Development and controls of the final Cretaceous black-shale event, Coniacian to lower Campanian (OAE 3): A reference section from the tropical Atlantic at Milankovitch time-scales

Dissertation
Zur Erlangung des Doktorgrades der Naturwissenschaften (Dr. rer. nat.)
am Fachbereich Geowissenschaften der Universität Bremen, Deutschland

Dissertation
Submitted for the Doctoral Degree in Natural Sciences (Dr. rer. nat.)
at the Faculty of Geosciences at Bremen University, Germany

vorgelegt von
presented by

Britta Beckmann

Bremen, August 2005

Tag des Kolloquiums:

08. November 2005

Gutachter:

Prof. Dr. T. Wagner

Prof. Dr. K.-U. Hinrichs

Prüfer:

Prof. Dr. K. Huhn

PD Dr. S. Kasten

General outline

This PhD thesis summarizes doctoral research, carried out between 2001 and 2005 at the University of Bremen, Germany. The central issue of the research deals with investigation of black shale deposition in the equatorial Atlantic and its relation to African climate variability during the Coniacian to Campanian Oceanic Anoxic Event (OAE) 3. The thesis opens with an introductory chapter (**chapter 1**), briefly reviewing climate conditions in the Late Cretaceous and a description of the concept of OAEs with a focus on the Cretaceous OAEs. In addition to a short summary of previous studies performed at ODP Site 959, a brief description of methods that were applied to the samples is given. **Chapters 2-5** comprise four scientific papers of which I am a co-author. The papers have been published or are in press in international peer-reviewed journals. **Chapter 6** summarizes the results and provides perspectives for ongoing investigations. New studies are briefly discussed.

To minimize duplication due to the organization of this thesis into a series of manuscripts, references have been removed from each paper and are cited in a single reference list at the end of this thesis. My contribution to the individual manuscripts is as follows:

Chapter 2. **"A millennial- to centennial-scale record of African climate variability and organic carbon accumulation in the Coniacian–Santonian eastern tropical Atlantic (Ocean Drilling Program Site 959, off Ivory Coast and Ghana)"**

Authors: Peter Hofmann, Thomas Wagner, Britta Beckmann

Status: published **Journal:** Geology, v. 31, p. 135-138

Contribution: analytical work (bulk organic analysis), data processing, contribution to geological interpretation, and authorship.

Chapter 3. **"Linking Coniacian-Santonian (OAE3) black shale deposition to African climate variability: a reference section from the eastern tropical Atlantic at orbital time scales (ODP Site 959, off Ivory Coast and Ghana)"**

Authors: Britta Beckmann, Thomas Wagner, Peter Hofmann

Status: published **SEPM Special Publication** v. 82, p. 125-143

Contribution: analytical work (selective and bulk organic geochemical procedures and subsequent analysis), data processing, graphical presentation, and principal writing.

Chapter 4. **"Euxinia and primary production in Late Cretaceous eastern equatorial Atlantic surface waters fostered orbitally driven formation of marine black shales"**

Authors: Thomas Wagner, Jaap S. Sinninghe Damsté, Peter Hofmann, Britta Beckmann

Status: published **Journal:** Paleoceanography, v. 19 (3), PA 3009, p. 1-13

Contribution: development of improved age model and accumulation records, contribution to interpretation, and authorship.

Chapter 5. **"Orbital forcing of Cretaceous river discharge in tropical Africa and ocean response"**

Authors: Britta Beckmann, Sascha Flögel, Peter Hofmann, Michael Schulz, Thomas Wagner

Status: published **Journal:** Nature, v. 437, p. 241-244

Contribution: analytical work (bulk organic analysis), data processing, graphical presentation, integration of modelling results, and principal writing.

Abstract

This study focuses on high-resolution investigation of marine sediments accumulated during the Coniacian-Campanian oceanic anoxic event 3 (OAE 3). These events, time envelopes of enhanced sequestration of marine organic carbon (OC), are one focus of current climate research as they provide fundamental information on the functioning of biogeochemical cycles and their internal and external feedback mechanisms during greenhouse conditions. To obtain a model of black shale formation in the Upper Cretaceous equatorial Atlantic Ocean, multi-parameter analyses of sediments from ODP Site 959 off Ivory Coast and Ghana were performed.

OC content and selected inorganic-geochemical parameters display cyclic fluctuations that can be attributed to orbital forcing of Milankovitch frequency. By combining biostratigraphic age-fixpoints with these cyclic records, a high-resolution timescale was obtained. This timescale allows the determination of changes in OC accumulation rates, biomarkers and trace elements; in addition it provides a detailed cyclostratigraphic age-model. Marine and continental geochemical proxy-data support the assumption of two depositional modes defining boundary conditions for marine black shale accumulation and OC-lean sedimentation in relation to African climate that persists throughout the OAE 3. While peak OC accumulation coincided with elevated detrital input from tropical regions, low OC levels were characterised by enhanced input from arid source areas. The transition between both modes was in the order of a few thousand years or even less and likely related to the repetitive displacement of the Intertropical Convergence Zone and African climate belts. Variable amplitudes in these continental proxy records suggest systematic climate contrasts alternating between arid and humid conditions. The long-term trend of the records supports gradual aridification of Africa from the Santonian onwards. Both mechanisms of continental runoff (i.e., riverine nutrient supply and the periodic development of an estuarine circulation generating a freshwater cap) were identified as main triggers for productivity cycles at Site 959. A more detailed study characterising organic matter composition and redox-conditions shows that OC and carbonate sedimentation were mainly controlled by dilution, and only in some cases superimposed by enhanced siliceous and calcareous plankton productivity. The distribution of molecular markers and trace-metal records indicate extreme variations in redox-conditions across the entire water column; euxinic conditions in surface waters were highly unstable and sensitive to the admixture of oxygenated water. Simulations using the global climate model GENESIS v. 2.0 validated the assumption of freshwater discharge resulting in circulation reversal and the development of ocean anoxia/euxinia and finally leading to black shale deposition. They indicate that ocean anoxia and black shale sedimentation was confined to specific periods of maximum discharge when northern spring equinox coincided with perihelion (the minimum distance between the Sun and the Earth).

Results from this study support a highly dynamic climate-ocean system during the Upper Cretaceous. Earth encountered a vigorous hydrologic cycle with large variations in atmospheric and marine circulation patterns in the Coniacian to Campanian "greenhouse world". These conclusions for the Cretaceous world imply that Earth not necessarily faces equable climate conditions during a possible future climate warming. However, further investigations of Upper Cretaceous sites are necessary to examine whether similar mechanisms and climate trends triggered black shale formation during the OAE 3 in different geographical settings in order to obtain a more global picture.

Zusammenfassung

Die vorliegende Studie befasst sich mit hochauflösenden Untersuchungen mariner Sedimente, die während des ozeanisch-anoxischen Ereignisses 3 (OAE 3) vom Coniac bis ins Campan akkumuliert wurden. Diese Ereignisse umfassen Zeitintervalle, die durch verstärkte Ablagerung von marinem organischen Kohlenstoff gekennzeichnet sind. Diese Intervalle stehen im Mittelpunkt der aktuellen Klimaforschung, da sie grundlegende Informationen sowohl zur Funktion biogeochemischer Zyklen als auch zu ihren internen und externen Rückkopplungsmechanismen während klimatischer Treibhausbedingungen liefern. Um ein Modell der Schwarzschiefer-Ablagerungen im äquatorialen Atlantik während der Oberkreide zu erhalten, wurden Multi-Parameter Untersuchungen an Sedimenten von ODP Kern 959 vor der Küste von Ghana und der Elfenbeinküste, durchgeführt.

Sowohl der Gehalt an organischem Kohlenstoff als auch organisch-geochemische Parameter zeigen zyklische Schwankungen, denen eine orbitale Steuerung auf Basis von Milankovitch-Frequenzen zugewiesen werden kann. Durch eine Kombination von biostratigraphischen Altersfixpunkten mit diesen zyklischen Datensätzen, wurde eine hochauflösende Zeitskala erstellt. Diese Zeitskala ermöglicht die Bestimmung von Änderungen in den Akkumulationsraten von organischem Kohlenstoff, Biomarkern und Spurenelementen. Zusätzlich liefert sie ein detailliertes zyklostratigraphisches Altersmodell. Marine und kontinentale geochemische Daten unterstützen die Annahme zweier unterschiedlicher Ablagerungsmodi. Diese bilden die Grenzbedingungen für marine Schwarzschiefer-Akkumulation und die Ablagerung organischer kohlenstoffarmer Sedimente bezogen auf das afrikanische Klima während des OAE 3. Während die maximale Akkumulation von organischem Kohlenstoff mit einem erhöhten detritischen Eintrag aus tropischen Regionen zeitlich zusammentrifft, werden Phasen niedriger organischer Kohlenstoffgehalte durch erhöhten Eintrag aus ariden Gebieten charakterisiert. Der Übergang zwischen beiden Modi umfasste eine Zeitspanne von wenigen tausend Jahren (oder weniger) und stand sehr wahrscheinlich mit der wiederholten latitudinalen Verschiebung der Innertropischen Konvergenzzone und damit verbundener afrikanischer Klimagürtel in Zusammenhang. Variable Amplituden in diesen kontinentalen Proxy-Daten lassen auf systematische Schwankungen zwischen ariden und humiden Klimabedingungen schließen. Der Langzeit-Trend dieser Daten unterstützt die Annahme einer graduellen Aridifizierung Afrikas ab dem Santon. Beide Mechanismen des kontinentalen Abflusses, fluvialer Nährstoffeintrag und das periodische Auftreten eines Frischwasserdeckels, hervorgerufen durch die Ausbildung einer estuarinen Zirkulation, stellen die Hauptauslöser zur Bildung von Produktivitätszyklen an Kern 959 dar. Detaillierte Untersuchungen zur Charakterisierung von Redox-Bedingungen und der Zusammensetzung des organischen Materials zeigen, dass die Ablagerung von Karbonat und organischem Kohlenstoff hauptsächlich durch Verdünnung kontrolliert wurde. Nur in einigen Fällen überlagert eine verstärkte Produktivität silikatischen

und karbonatischen Planktons diesen Prozess. Die Verteilung von Biomarkern und Spurenelementen zeigt extreme Variationen in den Redox-Bedingungen der gesamten Wassersäule an. Euxinische Bedingungen im Oberflächenwasser waren hochgradig instabil und empfindlich gegenüber der Zumischung sauerstoffhaltigen Wassers. Simulationen mit dem globalen Klimamodell GENESIS v. 2.0 bestätigen die Annahme, dass der Frischwasserabfluss zu einer Umkehr in der Zirkulation, der Ausbildung von ozeanischen Anoxia bzw. Euxinia, und schließlich zur Ablagerung von Schwarzschiefern führt. Die Simulationen zeigen, dass ozeanische Anoxia und Schwarzschiefer-Sedimentation auf bestimmte Perioden maximalen kontinentalen Abflusses beschränkt waren, wenn der nördliche Frühlingspunkt mit der kürzesten Distanz zwischen Sonne und Erde (Perihelion) zusammenfiel.

Ergebnisse dieser Studie unterstützen die Annahme eines hoch-dynamischen Klima-Ozean-Systems während der Oberkreide. Die Erde war zur Zeit der Treibhauswelt des Coniac-Campan einem intensiven Wasserkreislauf mit großen Schwankungen in atmosphärischen sowie marinen Zirkulationsmustern ausgesetzt. Diese Folgerungen für die kretazische Welt implizieren, dass die Erde während einer möglichen zukünftigen Klimaerwärmung nicht notwendigerweise vor gleichmäßigen Klimabedingungen stehen muss. Um ein globales Bild zu erhalten, ist es jedoch notwendig, weiterführende Untersuchungen an oberkretazischen Lokationen durchzuführen. Nur so kann geprüft werden, ob ähnliche Mechanismen und Klimatrends die Schwarzschieferbildung im OAE 3 an verschiedenen geographischen Positionen ausgelöst haben.

Table of Contents

Chapter 1. Introduction and outline of the thesis

1.1 Selected mechanisms of climate forcing

In the past decades, society's interest in and concern about future climate development has increased immensely. Before a quantitative assessment of how human activities affect current and future climate, it is essential to understand natural mechanisms and their related climate feedbacks first in modern times but also, as an analogue, in the geological past. As processes related to the interaction of the land-ocean-atmosphere-system take up a central part in climate research, a focus on these interactions is inevitable.

Major natural factors influencing climate at all scales are among others vegetation, continental topography, land-ocean distribution, solar insolation, and - intimately related to that - atmospheric greenhouse gases; most important being water vapour, CO_2, CH_4, and N_2O (Stocker & Schmittner, 1997). Several authors have identified the circulation and conservation of Earth's water (i.e., hydrologic cycle) and weathering chemistry to be primary drivers of global biogeochemical cycles and thus global climate variability (e.g., Allen & Ingram, 2002; Pierrehumbert, 2002; Rahmstorf, 2002). Climate is regulated by CO_2 and water (Pierrehumbert, 2002) as both affect Earth's radiation balance through greenhouse effects. From Figure 1, which gives a simplified overview of the hydrologic cycle, it is evident that solar radiation is the key driver for processes in the hydrologic cycle in determining

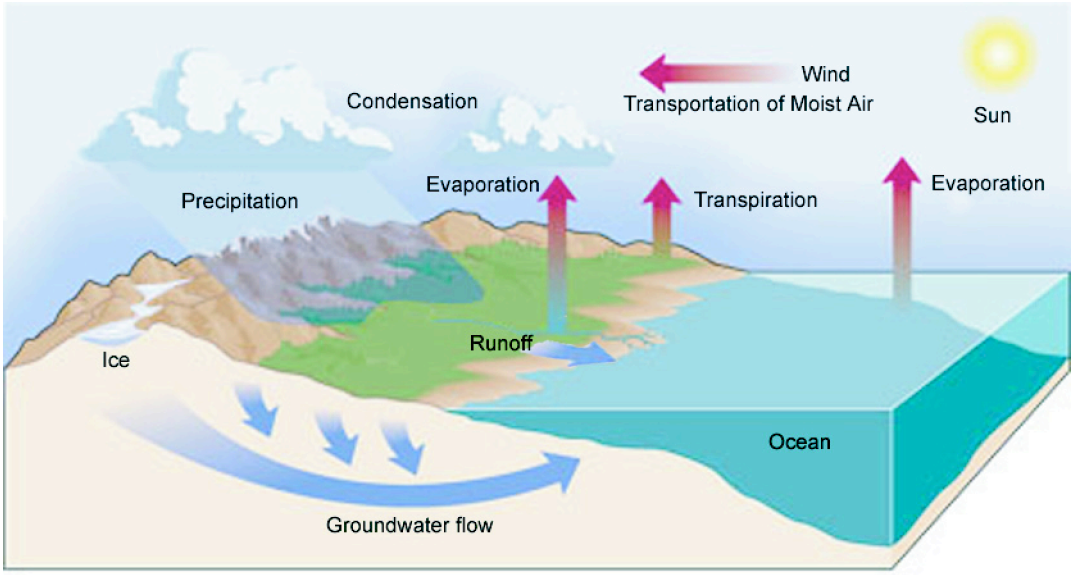

Fig. 1: Simplified model of the hydrological cycle (redrawn from www.jbpub.com/oceanlink2e/labeling/figures/c05f20.cfm). Water evaporates from lakes, rivers, and mainly the ocean, the vapour condensates to form clouds, which are transported around the globe. The water returns to the surface by precipitation where it either evaporates again, empties into lakes, rivers, and ocean as runoff, or form groundwater, which seeps into streams, rivers, and oceans or is released back into the atmosphere by transpiration.

evaporation rates, transportation of moisture, and precipitation. According to Pierrehumbert (2002) precipitation is the link between atmosphere and processes on Earth's surface and the seafloor, as water forms one main mode of energy transport in the atmosphere and the ocean. Additionally, the rate of precipitation determines the rate of chemical weathering of silicate rocks and thus CO_2 content of the atmosphere. Because changes in greenhouse gas concentration modulate insolation-driven climate, anthropogenic influence on these concentrations will ultimately affect global climate development over the next few thousand years (e.g., Broecker, 1997; Hay et al., 1997; Timmermann et al., 1999; Schmittner et al., 2000; Archer and Ganopolski, 2005). A focus of recent climate research is on CO_2, which is expected to dominate climate changes in the next century. Among other greenhouse gases it will force progressive global warming, however, the pacing and dimension of climate change and its consequences for mankind and ecosystems are difficult to predict.

Allen & Ingram (2002) stress a possibly stronger effect of large-scale rainfall distribution on global climate development rather than global warming. To their finding, regional details of precipitation response to greenhouse warming is much less constrained than the effect of increasing greenhouse gas concentrations, as are hydrologic feedbacks on the strength of oceanic circulation (e.g., Clark et al., 2002; Rahmstorf, 2002). Today's large-scale ocean circulation comprises a combination of currents driven by tides, wind, and fluxes of heat and freshwater (i.e., thermohaline circulation; e.g., Rahmstorf, 2002). The gravitational pull of Moon and Sun acts as one main source of turbulent energy to oceanic mixing. Wind-driven currents lead to climatic changes through their effect on upwelling near coasts and the Equator. Thermohaline circulation in general describes the effect of near-surface waters flowing to one of the three main deep-water formation areas (northern North Atlantic, Ross Sea, Weddell Sea) and recirculate at depth. Highest surface densities occur where water is coldest; additionally, salinity is involved in a positive feedback. Higher salinity in deep-water formation regions enhances the circulation and thus higher salinity water is transported to deep-water formation areas. The thermohaline circulation is a major contributor to the heat budget of the North Atlantic region and is sensitive to the amount of freshwater entering the North Atlantic. One popular effect of our modern situation could be a permanent shutdown of the Atlantic thermohaline circulation (e.g., Manabe & Stouffer, 1993; Stocker & Schmittner, 1997) with profound consequences to atmospheric operation and global climate (e.g., Broecker, 1997; Schmittner et al., 2000). Mechanisms of the hydrologic cycle and consequences for ocean chemistry and ecosystems therefore need to be explored in much more detail to improve climate predictions and help defining counter-actions. Key questions addressed by current climate research concern the effects of global climate development with respect to changes in sea level and flooding of continental margins, as well as the consequences if oceanic circulation is amplified, attenuated or changes its flow path.

1.2 Past periods of warm climate

To understand what Earth might face in the future, it is indispensable to analyze periods of past extreme warm climates. Detailed investigations of these intervals are necessary to assess the relationship between causes of climate variability and their effect on climate development during greenhouse climate. Changes in the Earth's orbit around the sun (variations in eccentricity, obliquity, and precession of the Earth) modify the seasonal distribution of solar radiation and thus climate and all sub-compartments of the hydrological cycle (e.g., Valdes 2000; Sloan & Huber, 2001; Philander & Fedorov, 2003). In order to resolve climate oscillations at short orbital time scales, high-resolution geological records of sufficient, uninterrupted total length and precise time-scales of these intervals are necessary (e.g., Sageman et al., 1998; Valdes 2000; Jenkyns, 2003). High-resolution multi-proxy studies, computer-based simulation of pre-Quaternary climate-ocean-systems, and model-data comparisons are powerful tools to explore possible scenarios, mechanisms, and feedback processes, especially when applied in combination to intervals of rapid change.

Earlier studies have identified several key mechanisms causing climate change: for instance large-scale accumulation of organic matter (OM) in the oceans resulting in marine black shales (e.g., Arthur et al., 1990; Martinez-Ruiz et al., 2000; Calvert & Fontugne, 2001), release of CO_2 by volcanic activity at spreading centres, subduction zones, and intraplate volcanism (e.g., Larson, 1991a&b; Berner, 1994), and catastrophic release of methane from marine gas hydrate dissociation (e.g., Gröcke et al., 1999; Hesselbo et al., 2000; Jahren, 2002; Jenkyns, 2003). The importance of the Tropics as driver of global ocean-atmosphere circulation and biogeochemical cycling during periods of extreme warmth is widely acknowledged (e.g., Hay et al., 1997; Wilson & Norris 2001; Norris et al., 2002). However, Flögel & Wagner (in press) present data from paleoclimate simulations linked to a geological model suggesting that mid-southern latitudes triggered tropical Atlantic black shale formation in the Late Cretaceous via precipitation and river discharge. Generally, continental margins react sensitive to fluctuations in hydrological and nutrient cycling, drastic changes in these settings are expected during intervals of global warmth, making them a focus area of current (paleo-) climate research.

1.3 Earth in the Late Cretaceous

Earth has encountered several phases of generally warm climate periods that were characterized by little or no ice and short-term intervals of contrasting climate, throughout its history (e.g., Frakes et al., 1992; Barron et al., 1995; Hay et al., 1997). The mid-Cretaceous to early Tertiary (105 – 55 Ma) was one of the warmest periods in the late Phanerozoic. As the late Cretaceous is among the best-investigated intervals with respect to terrestrial and marine fossil and geochemical records, it allows the detailed assessment of warming/cooling,

humidity/aridity and sea-level changes. These information are pivotal to understand how terrestrial and marine environments are coupled on a warmer Earth. Several factors influencing global climate were differently during the Cretaceous: e.g., land-ocean distribution and the related oceanic and atmospheric circulation pattern, vegetation cover, submarine volcanic activity, atmospheric CO_2 concentration, and the primary mode of cross-latitudinal energy transport by water vapour.

1.3.1 Climate conditions

Among the most remarkable features in the Upper Cretaceous are atmospheric pCO_2 levels (see Fig. 2) that were 2-12 times higher than the pre-industrial pCO_2 (e.g., Berner, 1992, 1994; Hay et al., 1997). This phenomenon has been related to the elevated production of oceanic crust in the Lower Cretaceous (Arthur et al., 1988; Larson, 1991a&b) and the emplacement of Large Igneous Provinces (LIPs, e.g., Ontong-Java Plateau and Kerguelen Plateau; Larson & Erba, 1999), and the catastrophic release of methane by gas hydrate dissociation (e.g., Gröcke et al., 1999; Hesselbo et al., 2000; Jahren, 2002; Jenkyns, 2003). As one consequence, maximum sea level during the mid-Cretaceous (Fig. 3a) was up to 250 m higher than today (Haq et al., 1987; Hardenbol et al., 1998).

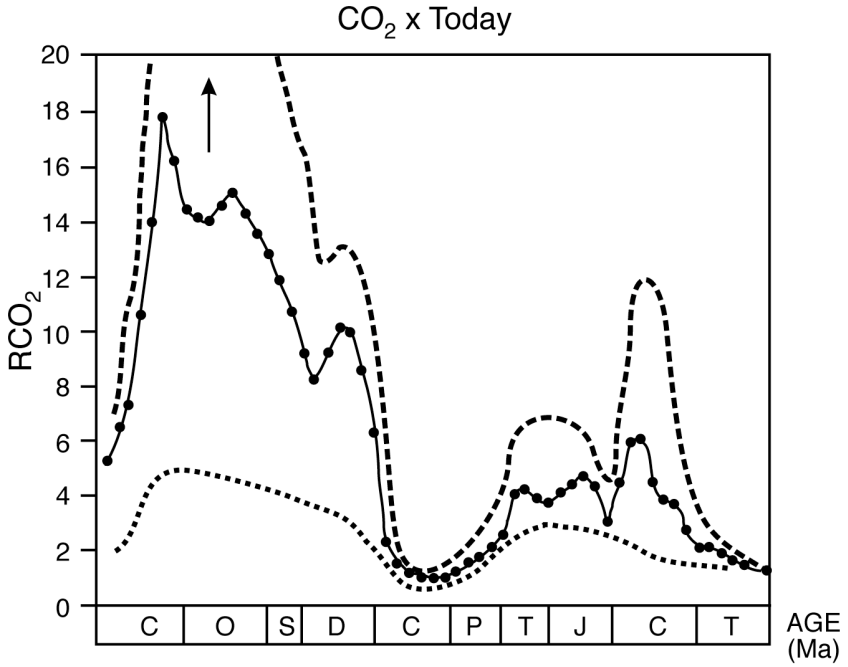

Fig. 2: Estimated CO_2 concentration at a given time normalized to the present day value (RCO_2) versus time. Dashed lines represent rough estimates of errors based on sensitivity studies (modified after Berner, 1991); arrow indicates that early Paleozoic RCO_2 values may have been higher.

Another consequence from significantly higher atmospheric pCO_2 was elevated global air- and ocean-temperatures (see Fig. 3b for paleo-position of sea-surface temperature - SST - 20°C isotherme). Several researchers found non-marine vertebrate fossil evidence for Late Cretaceous (Turonian to Coniacian) mean annual air temperatures exceeding 14°C in arctic regions (Markwick, 1998; Tarduno et al., 1998). Consistent with that fossil wood found on the

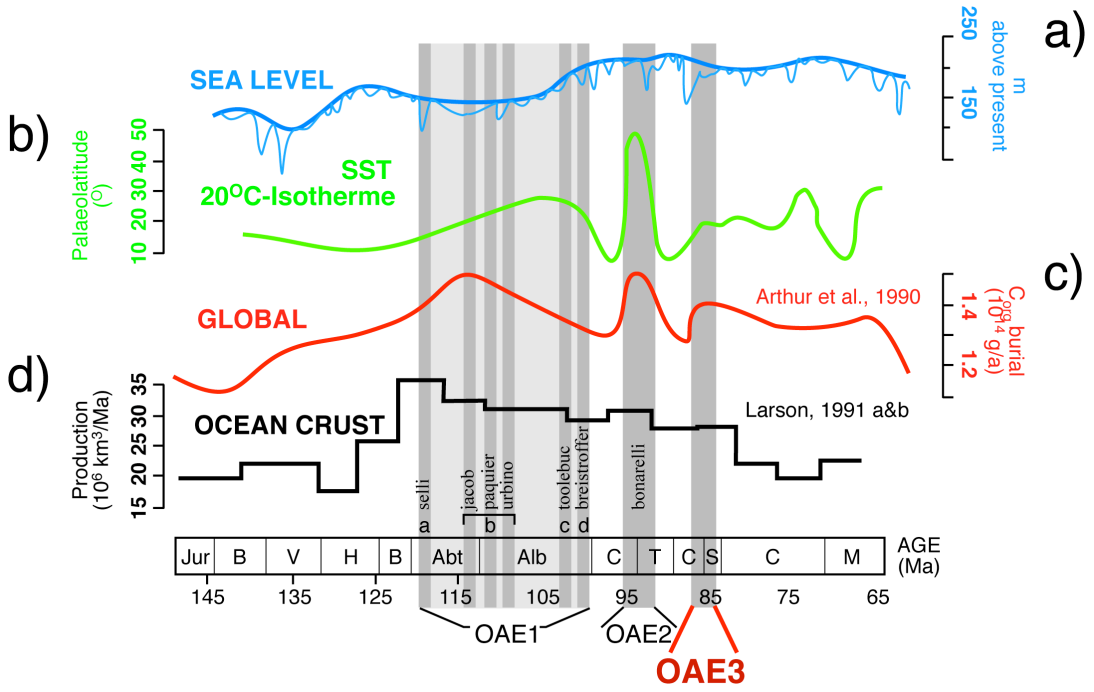

Fig. 3: Mid Cretaceous OAEs in the context of global sea-level development **(a)**, mean global sea surface temperature (SST) **(b)**, global OC burial **(c)**, and ocean crust production **(d)** (modified after Arthur et al., 1990; Larson 1991a, b).

northern Antarctic Peninsula suggested peak air temperatures in the range of 16-23°C during the Coniacian to early Campanian (Francis & Poole, 2002). These observations imply that polar temperatures were warm rather than near freezing and supports the idea of generally absent polar ice caps during these times. Recent studies confirm that Late Cretaceous surface ocean paleotemperatures exceeded 32°C in the tropical Atlantic during the Cenomanian-Turonian (Norris et al., 2002; Wilson et al., 2002) and Maastrichtian (Pearson et al., 2001), 30°C in the southern high latitudes during the late Turonian to lower Campanian (Huber et al., 1995; Bice et al., 2003), and exceeded 20°C in the Arctic Ocean during much of the Cenomanian-Turonian interval (Jenkyns et al., 2004). Bathyal temperatures reached 20°C in the subtropical North Atlantic between the Albian and Coniacian interval (Norris & Wilson, 1998; Fassell & Bralower, 1999; Huber et al., 1999) and varied between 14 and 16°C in high-latitude oceans from late Cenomanian to early Campanian (Huber, 1998). Warmest SSTs yet for the Cretaceous and Cenozoic were reported for the Cenomanian to Turonian. Schouten et al. (2003) found biomarker evidence for early Albian to early Turonian tropical SSTs in the proto-North Atlantic of 32-36°C. The pole to equator temperature gradient defines meridional heat transport by atmosphere and ocean and ultimately defines climate (Pierrehumbert, 2002). While generally warm climates have smaller temperature gradients, the concentration of water vapour increases with temperature (Pierrehumbert, 2002).

A different paleogeographic setting as well as enhanced air and surface water temperatures led to oceanic circulation patterns during the Cretaceous interval principally

different from Quaternary's thermohaline circulation with three major deep-water formation areas. Poulsen et al. (2001) for example used an ocean general circulation model (OGCM) to simulate significant changes in surface and deep oceanic circulation within the Atlantic basins from stagnant circulation in the North Atlantic basin and lagoonal circulation in the South Atlantic during the Albian, to thermohaline circulation ventilating both basins in the Turonian. According to DeConto et al. (2000), Campanian simulation using an OGCM predict most deep water formation via convection in the southern high latitudes, a process similar to the one found in today's North Atlantic. Bush & Philander (1997) simulated global mean temperatures being approx. 4°C warmer than today and a persisting seasonal cycle with certain regions evidencing temperatures below freezing. They reconstructed a vigorous wind-induced ocean circulation with a magnitude of convergence of surface winds (i.e., Intertropical Convergence Zone; ITCZ) remaining comparable with the present day situation; according to their simulations the evolving Equatorial Atlantic Gateway (Wagner & Pletsch, 1999) was characterized by salinities exceeding 38.5‰. Similar results were drawn from global climate modelling by Otto-Bliesner et al. (2002), who simulated a very salty narrow South Atlantic (> 38‰) with a large deep overturning cell in the Upper Cretaceous.

With few exceptions most biostratigraphic or geochemical studies of Cretaceous organic carbon (OC)-rich sediments in the past were relatively low resolution, hampering the identification of higher frequency fluctuations that illustrate the cause-effect relationships of Cretaceous climate variability and OC deposition. However, general interactions of the Cretaceous climate-ocean system are widely investigated and reasonably well constrained. Various mechanisms have been identified capable to drive short-term, but strong fluctuations in global greenhouse conditions. One fundamental mechanism involves strongly enhanced deposition of OM leading to massive drawdown of atmospheric CO_2, a shift in the carbon isotopic signature, and consequently global cooling (e.g., Arthur et al., 1990; Kuypers et al., 1999). Based on carbon isotope analysis of n-alkanes from leaf-waxes, Kuypers et al. (1999) estimated a reduction of atmospheric CO_2 on the order of 40-80% for the Cenomanian/Turonian that occurred in 60 kyrs parallel with the onset of the Cenomanian/Turonian Boundary Event. Apart from large rapid shifts in atmospheric pCO_2 and paleogeographic changes (e.g., opening of the Equatorial Atlantic Gateway; Wagner & Pletsch, 1999; Wagner, 2002), Upper Cretaceous sedimentary records bear evidence of orbital changes through cyclic bedding rhythms with periodicities in the Milankovitch frequency band (e.g., Kuhnt et al., 1997, 2001; Dean & Arthur, 1998; Floegel et al., 2005; Kuypers et al., 2004).

The final goal was to assess global and regional controls on enhanced OC deposition using multi-parameter records. Detailed analysis of Coniacian to early Campanian sediments from ODP Site 959 not only supports the information gained from other high-resolution studies, it highlights a critical geological period that has never been investigated at this time resolution before.

1.3.2 The concept of oceanic anoxic events

One prominent feature during a warm climate mode is the deposition of black shales in the ocean. Accumulation of these dark coloured, bituminous, OC-rich marine sediments occurred during specific periods of Earths history, confined to short time-intervals of poor oceanic mixing and widespread expansion of oxygen minimum zones (OMZ) to the open ocean, commonly termed "oceanic anoxic events" (OAE; e.g., Schlanger & Jenkyns, 1976; Arthur & Schlanger, 1979; Jenkyns, 1980). Later on, the term OAE was used for time envelopes during which black shale deposition was particularly prevalent; it did not specifically distinguish between events of long- or short-time duration (Arthur et al., 1987; 1990). Stratigraphically restricted horizons of enhanced OC-rich black shale can be correlated across large distances (e.g., Schlanger & Jenkyns, 1976). Specifically the Cenomanian-Turonian black shales were widespread and found in a variety of settings (e.g., broad rises and plateaus in the open Pacific, Tethyal margins, shallow shelf areas of northeastern Europe). This led to the conclusion that the world oceans underwent fundamental chemical and/or biological changes during the OAEs, with oxygen deficiency at the sea floor (Arthur & Schlanger, 1979; Jenkyns, 1980) and radiation and extinction of organism groups (Erba, 1994; Erbacher & Thurow, 1997; Leckie et al., 2002). Initially, OAEs have been related to sea level transgressions, as the expansion of epicontinental seas led to an increase of OC production while the amount of O_2 renewal in bottom water decreased (e.g., Schlanger & Jenkyns, 1976; Jenkyns, 1980). OAEs are commonly characterized by positive $\delta^{13}C$ shifts (e.g., Arthur et al., 1990; Erba, 1994; Jenkyns et al., 1994; Erbacher et al., 1996; Kuypers et al., 2002; Leckie et al., 2002; Erba 2004). These positive $\delta^{13}C$ isotopic anomalies were explained by large-scale burial of isotopically light OC and an enrichment of the heavy ^{13}C isotope in the world's ocean and precipitates therein. OAEs not only occurred during the Cretaceous, e.g., the early Toarcian OAE (e.g., Jenkyns, 1999; 2003; Erba, 2004). Cretaceous OAEs, however, are of particular scientific interest because they provide evidence for the reoccurrence of extreme modes of the open ocean with rapid fluctuations in ocean chemistry compared to their duration on the order of few 100 ka (e.g., Arthur et al., 1990; Bralower et al., 1994; Kuhnt et al., 1997, Leckie et al., 2002; Kolonic et al., 2005).

In general, three Cretaceous OAEs have been identified, while the first has been further divided into 4 sub-events (see Leckie et al., 2002 for summary; Fig. 3). After a detailed look at the Cretaceous OAEs, the initial stratigraphic concept of OAEs relating them to positive $\delta^{13}C$ excursions is unsustainable as there is a mismatch in timing of black shale deposition relative to global isotopic carbon excursions. Additionally to the stable carbon isotope signal, several other general conditions were different for individual OAEs. The globally distributed early Aptian OAE 1a ("Selli" event – 120.5 Ma) was preceded by a negative $\delta^{13}C$ excursion linked to the eruption of the Ontong-Java LIP (Fig. 3d) forcing global warming and followed by an abrupt positive $\delta^{13}C$ excursion due to increased marine

productivity and black shale deposition (Erba, 1994; Föllmi et al., 1994; Menegatti et al., 1998) and parallel sea-level rise. Contrasting this, Erbacher et al. (2001) identified an increase in $\delta^{13}C$ of planktic foraminifera shortly below the OAE 1b (further subdivided into "Jacob", "Paquier", and "Urbino" events – 113-109 Ma) followed by a negative $\delta^{13}C$ excursion at the base of the black shale. They state that instead of productivity, degassing of CO_2 from surface water and a decreasing supply of negative carbon from deep water caused the positive $\delta^{13}C$ excursion, relating OAE 1b to a "super-sapropel" stage of restricted ventilation caused by partial tectonic isolation, low sea level, and the initiation of warm global climate. Both, the late Albian OAE 1c ("Toolebuc" event – 101 Ma), as well as the latest Albian OAE 1d ("Breistroffer" event – 99.5 Ma) were less pronounced and have only regional significance (Erba, 2004). The Cenomanian/Turonian Boundary Event, OAE 2 ("Bonarelli" event – 93.5 Ma) was the most widespread (Leckie et al., 2002) and probably the most intense OAE in respect to global OC burial rates (Fig. 3c).

The OAE 2 is characterized by a distinct positive $\delta^{13}C$ excursion that has been divided into three major phases – an initial rapid shift in 60 kyrs, a plateau with maximum $\delta^{13}C$ values for about 400 kyrs, and a recovery phase of approx. 500 kyrs (Kuypers et al., 2002); it was not preceded by a negative $\delta^{13}C$ shift (Jenkyns, 2003). Kuypers et al. (2002) find geochemical and biomarker evidence that parts of the proto-North Atlantic were already periodically anoxic before the OAE, thus a combination of preservation and enhanced productivity led to the widespread development of OAE 2 black shales. Leckie et al. (2002) relate high productivity during the OAE 2 to changes in intermediate or deep-water circulation and/or source of water mass production and conclude that primary productivity was further enhanced by widespread transgression.

The final Cretaceous event is the Coniacian/Santonian OAE 3 (86-85 Ma), which was restricted to marginal marine settings as the deep ocean was fully oxic during that interval, evident from widespread deposition of Cretaceous oceanic red beds (e.g., Arthur & Fisher, 1977; Galeotti et al., 2002; Leckie et al., 2002; Wang et al., 2005; Hu et al., 2005).

1.3.3 The oceanic anoxic event 3 in the Coniacian-Santonian

The OAE 3 is characterized by a moderate carbon isotope excursion on the order of 0.2 – 0.3‰ that has been identified in several settings (Jenkyns et al., 1994; Perez-Infante et al., 1996; Crespo de Cabrera et al., 1999). De Romero et al. (2003) report carbon isotope excursions up to 5‰, which they tentatively relate to the OAE 3. During the late Santonian to early Campanian, extended siliceous deposits have been identified that were interpreted to represent an open-marine productivity event, related to the lowering of the Calcite Compensation Depth (CCD; e.g., Kuhnt, 1992; Kuhnt et al., 1989; 1998 and references cited therein). However, this so called Lower Campanian event (LCE) did not belong to the Coniacian/Santonian OAE in the original definition of the OAE 3.

Apart from few sites situated in higher latitudes (e.g., Stein et al., 1989; Leith et al., 1992; Dam et al., 1998), many of the known OAE 3 sections were deposited in low latitudes along continental margins (e.g., in northern South America, Brazilian Marginal Basins, Angola Basin, and Deep Ivorian Basin (DIB); see chapters 3 and 4 for overview) and intercontinental connections between them (Western Interior Seaway). The South American La Luna and Querecual Formations are among the geographically most extensive deposits of OAE 3 OC-rich sediments. Because of their geographic position in the Tropics on the conjugate South American margin, these formations are expected to represent the closest similarities in terms of mechanisms and sedimentary facies with the deposits from ODP Site 959. OC-rich, marine shales were deposited from the Turonian to Santonian (e.g., Mongenot et al., 1996; Perez-Infante et al., 1996; Alberdi-Genolet & Tocco, 1999; Davis et al., 1999; Erlich et al., 1999; Cotillon et al., 2000), regionally up into the basal Campanian interval (Zapata et al., 2003). However, time resolution of analyses from those sediments is often insufficient to identify cause-effect relationships between the atmosphere and the ocean and relate triggers and responses of black shale deposition. Several authors related intensive primary production coupled with enhanced preservation due to recurrent episodes of anoxia (Alberdi-Genolet & Tocco, 1999; Erlich et al., 1999) and sulphidic bottom-water (Mongenot et al., 1996; Davis et al., 1999) to the cyclic deposition of OAE 3 black shales. Erlich et al. (1999) instead attribute paleobathymetric barriers connected with basin uplift of the Maracaibo and Apure Basins with enhanced black shale deposition. Segmentation and restriction of seaways led to restricted circulation patterns with little or no exchange of oxygenated bottom-waters with open-marine environments in these epeiric basins (Macsotay et al., 2003; Zapata et al., 2003). Rey et al. (2004) describe consistent anoxia or low dissolved oxygen content based on geochemical and microbiological data. They find evidence that seasonal ventilation via turbidites or major storms was uncommon, while stagnant and anoxic bottom-water conditions rarely changed, concluding that dry conditions prevailed during the accumulation of the La Luna Formation. Contrasting this scenario, the Querecual Formation evidences periods of strong anoxia, punctuated by phases of intermittent oxygenation as seasonally modulated wet and dry cycles resulted in fluctuations in the OMZ (Macsotay et al., 2003). Geochemical, palaeontological, and sedimentological parameters bear evidence of rainy climate and consequently enhanced terrigenous input via continental runoff, associated dilution of biogenic carbonate and due to intensified stratification, elevated OC preservation during the early deposition of the La Luna Formation (Rey et al., 2004). A change in Cretaceous climate towards cool and arid conditions led to reduced runoff, increased upwelling and ultimately to destabilized stratification and decreasing OC preservation (Rey et al., 2004).

The OAE 3 is of special interest, because the Coniacian-lower Campanian interval marks the beginning of a global cooling trend that persists well into the Tertiary. Its potential connection with the enhanced accumulation of OM-rich sediments has only rarely been

investigated beforehand, mostly due to low sedimentation rates, hiatuses, and poor core recovery of the respective sediment cores that were retrieved from other sites surrounding the ocean margins. Few authors have identified the influence of climate variability at Milankovitch or sub-Milankovitch timescales on the Coniacian to Campanian equatorial Atlantic. Cotillon et al. (2000) identified several high frequency cycles (varves, El Niño and cycles of solar activity) by microscope analyses of core material and field observations. Whereas Rey et al. (2004) report eccentricity and obliquity cycles in OC and $CaCO_3$ records; they did not observe cycles of higher order due to insufficient sample resolution.

1.4 Aims of this study

ODP Site 959 was selected as a reference site to study the continuous transition from peak greenhouse conditions during the Turonian to gradually cooler climates in the lower Campanian at a tropical Atlantic setting because of the high core recovery of approx. 96% for the upper Turonian to lower Campanian interval (Mascle et al., 1996), and the existing detailed biostratigraphy (e.g., Watkins et al., 1998).

The study presented here was performed to establish an unprecedented reference section for the tropical Atlantic to investigate regional and global controls of enhanced OC accumulation during the OAE 3 using multi-parameter records. High-resolution organic and inorganic geochemical datasets are necessary to identify and understand the mechanisms and feedbacks of rapid climate changes superimposed on longer-term trends from greenhouse climate in the Upper Cretaceous to the Tertiary cooling trend and its impact on continental margin chemistry. Several specific questions were addressed by investigation of various marine and terrigenous proxy records to reconstruct mechanisms and feedbacks of orbital forcing, land-sea interaction, and phasing of terrigenous and marine records. These questions concerned the timing of the OAE 3, as well as identification of mechanisms forcing the enhanced accumulation of black shales.

Preliminary investigations have shown that OC-rich sediments occurred throughout almost the entire Cretaceous section, but black shale deposition only commenced after the separation of Africa and South America was far enough to allow permanent oceanic mid-water exchange in the late Albian (Wagner & Pletsch, 1999). These studies of the Upper Cretaceous sequence of ODP Site 959 include geochemical and pyrolytical data that led to a tentative sub-division of the OAE 3 into three phases of OM accumulation (Wagner & Pletsch, 1999; Pletsch et al., 2001). The OAE 3a and b were described as two periods of enhanced, highly variable OC sedimentation from the uppermost Turonian through the Santonian. Foraminiferal assemblages and calcareous nannoplankton further suggest elevated carbon flux and the existence of an oxygen minimum zone (Kuhnt et al., 1998; Watkins et al., 1998; Holbourn et al., 1999). The lower Campanian OAE 3c evidenced a less variable but still enhanced OC deposition. This sub-event correlates with the LCE, an interval characterised by

elevated carbon and biogenic silica flux even to the deep sea floor. Slightly elevated C/S ratios during the OAE 3c indicate decreasing preservation of labile OM (Wagner & Pletsch, 1999). The occurrence of agglutinated foraminifera and absence of calcareous nannoplankton in the early Campanian was interpreted to mirror the subsidence of Site 959 below the local CCD (Watkins et al., 1998; Kuhnt et al., 1998). Hence, sediments from ODP Site 959 allow the investigation of the continuous development of Upper Cretaceous black shale formation from shallow to deep-water environments (Holbourn et al., 1999), as Site 959 subsided from lower shelf to abyssal depths during the opening of the central Atlantic Ocean. Continuously rising input of mainly detrital quartz and the lack of minerals evidencing more humid climate conditions in the OAE 3c were interpreted to illustrate the development towards more arid climate (Wagner & Pletsch, 1999; Pletsch et al., 2001).

1.5 Material and analytical approach

ODP Site 959 was drilled during Leg 159 off Ivory Coast and Ghana (3°37.656'N, 2°44.149'W) at approx. 2100 m water-depth. As the site is situated along the Côte d'Ivoire Ghana Transform Margin (see Fig. 4a), its sedimentary record is intimately linked to the plate tectonic and paleoceanographic evolution of the equatorial Atlantic gateway (Pletsch et al., 2001; Wagner & Pletsch, 1999). The formation of a basement ridge on the south-eastern border of the transform margin provided efficient shelter against erosive and potentially oxidizing currents from the southern Atlantic (see migrated multi-channel seismic line in Fig. 4b).

After a detailed core description on the respective archive halves, identifying lithology, bioturbation, and lamination (see chapter 3), samples from cores 67R to 63R, covering the late Turonian to lower Campanian, were taken at 1 cm increments in order to ensure appropriate time-resolution for the anticipated detailed look at climatic changes. All samples were dried at 35°C and except for organic petrology samples homogenized prior to analysis. Figure 5 illustrates the analyses performed, a more detailed description on the methods used can be found in chapters 3 and 4. LECO and mineral analyses, organic petrology as well as part of the isotopic analyses were performed at the Department of Geology at the University of Bremen. Rock Eval pyrolysis was carried out at the Federal Institute for Geosciences and Natural Resources (BGR) in Hannover, biomarker and additional isotopic analyses were conducted at the Netherlands Institute for Sea Research (NIOZ), Texel, while major and minor element analysis was performed at the Geological Institute of the University of Cologne.

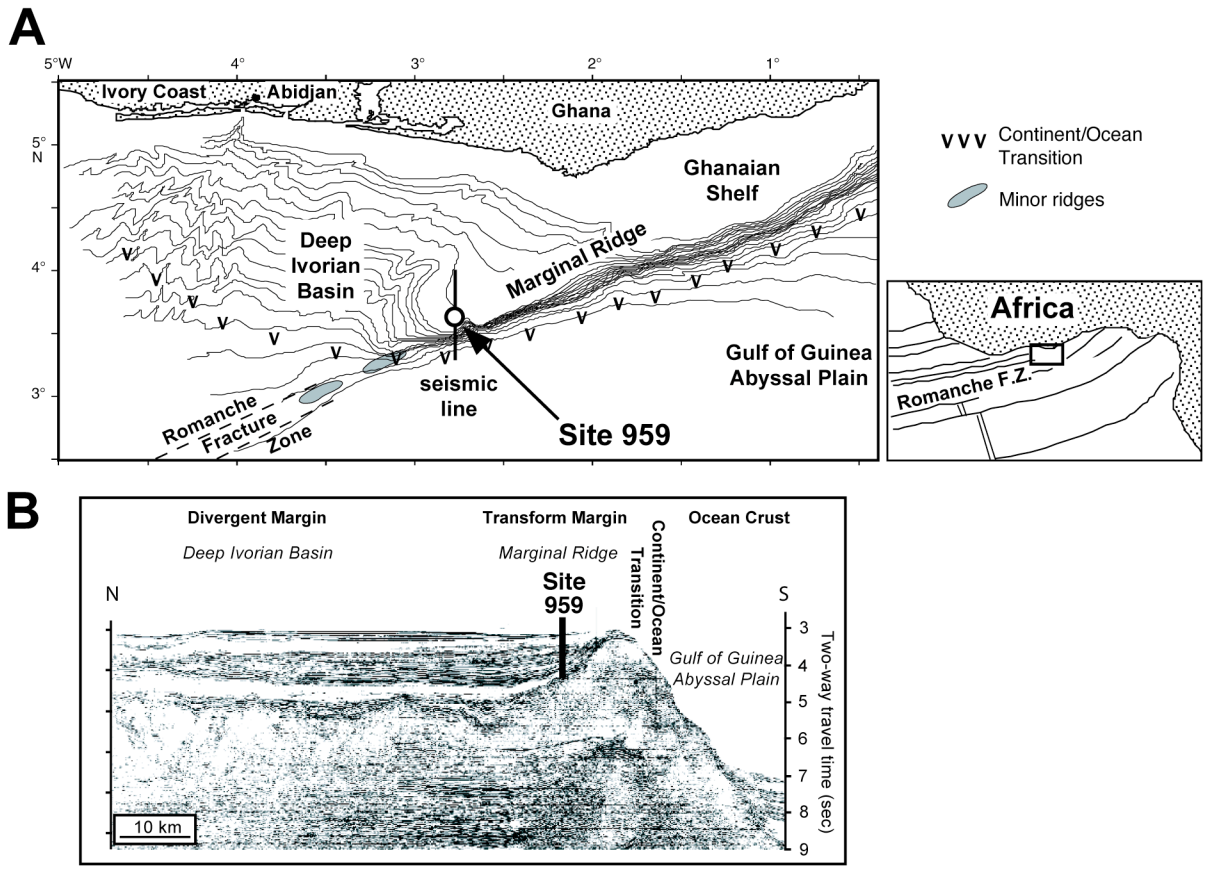

Fig. 4: (a) Location of ODP Site 959 (modified from Pletsch et al., 2001). **(b)** Migrated multichannel seismic line across the Côte d'Ivoire Ghana Transform Margin and the Deep Ivorian Basin (from Mascle et al. 1996).

1.6 Overview of own research

In **chapter 2** (Hofmann et al., 2003), a depositional model for black shale accumulation in equatorial regions during the OAE 3 was developed covering the late Turonian to late Santonian interval of the profile. The identification of a strong cyclic signal in proxy records of marine sedimentation (OC; occurrence of black shale) and continental supply (Si, K, and Al; abundance of quartz and clay minerals) relates the periodic deposition of black shales in the DIB and was linked to orbitally forced climate variability across Africa. The proposed depositional model relates enhanced OC accumulation to phases when the Intertropical convergence zone (ITCZ) was located at a southern position, leading to high precipitation and excess runoff resulting in enhanced freshwater and nutrient supply and a temporal formation of estuarine circulation. Different from that background deposition with lower OC accumulation occurred while the ITCZ was in a northern position fostering the SE trades to transport of dust from southern latitudes and generally drier conditions to the study site. Cycle analysis and orbital tuning of the terrigenous proxies Si/Al and K/Al for the biozone CC15 (85.7 to 84.9 Ma) provides a high-resolution cyclostratigraphic time frame.

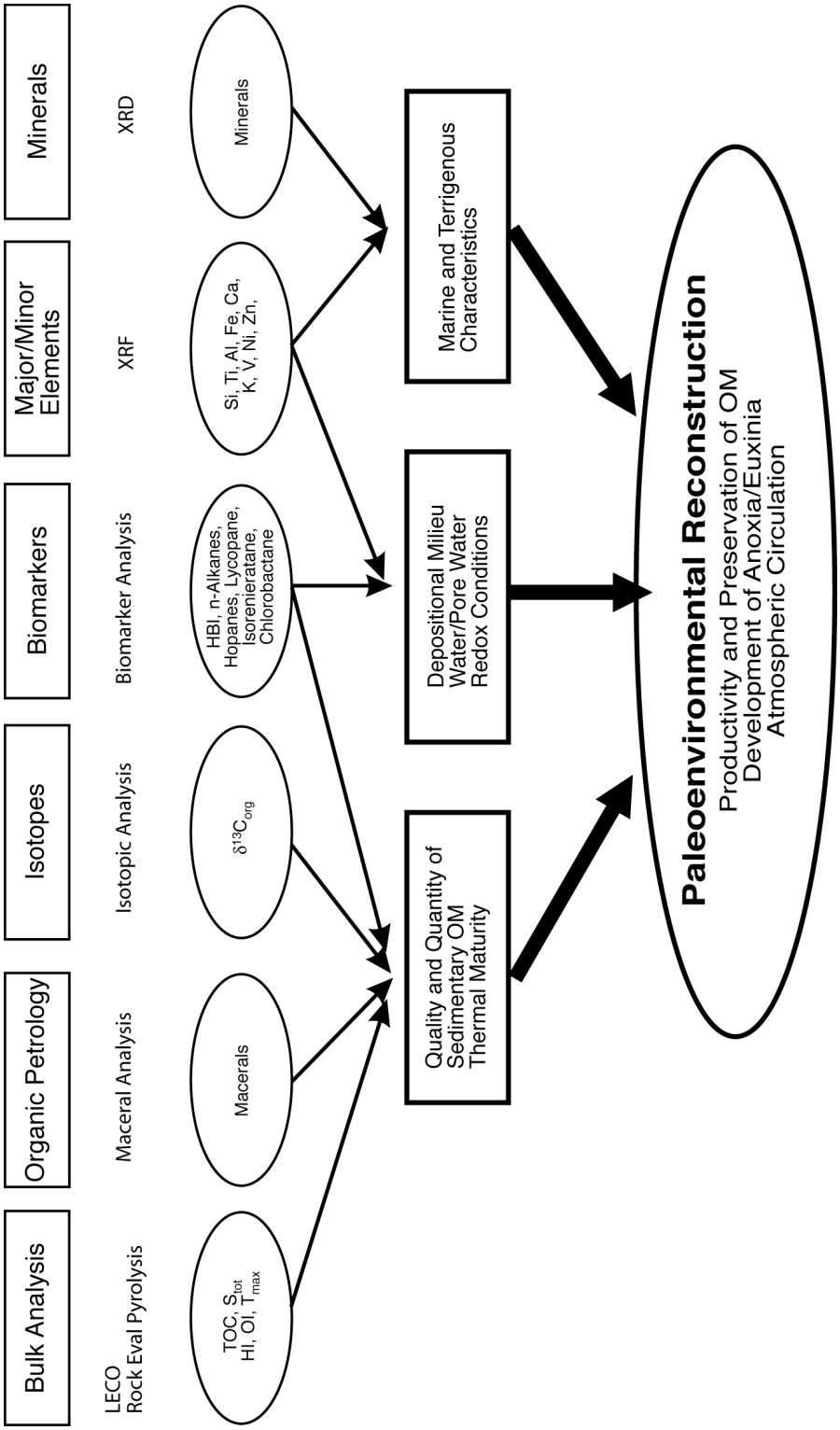

Fig. 5: Schematic flow chart for analyses of investigated black shales.

Chapter 3 (Beckmann et al., 2005) introduces ODP Site 959 as a reference section for the investigations of the linkage of OAE 3 organic sedimentation to African climate variability, offering a more detailed examination of the proposed depositional model. Marine derived OC

dominates the sediments as deduced from maceral analysis, stable carbon isotopes of OC ($\delta^{13}C_{org}$), and Rock Eval pyrolysis (hydrogen index, HI and oxygen index, OI). Relative contributions of OM from marine and minor contributions of terrigenous sources remain fairly constant across the record. Preservation conditions of OM in contrast were clearly variable as indicated by records from redox-sensitive trace elements (V, Ni, Zn) obtained by X-ray fluorescence and Fe-OC-S relationships in support of oxygen-depleted to euxinic environments with iron-limitation during times of deposition. The application of a cyclostratigraphic age model allows an identification of the temporal relationship between OC and carbonate records. Maximum black shale accumulation on average lasted for approximately 5 ka (i.e. 1/4 of a precession cycle). Based on the cyclostratigraphic time model, accumulation rates of individual compounds were calculated. Lead-lag relationships of marine and continental proxies were recognized providing robust estimates for average transient times from oxygenated to oxygen-depleted environmental conditions. The relationships suggest that marine sedimentation in the Upper Cretaceous tropical Atlantic reacted to atmospheric circulation (i.e., movement of the ITCZ) and hydrological cycling rather than drove them.

Chapter 4 (Wagner et al., 2004) further addresses the composition of primary producers and the development of photic zone euxinia in the Upper Cretaceous DIB by analysis of molecular markers. Alkenone-derived organic compounds and highly branched isoprenoids (HBI) indicate that calcareous nannoplankton and diatoms were primary producers in the DIB. Consistent with interpretatiosn from bulk geochemistry, diagnostic terrestrial biomarkers are absent. The accumulation of HBIs further indicates high nutrient levels favouring siliceous plankton production. In addition to trace metal accumulation presented in chapter 3, biomarkers for green sulphur bacteria (i.e. isorenieratane and chlorobactane) evidence extreme variations in redox conditions and intervals of photic zone euxinia (PZE). Reconstruction of the position of the chemocline using isorenieratane and chlorobactane shows that anoxic condition extended periodically into the bottom water with PZE occurring during maximum OC accumulation. Black shale deposition, however, was fostered by but not restricted to euxinic conditions in the Upper Cretaceous DIB as evident from OC-rich invervals without markers for PZE. The biomarkers records confirm that chemical boundary conditions in the ocean were as extreme as during the global OAE 2, these conditions however were likely more restricted in extend and duration. The data further propose a larger-scale belt of PZE along West Africa during main parts of the OAE 3 despite the free exchange of deep and surface water masses in the Cretaceous South Atlantic.

Chapter 5 (Beckmann et al., in press) finally discusses the impact of climate variability and river discharge on the DIB using an approx. 40m long record of marine and terrigenous proxies from ODP Site 959. The continuation of the record well into Campanian sequences allows the deduction of long-term trends and shorter-scale variations in the tropical atmosphere-ocean system. Time-frequency analyses of K/Al and OC records show the

continuity of one dominant period with approx. 1.3 cycles/m wavelength across a core gap into the lower Campanian interval. Considering the uncertainties in the available age model, this period lies close enough to 22 ka to support precessional forcing. The persistent cyclicity and accumulation pattern of climate tracers implies that black shale sedimentation was controlled by the same mechanism throughout the Upper Cretaceous. The record that has been estimated to represent 1.46 Ma based on the continuation of the cyclostratigraphic approach discussed earlier (see chapters 2 and 4) and based on the results of time-frequency analysis. It allows the detailed assessment of African climate development into the lower Campanian. Aluminium normalized terrigenous proxy data suggests a gradual aridification of Africa, while the arid proto-Kalahari remained constant in extension and geographical position. Variance records of terrigenous proxies demonstrate the existence of variable climate contrasts in tropical Atlantic region, fluctuating between strong contrast between arid and humid conditions and moderate arid-humid alternations. As river discharge is of specific interest for black shale accumulation, precession-driven runoff patterns for the DIB and adjacent areas were simulated utilizing the GCM GENESIS v. 2.0. GCM simulation yielded a pronounced wet season in spring and a dry season from July to February. Strongest seasonal contrasts in the runoff pattern were recognized when northern spring equinox occurred at perihelion (earth's closest approach to the sun). Black shale formation was restricted to phases when maximum insolation during perihelion occurred during the wet season, fostering seasonal contrasts and massive spring river discharge. The simulation provides first threshold values for river discharge to trigger a shift into the black shale mode and offers an estimation of the thickness of the resulting freshwater cap in the DIB.

Chapter 2.

A millennial- to centennial-scale record of African climate variability and organic carbon accumulation in the Coniacian–Santonian eastern tropical Atlantic (Ocean Drilling Program Site 959, off Ivory Coast and Ghana)

Peter Hofmann, Thomas Wagner, Britta Beckmann

[1] *Department of Geosciences, University of Bremen, Klagenfurter Str, 28357 Bremen, Germany*

[2] *Geological Institute, University of Cologne, Zülpicher Str. 49a, 50674 Köln, Germany*

Status: published Geology (2003), v. 31, p. 135-138

2.1 Abstract

Millennial- to centennial-scale geochemical records of Coniacian to Santonian deposits from the Deep Ivorian Basin are used to develop a model for the accumulation of black shales in equatorial regions during the final of the Cretaceous oceanic anoxic events (OAE). Proxy records from ODP Site 959 document a strong precessional signal in the occurrence of black shales, the abundance of quartz, and clay mineralogy during OAE 3. We hypothesize that this signal reflects changes in atmospheric circulation patterns, which in turn caused latitudinal shifts of continental climate belts across western Africa. Furthermore we propose that the periodic deposition of black shales occurred in response to adjustments of oceanic circulation in the Deep Ivorian Basin resulting from climate controlled fluctuations in continental runoff. A new high-resolution, cyclostratigraphic framework allowed us to estimate a rapid change—within <1000 yr—from dysoxic (background) to anoxic or euxinic (black shale) environmental conditions, followed by black shale deposition for ~10 k.y. and a gradual return to the initial dysoxic conditions. Our findings imply a highly dynamic Late Cretaceous atmosphere-ocean system.

2.2 Introduction

The importance of Cretaceous oceanic anoxic events as key mechanisms for the development of large organic carbon sinks and their relationship to rapid climate changes is widely acknowledged. The Coniacian–Santonian oceanic anoxic event (OAE 3) is thought to be the last of the Cretaceous OAEs (e.g., Arthur et al., 1990). However, compared to extensive research on the Early Cretaceous OAE 1 and middle Cretaceous OAE 2, only a few studies have addressed the evolution and associated controls on organic carbon burial during this time period (e.g., Davis et al., 1999; Erlich et al., 1999). Atmospheric circulation models (e.g., Poulsen et al., 1999; Floegel, 2002) and sea-surface temperature records of the equatorial Atlantic (e.g., Wilson and Norris: 2001; Norris et al., 2002; Wilson et al., 2002) identify low latitude regions as key areas that were subjected to and may even have triggered global climatic fluctuations on seasonal to orbital time scales during Cretaceous greenhouse periods. For the OAE 1b, Erbacher et al. (2001) demonstrated that increased continental runoff is one process that affected marine black shale formation. They presented stable isotope data from Ocean Drilling Program (ODP) Site 1049 in the western subtropical Atlantic indicating that processes leading to the elevated organic carbon burial were similar to those that led to the Pliocene–Pleistocene Mediterranean sapropels (Emeis et al., 2000), thereby closely linking continental climate variability to marine organic sedimentation.

In this study we present geochemical evidence for orbitally forced climate variability in Africa, which caused extensive but short-term carbon sequestration in the adjacent Deep Ivorian Basin. Millennial- to centennial-scale proxy records of marine sedimentation (total organic carbon, TOC) and continental supply (Si, K, Al) from ODP Site 959 link regional African climate development and organic carbon burial, i.e., black shale development in the sheltered Deep Ivorian Basin. The results yield new insight into the controls on organic carbon burial in Late Cretaceous equatorial regions and the rate of change between depositional modes; the results also provide a high-resolution framework to test annual- to precession-scale climate predictions as derived from Late Cretaceous general circulation models.

2.3 Samples and methods

Recent studies have shown that extensive black shale deposition occurred in the Deep Ivorian Basin from Turonian to Campanian time (Wagner and Pletsch, 1999; Wagner, 2002). The most complete record of black shale accumulation during OAE 3 was encountered at ODP Site 959 (Fig. 1). Sedimentological and paleontological studies have already indicated that black shale deposition followed a highly cyclic pattern during the Coniacian to Santonian interval (Pletsch et al., 2001). This interval is characterized by average sedimentation rates of up to 15 m/m.y., providing an excellent base for a high-resolution time study (millennial

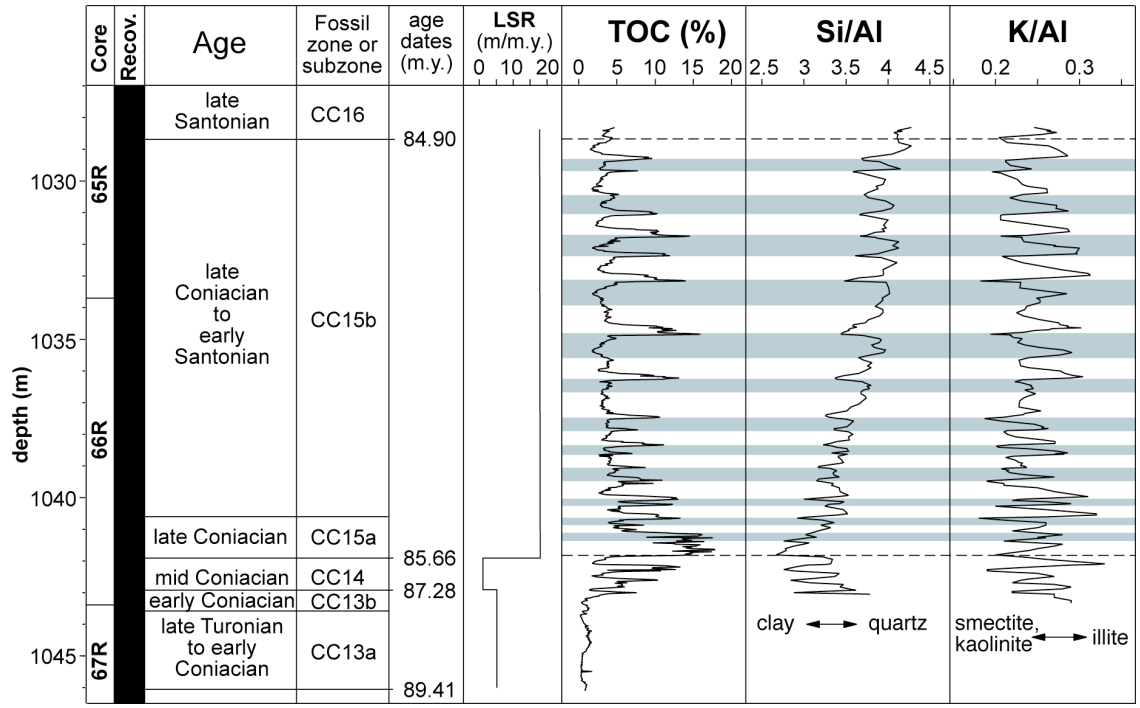

Fig. 1: Profiles of cyclic fluctuations of total organic carbon (TOC), Si/Al, and K/Al with depth for nannofossil zones CC 14 and CC 15. Minima in Si/Al and K/Al ratios generally coincide with maxima in organic carbon deposition. Ages and nannofossil zones and subzones from Watkins et al. (1998); linear sedimentation rates (LSR) were calculated from age dates provided by Hardenbol et al. (1998). Recovery (Recov.) for cores 65 and 66 was 100%.

scale, Fig. 1). Cores 959D-65R and 959D-66R were sampled at 1 cm increments. To measure oceanic productivity, TOC analyses were conducted on every other sample with a LECO instrument to provide an average 1250 yr time resolution for biozone CC 15. Major element chemistry was used to trace climate variability via changes in sediment composition, because distinct source areas can be discriminated by variations in the abundance of quartz and illite versus clay-mineral content (smectite, kaolinite, illite; Wagner and Pletsch, 1999). The chemical composition of the sedimentary rocks was determined by X-ray fluorescence analysis on samples with an average spacing of 5 cm.

2.4 Results and discussion

2.4.1 Record of high-frequency cycles at ODP Site 959

Organic carbon and aluminum-normalized element records for Site 959 clearly document cyclical variations in sediment composition for nannofossil zones CC 14 through CC 15 (Fig. 1). Organic carbon content ranges from minimum values between 2 and 5% to maximum values between 7 and 17% TOC. Hydrogen indices from 180 to 620 mg HC per gram of TOC in combination with visual inspection of sedimentary organic matter demonstrated a dominantly marine origin for the bulk organic matter (Wagner and Pletsch,

1999). TOC cycles were, therefore, caused by fluctuations in productivity and/or preservation. Si/Al ratios reach a minimum at the transition from nannofossil zone CC 14 to CC 15 and show a gradual increase from the base to the top of CC 15. Superimposed on this long-term trend are pronounced cyclic fluctuations of the Si/Al ratios with variable amplitudes. K/Al ratios range from 0.17 to 0.32 and fluctuate around a mean value of ~0.25%. Minima in Si/Al and K/Al ratios coincide strikingly with black shale deposition.

On a low-resolution scale Wagner and Pletsch (1999) have shown that the silicate content for the Coniacian to Santonian interval of Site 959 is controlled by the abundance of quartz, smectite, illite, and kaolinite. Biogenic silica (e.g., opal from radiolaria and diatoms) is generally absent. Si/Al and K/Al ratios, therefore, reflect temporal fluctuations in the delivery of quartz and illite vs. smectite and kaolinite to the Deep Ivorian Basin. Current climate simulation models (DeConto et al., 1999) and geologic data (Maley, 1996) suggest the presence of distinct climate belts across the African continent during Late Cretaceous time. Extensive areas in southern parts of Africa were characterized by arid climates with desert-like conditions and sparse vegetation. Bauxite, laterite, and coal deposits in areas surrounding the equatorial western African margin indicate tropical conditions with intense weathering and a dense vegetation cover (Scotese, 1997; DeConto et al., 1999). These contrasting climate belts in tropical and Southern Hemisphere subtropical Africa were separated by a zone of prairie to shrub land, which received low to intermediate amounts of precipitation (DeConto et al., 1999). The cofluctuation of quartz and illite, and smectite and kaolinite at Site 959 documents changing sediment supply from either desert (southern) or tropical (northern) source areas. The observed alternation of dominant source areas during each depositional cycle indicates that transport mechanisms controlling the delivery of sediment components to the southern slope of the Deep Ivorian Basin shifted consistently in the same manner throughout the Coniacian–Santonian OAE 3.

We interpret the observed cyclic input pattern to document the repetitive and rapid latitudinal displacement of the paleo–intertropical convergence zone (ITCZ) and the African climate belts in the Southern Hemisphere (Fig. 2). As a result of the prominent fluctuations in low-latitude atmospheric pressure systems, we propose that the southeasterly trade winds reached the DIB when the paleo-ITCZ moved northward to somewhere in northern to central Africa or decreased in strength as the paleo-ITCZ moved south. In conjunction with these dynamic changes in atmospheric circulation, marine and terrigenous bulk-sediment-accumulation rates fluctuated drastically throughout time to produce the observed sedimentary cyclicity at Site 959.

The mechanisms that operated during the black shale mode (when the ITCZ was at its southern position) promoted periods of high precipitation and excess continental runoff from extensive laterite deposits. The resulting freshwater supply from tropical areas enhanced the availability of dissolved nutrients and may have temporarily induced estuarine circulation in the semi-enclosed basin, thus sustaining black shale formation. In contrast, a more northern

position of the ITCZ is thought to have enabled the southeasterly trade wind system to extend far enough north to approach the Ivory Coast region, which both increased the transport of dust from southern latitudes to the Deep Ivorian Basin and also caused generally dryer conditions over the equatorial regions of western Africa. This interpretation is supported by general circulation models for the Cenomanian–Turonian that identify fluctuations in the trade-wind system to be essential for the precipitation balance over western Africa (Poulsen et al., 1999; Floegel, 2002) on both seasonal and precessional time scales. Park and Oglesby (1991) further demonstrated that the evaporation-precipitation balance of the South Atlantic on longer time scales was sensitive to precession forcing.

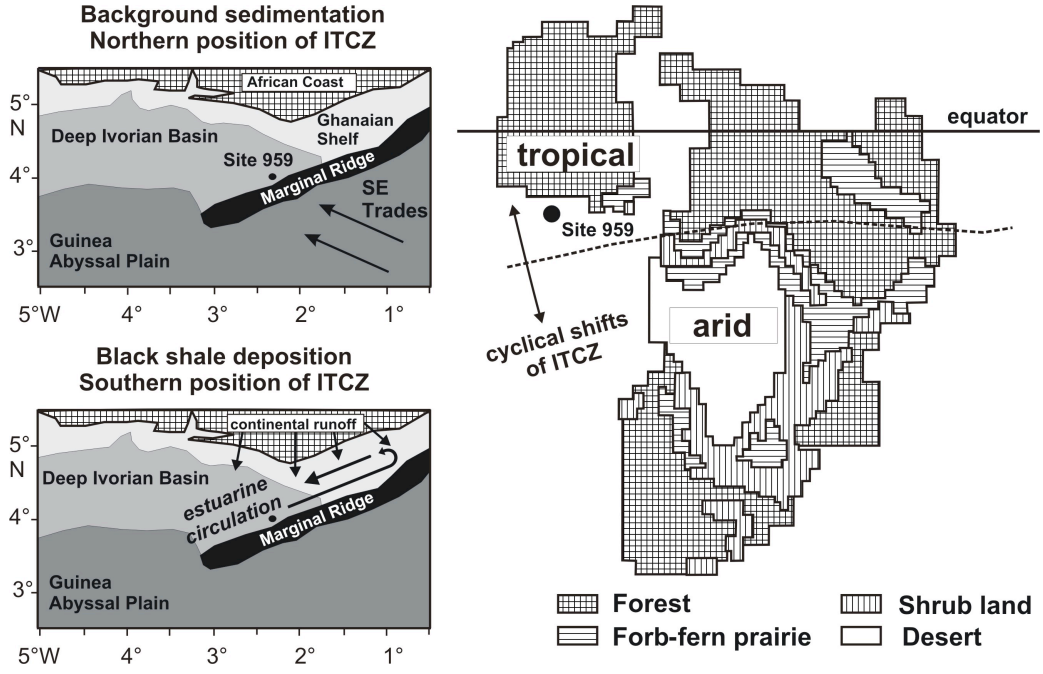

Fig. 2: African climate belts modeled for Campanian with GENESIS-EVE (DeConto et al., 1999) are characterized by tropical forests along paleoequator and shrub land and desert in southern Africa. Repetitive latitudinal displacement of paleo-intertropical convergence zone (ITCZ) and African climate belts is thought to have influenced sedimentation patterns at Site 959. Dominant atmospheric processes at Site 959 during background sedimentation of organic carbon (northern position of paleo-ITCZ) transport material from arid, southern source areas toward Site 959 via southeasterly trade winds. During black shale deposition (southern position of paleo-ITCZ), sediment from tropical areas was delivered via continental runoff to Site 959. The expected associated freshwater input to the DIB enhanced the nutrient supply and is hypothesized to have induced estuarine circulation.

2.4.2 Orbital control of the cycle pattern of CC15

A major feature of the Cretaceous sedimentary record is cyclic bedding rhythms that display periodicities in the Milankovitch frequency band (e.g., Dean et al., 1984; Kuhnt et al.,

1997, 2001). Results from climate-simulation models (e.g., Park and Oglesby, 1991) and sedimentary bedding rhythms (e.g., Herbert et al., 1999) provide evidence for orbital forcing that was mainly controlled by precession in the Cretaceous South Atlantic. Accordingly, we interpreted the cycle pattern of Site 959 to reflect orbital forcing and conducted orbital tuning for biozone CC 15. CC 15 spans from 85.7 to 84.9 Ma and thus represents 0.76 m.y. (Hardenbol et al., 1998). Biostratigraphic studies confirm the presence of nannofossil subzones CC 15a and CC 15b (Watkins et al., 1998), suggesting a complete record.

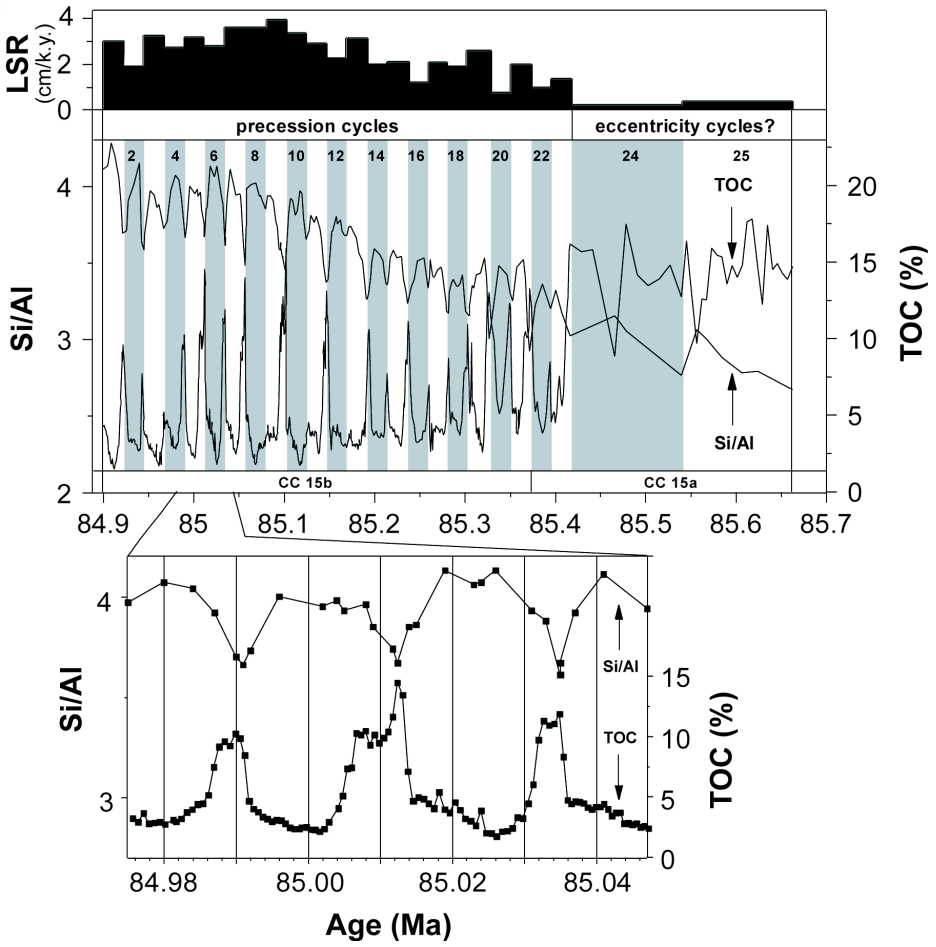

Fig. 3: Si/Al and TOC record of nannofossil zone CC 15 in time framework developed by orbital tuning of Si/Al record. Minima of Si/Al were selected as cycle boundaries. CC 15 is interpreted to be represented by 23 precession cycles and 2 cycles which were tentatively assigned to eccentricity. Total duration estimated for biozone CC 15 based on this tuning model is 763 k.y., which is consistent with data from Hardenbol et al. (1998). Note cores 65R and 66R were rotary drilled. However, K/Al and Si/Al cycle patterns provide no evidence for lost section due to drilling. Uncertainty in the exact depth assignment of the CC 15 to CC 16 boundary is estimated to change the time model by less than one precession cycle. For uncertainties in the assignment of the time content of cycles 24 and 25 see text. Linear sedimentation rates (LSR) for each individual cycle were derived from the tuning model.

Orbital tuning was conducted for the terrigenous proxies Si/Al and K/Al indicative of African climate dynamics. Minima in the Si/Al ratio were chosen as cycle boundaries, as they coincide with minima in the K/Al record and generally correspond to TOC maxima. The

results of using this approach indicate that CC 15b contains 21 cycles and 15a contains 4 cycles (Fig. 3). To match the total expected duration of 760 k.y. for CC 15, cycles 1 to 23 (Fig. 3) were interpreted to record 22.481 k.y., the characteristic precession cycle length for the Late Cretaceous (e.g., Berger et al., 1992) resulting in a time content of 517 k.y. Cycles 24 and 25 of the Si/Al record show do not show the same pattern for the TOC record as cycles 1 to 23. A condensed interval characterized by low sedimentation rates for Si/Al cycles 24 and 25 is suggested by the overall decrease in linear sedimentation rate from cycle 9 to 23 (Fig. 3) and the low linear sedimentation rate of 0.072 cm/k.y. for CC 14 (Fig. 1). We speculate that if CC 15 is completely preserved cycles 24 and 25 may represent precession cycles with a periodicity of 123 k.y. The time content of biozone CC 15 based on this tuning model is 763 k.y.

2.4.3 Time relationships for input variation within the depositional model

The fine time resolution allows the assessment of the speed of climate change and the associated oceanographic response for biozone CC 15b. Minima in Si/Al and K/Al closely correspond to the TOC maxima in each precession cycle (Fig. 3), whereas maxima in Si/Al and K/Al precede the following TOC maximum on average by ~8800 and ~17,300 yr, respectively. This phase relationship supports the interpretation that an enhanced supply of material from arid regions did not stimulate organic matter accumulation, i.e., the oceanographic response, but is clearly linked to the input from tropical African regions. Increasing runoff probably enhanced the nutrient supply and may have induced estuarine circulation in the DIB.

Furthermore, individual organic carbon peaks display a distinct asymmetry, showing a rapid initial rise in TOC followed by a gradual return to the original level. The transition from the background mode to the black shale depositional mode required on average 4000 yr, but also occurred in <1000 yr (e.g., cycles 9 and 10, Fig. 3). The gradual return to the background depositional mode lasted ~6000 yr. The observed timing across individual organic matter peaks is not an artifact of the cycle boundary selection, as demonstrated by time relationships for cycles with identical LSR (cycles 7 and 8; Fig. 3). Shifts in sedimentation rate across individual precession cycles, however, could alter the results and cannot be ruled out. Our observations of the OAE 3 dynamics in the tropical Atlantic indicate a rapidly changing ocean-atmosphere system and corroborate Cretaceous OAE findings by other workers who have consistently proposed short-term climate change during greenhouse periods (e.g., Cotillon et al., 2000; Kuhnt et al., 2001; Wilson and Norris, 2001).

2.5 Conclusions and implications

In the tropical Atlantic, the time period corresponding to the Coniacian–Santonian OAE 3 is documented by a periodic rather than a constant phase of black shale sedimentation. The deposition of black shale cycles in biozone CC 15 consisted of ~10-k.y.-long periods of black shale sedimentation followed by ~12-k.y.-long periods of background sedimentation. In the Coniacian–Santonian tropical Atlantic, atmospheric circulation apparently triggered marine black shale sedimentation as a response to orbitally forced shifts in continental climate belts. The proposed mechanism for black shale sedimentation off equatorial western Africa is climate controlled fluctuation in continental runoff, which is comparable to the scenario for sapropel formation in the Pliocene–Pleistocene Mediterranean (e.g., Emeis et al., 2000) and in the Early Cretaceous North Atlantic (OAE 1B, Erbacher et al., 2001). Our depositional model predicts the behavior of key climate elements of the equatorial Atlantic (wind system, evaporation-precipitation balance, position of the ITCZ), which can then be used to test climate circulation models for this time period and define the natural behavior of the planet during ancient counterparts of the present-day climate change. More generally, our records provide new geological evidence in support of the concept of a dynamic "greenhouse climate system" with an enhanced hydrological cycle operating in equatorial regions during the mid-Cretaceous (Wilson et al., 2002).

2.6 Acknowledgements

This study was funded by the Deutsche Forschungsgemeinschaft (Ocean Drilling Program, grant Wa1036/7 and Ho2188/1). Reviews by K. L. Bice and P. A. Wilson helped to improve the manuscript.

Chapter 3.

Linking Coniacian-Santonian (OAE3) black shale deposition to African climate variability: a reference section from the eastern tropical Atlantic at orbital time scales (ODP Site 959, off Ivory Coast and Ghana)

Britta Beckmann[1], Thomas Wagner[1], and Peter Hofmann[2]

[1] *Department of Geosciences, University of Bremen, Klagenfurter Str, 28357 Bremen, Germany*

[2] *Geological Institute, University of Cologne, Zülpicher Str. 49a, 50674 Köln, Germany*

Status: published SEPM Special Publication No. 82, p. 125-143

3.1 Abstract

Black-shale cycles deposited in the Late Cretaceous tropical Atlantic at ODP Site 959 were analyzed to reconstruct processes for organic-matter sequestration during the Coniacian-Santonian "oceanic anoxic event" (OAE3). The results from bulk organic and inorganic geochemistry suggest that black-shale accumulation was intimately linked to orbitally forced cycles in the Deep Ivorian Basin (DIB) that alternated between eutrophic conditions stimulating organic-walled plankton productivity followed by less trophic conditions associated with calcareous production. Results from Rock Eval Pyrolysis, bulk $\delta^{13}C_{org}$ analysis, and maceral analysis demonstrate a dominantly marine origin of the organic matter (OM) with only a subordinate proportion from terrestrial sources. Intervals of high organic carbon (OC) accumulation display high hydrogen indices (HI) up to 720 mg HC/g OC, low oxygen indices (OI) of 20 mg CO_2/g OC, and bulk $\delta^{13}C_{org}$ varying between –28 to –26.5‰. The enrichment in redox-sensitive trace metals up to 2500 µg/g for vanadium, for example, as well as carbon-sulfur relationships in black shale intervals suggest intermittently anoxic conditions, on occasion as extreme as during the Cenomanian-Turonian OAE2. We propose that the black-shale cycles were directly linked to the climate development in equatorial Africa via the hydrological cycle. The mechanism for carbon sequestration that operated in the DIB may have worked in a similar way in other equatorial regions of Africa and South America, implying that the tropics acted as a prominent sink for OC, and consequently atmospheric CO_2, during the Coniacian-Santonian OAE3.

3.2 Introduction

There is increasing evidence from marine proxy records that tropical regions during the late Cretaceous were hotter than previously reported (Huber et al., 2002; Norris et al., 2002; Wilson et al., 2002) and far exceeded modern average temperatures. Tropical sea-surface temperatures in the range of 32-36°C apparently lasted from the latest Cenomanian to the early Campanian (Huber et al., 2002). A fundamental consequence of superheated Cretaceous tropics is a vigorous hydrological cycle operating in equatorial regions. Geological evidence supporting an enhanced hydrological cycle during the late Cretaceous hothouse period was recently reported for ODP Site 959 (Fig. 1) from the Deep Ivorian Basin (DIB) off equatorial West Africa (Hofmann et al., 2003). Millennial-scale marine and terrigenous proxy records from that site document short-term environmental variability during the Coniacian-Santonian and imply orbital controls on climate development. These results support other recent studies that emphasized the importance of the tropics in driving global ocean-atmosphere circulation during peak greenhouse conditions, and stressed astronomically driven long-term climate control (Park and Oglesby, 1991; Dean and Arthur, 1998; Poulsen et al., 1999; Flögel, 2001; Norris et al., 2002; Otto-Bliesner et al., 2002; Wilson et al., 2002).

Hofmann et al. (2003) suggested a direct link between low-latitude continental climate variability and marine black-shale formation during Oceanic Anoxic Event 3 (OAE3) for the tropical South Atlantic (off Ivory Coast and Ghana). Accordingly, tropical atmospheric and oceanic circulation about 85 million years ago were intimately linked via insolation-driven changes in continental precipitation and runoff that may have forced a local reversal in ocean circulation, water-mass stratification, progressive oxygen deficiency, and, finally, enhanced organic-carbon (OC) burial. This mechanism could explain enhanced carbon storage in tropical regions during hothouse conditions and hence enforced removal of CO_2 from the atmosphere, thereby reducing concentration of greenhouse gases, and, ultimately, initiating a longer-term cooling trend. However, the processes and driving forces that link the atmospheric component of the climate system to its oceanic expression in tropical regions are still poorly understood and need more detailed examination. The suggested mechanism for carbon burial may have important implications for the global carbon budget, considering that many OC-rich OAE3 sections are reported from the low latitudes, e.g., La Luna Formation Venezuela, DIB, Brasilian Marginal Basins, and Angola Basin (e.g., Mello et al., 1995; Davis et al., 1999; Erlich et al., 1999; Wagner and Pletsch, 1999).

Geological climate data (e.g., Maley, 1996; Scotese, 1997) and recent climate simulation models (e.g. DeConto et al., 1999; Flögel, 2001) suggest the presence of distinct climate belts across continental Africa during the late Cretaceous (Fig. 2). Accordingly, large areas in southern Africa were characterized by arid climate with desert-like conditions, representing a type of Mega-Proto-Kalahari that extended between about 15and 40° S (DeConto et al., 1999). Bauxite, laterite, and coal deposits, in contrast, surrounded the

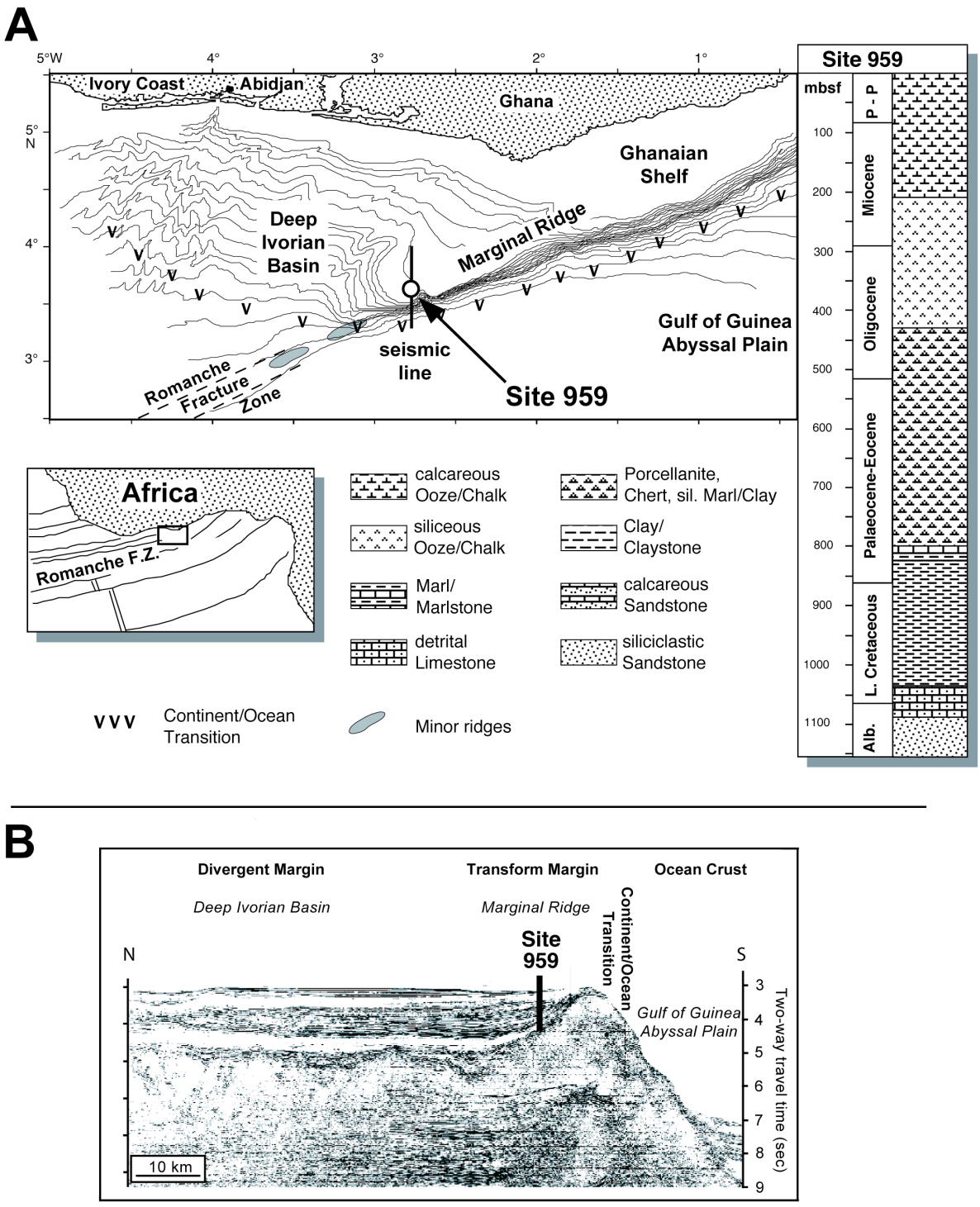

Fig. 1: (a) Location, stratigraphy, and generalized lithology of Site 959 (modified from Pletsch et al., 2001), **(b)** Migrated multichannel seismic line across the CIGTM and the Deep Ivorian Basin (from Mascle et al. 1996).

equatorial, tropical belt with intense weathering and dense vegetation (Scotese, 1997). These contrasting climate and vegetation zones in continental Africa were separated by a relatively narrow sector of prairie to shrub land that received low to intermediate amounts of precipitation (DeConto et al., 1999).

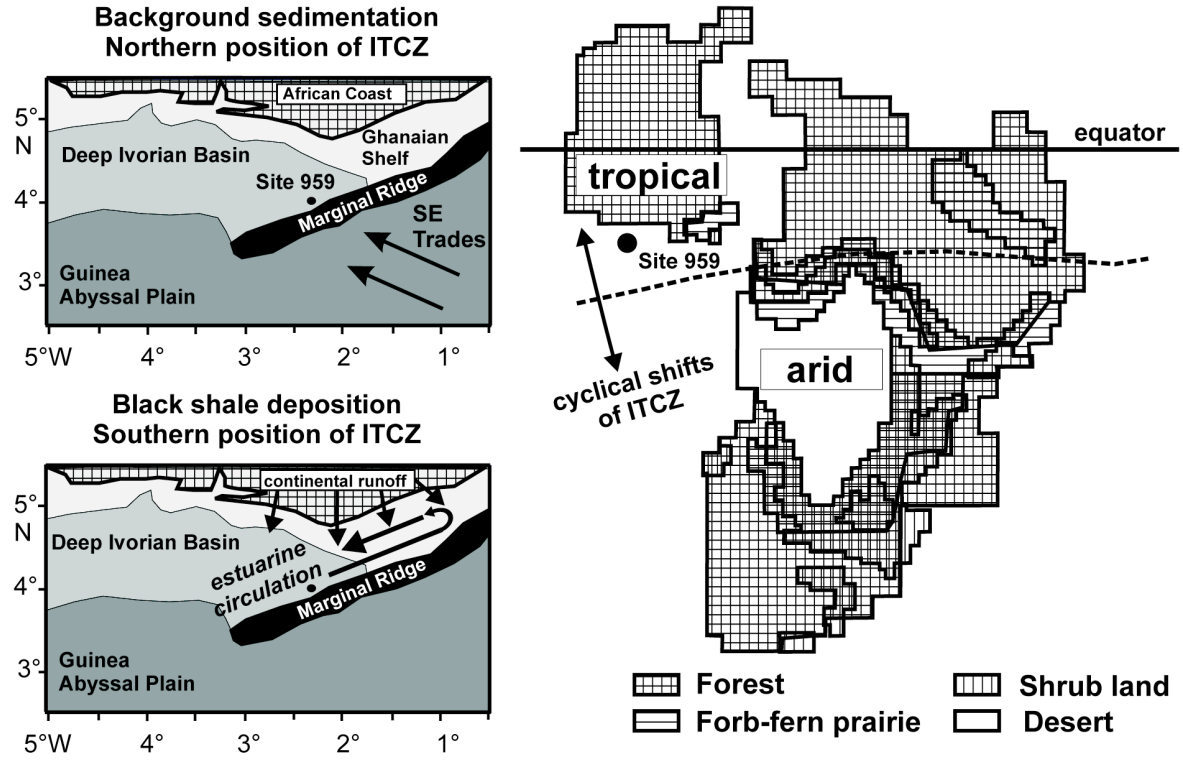

Fig. 2: Depositional model for the upper Cretaceous Deep Ivorian Basin (DIB) as proposed by Hofmann et al. (2003). Shrub land and desert in southern Africa and tropical forests along the paleo-equator characterize Campanian African climate belts (modeled with GENESIS-EVE, DeConto et al. 1999). The repetitive latitudinal displacement of the Upper Cretaceous Intertropical Convergence Zone (ITCZ) and African climate belts is thought to have triggered the sedimentation pattern at Site 959. Enhanced southeasterly trade winds during OC-lean background depositional conditions (ITCZ at its northern position) transported dust from southern, arid African source regions towards Site 959. During black shale deposition (southern position of the ITCZ), huge amounts of sediment from tropical African source areas were delivered via continental run-off towards the DIB. The expected associated freshwater input to the DIB is hypothesized to have enhanced nutrient supply and induced estuarine circulation.

Hofmann et al. (2003) showed that the sedimentary record at ODP Site 959 is characterized by periodically fluctuating Si/Al and K/Al ratios, and OC content documenting two principal depositional modes. These are (1) a black-.shale mode with elevated OC levels (up to 18%) which are closely corresponded by minima in the Si/Al and K/Al ratios, and (2) a background mode where OC content varies between 2% and 4%, accompanied by elevated Si/Al and K/Al ratios. The fluctuation in Si/Al and K/Al ratios is determined by the abundance of quartz, illite, smectite, and kaolinite (Wagner and Pletsch, 1999; Pletsch et al., 2001), whereas biogenic silica is, on the basis of smear-slide analyses from Site 959, generally absent (Mascle et al., 1996). Kaolinite and smectite are products of intense tropical weathering, whereas quartz and illite can be attributed to more arid source regions dominated by physical weathering processes (Hofmann et al., 2003). Cyclic variations in Si/Al and K/Al ratios, therefore, document fluctuating supply from different continental source areas, i.e., a tropical low-latitude area and a higher latitude arid area (Fig. 2). On the basis of these

assumptions it was hypothesized that the input from the respective source areas to the DIB was controlled by shifts in the position of the Intertropical Convergence Zone (ITCZ). The modern and probably also the Cretaceous ITCZ marks a narrow belt where the trade winds of the Northern and Southern Hemisphere converge, characterized by heavy rainfall and generally west- and equator-bound wind directions. Latitudinal variation in the position of the ITCZ on seasonal to orbital time scales directly affects precipitation in the related areas (e.g., pronounced monsoon during boreal summer over today's southeastern Asia), leading to a rhythmic succession of drier and wetter climate periods over western Africa and the adjacent eastern tropical Atlantic. Hofmann et al. (2003) considered a similar mechanism for the late Cretaceous DIB. They propose that southeasterly trade winds approached the DIB when the ITCZ was located in a northern position, equivalent to the modern boreal summer configuration. The trade winds transported dust from southern African source areas northwards into the eastern Equatorial Atlantic. This situation changed significantly when the ITCZ shifted towards a more southern position, equivalent to the modern boreal winter configuration, resulting in a weakened influence of the dust-loaded southeasterly trades on the sediment supply to the DIB but a much stronger supply from tropical African regions with their vigorous monsoonal climate (Fig. 2). Black-shale deposition was confined to the latter configuration, when huge amounts of sediment, nutrients, and freshwater from tropical areas were drained into the DIB. The onset of continental runoff and the associated freshwater influx with enhanced nutrient supply to the DIB is thought to have induced an estuarine circulation in the DIB. Intervals with enhanced sediment supply from tropical regions are indicated by a high supply of kaolinite and smectite to the DIB (e.g., minima in the Si/Al and K/Al curves) whereas intervals with high Si/Al and K/Al ratios and relatively low OC content on the other hand are indicative of a stronger influence of the southeasterly trade-wind system and represent generally drier conditions in the DIB region.

The aim of this study is to further examine the consequences of climate fluctuations for marine sedimentation in the DIB. We discuss the sources of OC and their respective contributions to black-shale formation in the DIB, together with the processes that controlled carbonate and OC productivity and burial and the development of bottom-water anoxia in the DIB.

3.3 Geological setting and lithology

ODP Site 959 was drilled on a small plateau on the southern shoulder of the DIB, at 2102 m water depth (Fig. 1; Mascle et al., 1996). The DIB is a semi-sheltered basin whose formation is closely related to the development of the opening Equatorial Atlantic Gateway. The Côte d'Ivoire Ghana Transform Margin has resulted from major transform motions between plate boundaries of the South American and African continents during the formation of the equatorial Atlantic, and represents the continuation of the oceanic Romanche Fracture Zone

onto continental crust (Pickett and Allerton, 1998). Cretaceous sedimentation at Site 959 was closely related to the tectonic evolution of the margin (Wagner and Pletsch, 1999; Pletsch et al., 2001; Wagner, 2002). Deposition of black-shales commenced in the Turonian when margin differentiation started and continuous subsidence generated a semi-enclosed sub-basin. Continuous deposition of OC-rich sediments lasted from the Turonian throughout the Danian, when fully open ocean conditions were finally established (Wagner and Pletsch, 1999). Peak black-shale deposition took place during the Coniacian and Santonian, a time period corresponding to OAE3 (Arthur et al., 1990), which has also been recognized for its OC-rich strata in the basins surrounding the Atlantic Margins (e.g. Dean et al., 1984; Mello et al., 1995; Davis et al., 1999; Erlich et al., 1999; Holbourn et al., 1999; Holtar and Forsberg, 2000; Schoellkopf and Patterson, 2000).

The late Turonian to late Santonian section at Site 959 consists mainly of carbonate-poor gray to black claystones and carbonate-rich, light gray nannofossil claystones (Fig. 3). The lower part of the profile (1044 to 1038.5 mbsf) exhibits several hardgrounds and contains various layers of phosphate clasts representing periods of reduced sediment accumulation. The duration of these periods of reduced sedimentation is difficult assess, but the consistency and persistence of the cyclic pattern observed in all proxy records suggest that periods of hardground formation were short and apparently did not hamper the formation of a continuous sedimentary record during the late Coniacian to early Santonian nannofossil zone CC15. Pyrite occurs throughout the analyzed interval, either dispersely distributed within the sediment or as pyrite clasts. Bioturbation is common and can occur as distinct burrows even within laminated strata (Fig. 3). X-ray diffraction analyses by Pletsch et al. (2001) reveal a clay-mineral assemblage in the Coniacian–Santonian sediments from Site 959 consisting of dominantly smectite with minor amounts of illite and kaolinite; chlorite is present only below 1040.5 mbsf.

Holbourn et al. (1999) attributed outer-shelf or upper-slope conditions to the deposits, on the basis of their analysis of benthic foraminifera assemblages. A general deepening trend of Site 959 is documented in the shift to middle bathyal to lower bathyal foraminifera assemblages around 1030.5 mbsf (Fig. 3).

3.4 Material, methods, and chronology

Samples from ODP Leg 159, Site 959D cores 65W-66W were taken continuously at 1 cm increments at the Bremen Core Repository. Samples were split, dried at 35°C, except for microscope samples, and homogenized prior to analysis. Determination of OC and totalsulfur (S_{tot}) content was performed after removal of inorganic carbon with 0.25 N HCl, using a LECO CS-300 carbon-sulfur analyzer on every other sample. Rock-Eval pyrolysis (hydrogen index, HI; oxygen index; OI) of selected bulk sediments was conducted on a Rock-Eval 6 with S3, following the procedures outlined by Espitalié et al. (1977). The average spacing of

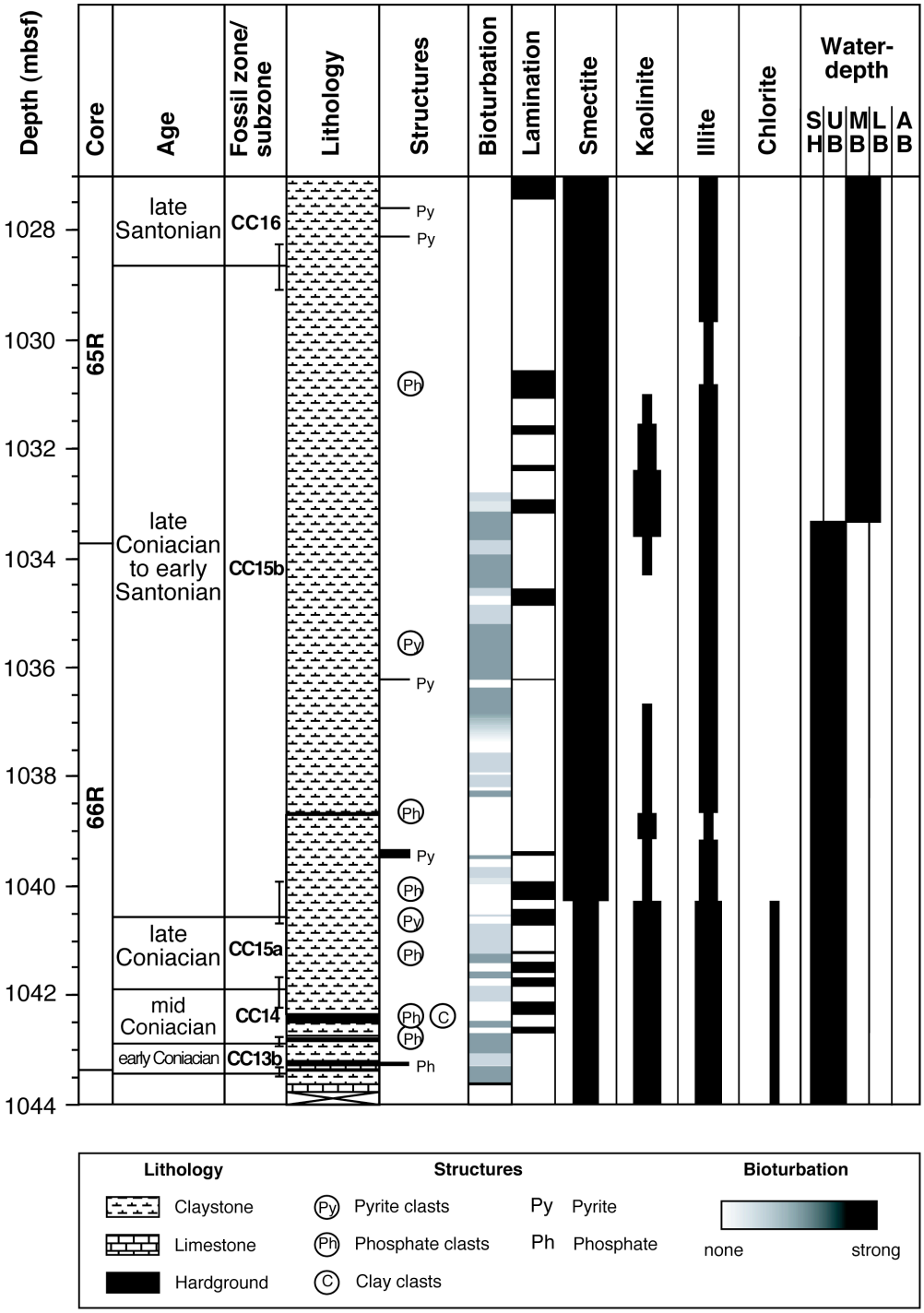

Fig. 3: Generalized lithology including sediment structures, bioturbation, and lamination for nannofossil between 1027 and 1044 mbsf. Ages, nannofossil zones, and uncertainties in the assignment of biozone boundaries according to Watkins et al. (1998), clay mineral content (smectite, kaolinite, illite, and chlorite) from Pletsch et al. (2001). Width of bars for clay minerals relates to estimated quantity. Water depth from Holbourn et al. (1999); SH: shelf, neritic; UB: upper bathyal; MB: middle bathyal; LB: lower bathyal; AB: abyssal.

samples for Rock-Eval analysis was 2 cm for intervals with high OC content and approximately every 8 cm for intervals with low OC content.

Major-element chemistry was determined by X-ray fluorescence analysis on samples with average spacing of every 6 cm, following the procedure outlined by Hofmann et al. (2001). Maceral composition was studied on selected polished blocks, using a Zeiss Axiophot microscope equipped with incident white and ultraviolet light. Stable carbon isotope ratios of OC ($\delta^{13}C_{org}$) were measured on decalcified samples. After combustion at 1050°C, the resulting CO_2 was trapped and analyzed with a Finnigan MAT Delta E mass spectrometer. All $\delta^{13}C_{org}$ values are reported relative to the V-PDB standard. Tabulated data of this manuscript is available at http://www.pangaea.de/PangaVista2?query=beckmannb.

The Coniacian-Santonian interval between 1044 and 1027 mbsf covers nannofossil biozones CC13b to CC16 (Fig. 3; Watkins et al., 1998). Watkins et al. (1998) assigned sample 65R3W144-146 to biozone CC16 and sample 65R4W77-79 to biozone CC15 (maximum uncertainty in depth assignment is 85 cm); sample 66R6W47-50 is the first of biozone CC15 and sample 66R6W104-106 is the last sample attributed to biozone CC14 (maximum uncertainty in depth assignment is 57 cm). Our boundaries for biozones CC16/CC15 and CC15/CC14 were placed in samples 65R4W32-33 (last sample CC15) and 66R6W62-63 (first sample CC15), both lying well within the uncertainty presented by Watkins et al. (1998). We assigned chronological ages to the respective boundaries following the absolute age dates presented by Hardenbol et al. (1998). They give dates for the transition of CC16/CC15 (84.9 Ma) and CC15/CC14 (85.66 Ma), but they do not provide any error for these absolute ages, which, however, may well be in the order of a few hundred thousand years. Applying the outlined age model, average linear sedimentation rates (LSR) in biozone CC15 are 17.4 m/Myr. If the largest and smallest depth intervals defined by the uncertainties of the CC16/CC15 and CC15/CC14 boundaries are applied, average LSR increase to 18.4 m/Myr or decrease to 16.6 m/Myr, respectively.

In order to be able to compare the record at Site 959 of the DIB with other depositional settings, selected data were converted into accumulation rates. We used the time model for CC15 by Hofmann et al. (2003), who interpreted cycles 1-23 as precession cycles (~ 22.5 kyr) and cycles 24 and 25 as eccentricity cycles (~123 kyr; Fig. 4). The justification for the interpretation as precession cycles comes from climate simulation experiments which clearly show that precessional forcing is the dominant motor for climate cycles in the late Cretaceous South Atlantic (e.g., Park and Oglesby, 1991; Flögel, 2001). The time span covered by CC15 is in the order of 0.76 Myr (Hardenbol et al., 1998). The 25 cycles of CC15 at Site 959 cannot account for that length of time if all cycles are interpreted to be precession cycles (Fig. 4). We therefore assume that cycles 24 and 25 represent eccentricity cycles to approach the actual duration of CC15. This interpretation suggests low sedimentation rates for the basal part of CC15a (cycles 24 and 25, Figure 4), which is in good agreement with the low sedimentation rates recorded for the underlying nannofossil zone CC14. In addition, e.g., the OC curve shows a clear shift in the accumulation pattern after cycles 24 and 25, which may be a result of the gradual increase in sedimentation rate from this point on.

Linear sedimentation rates (LSR) were calculated according to

LSR[m/Myr] = (depth 2 [mbsf] – depth 1 [mbsf])/cycle duration [kyr] * 1000

Accumulation rates (AR) for individual components were calculated according to Van Andel et al. (1975) and Müller and Suess (1979):

AR_{comp} [g/m^2/yr] = LSR [cm/kyr] * DBD [g/cm^3] * Comp [wt%]/10

where Comp is weight percent of component and DBD is dry bulk density, calculated according to:

DBD [g/cm^3] = TOC [%]/100 * 1.1[g/cm^3]
+ (100 – TOC [%]) * 2.1[g/cm^3]/100

1.1 [g/cm^3] is the average density of organic carbon (Stach et al., 1982); 2.1 [g/cm^3] is the average sediment density (from Mascle et al. 1996).

3.5 Results and discussion

3.5.1 Pattern of geochemical cycles at Site 959

Among other data, the records of OC as well as the Si/Al and K/Al ratios display a pronounced and consistent cycle pattern throughout nannofossil zone CC15 (Fig. 4). Cycle boundaries are defined by minima in the Si/Al and K/Al record, which generally correspond to maxima in the OC record. However, if the cycle pattern of Si/Al and K/Al is compared to OC in detail it is evident that some OC peaks expected from the Si/Al pattern are not developed. Notably, the transitions between cycles 8/9, 10/11, and 12/13 exhibit no maxima in OC (Fig. 4), which excludes the use of the OC record to define cycle boundaries. Compared to OC, carbonate reveals a less distinct cyclic pattern. The shortest cycle (cycle 20) spans 16 cm, and the longest cycle (cycle 9), 86 cm. Cycles in the lower part of CC15, below 1038 mbsf, are generally more condensed than the ones preserved in the upper part of CC15.

Over the entire record Si/Al values fluctuate between 2.75 and 4.25, with average ratios increasing gradually from approximately 3.0 at the bottom of the profile to 4.2 at the top. The corresponding K/Al ratio varies between 0.18 and 0.33, but it shows no superimposed trend across the profile. As pointed out before, fluctuations in Si/Al and K/Al ratio are related to variation in the abundance of quartz and illite on the one hand versus smectite and kaolinite on the other hand. These compositional variations are thought to reflect sediment supply from a tropical and a more arid source region to the DIB.

OC content fluctuates between 2% and 18% throughout the record (Fig. 4), with highest values in the lower part of CC15a (1042-1041 mbsf). Carbonate content varies between 0% and 50% in biozone CC15. Highest values, exceeding 80%, are reached below the base of the study interval (1042 mbsf) in biozones CC13 and CC14. Starting from 1037.3 mbsf, the average carbonate content decreases towards the upper part of the record, progressively

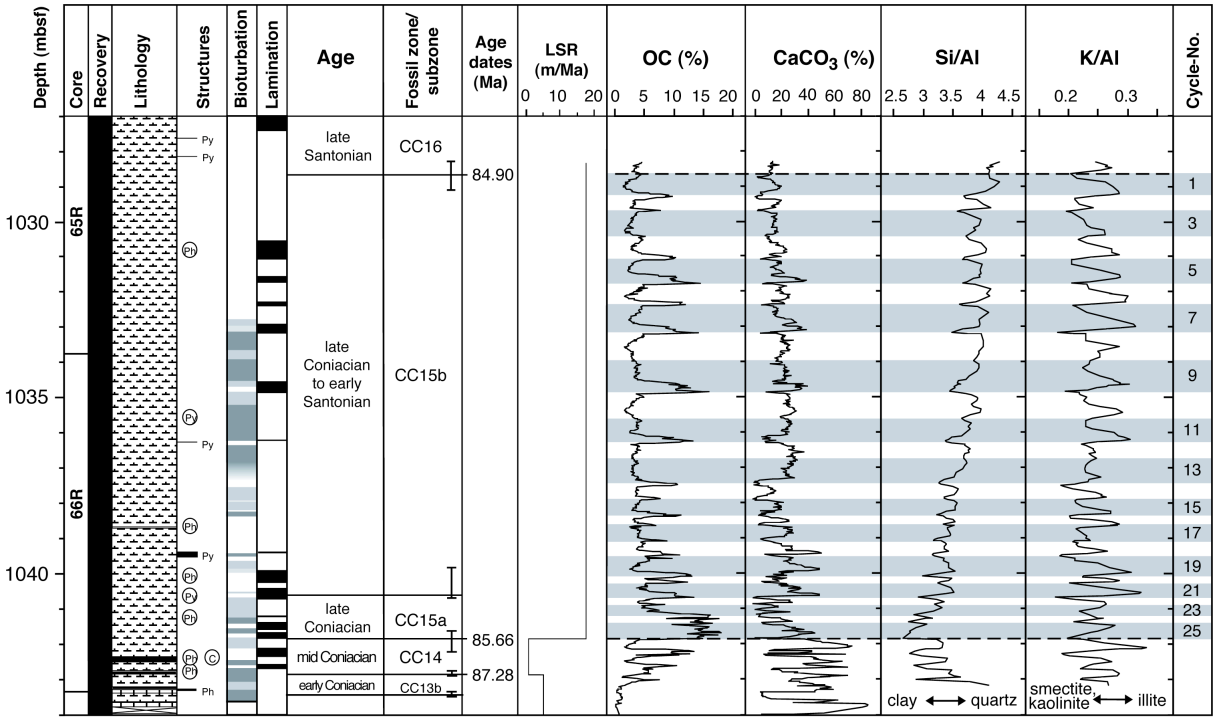

Fig. 4: Depth profiles of organic carbon (OC) and carbonate ($CaCO_3$) content, and Si/Al and K/Al as terrigenous proxies for nannofossil biozones CC13 through CC15 (from Hofmann et al. 2003). Si/Al and K/Al ratios document temporal variations in the delivery of quartz and illite versus smectite and kaolinite to the DIB suggesting cyclic changes in continental sediment supply from an arid (southern) and tropical (northern) African source area. Minima in Si/Al and K/Al generally correspond to maxima in organic carbon deposition. Generalized lithology, sediment structures, bioturbation, and lamination for nannofossil biozones CC13 to CC16 from figure 3; ages, fossil zones, and error bars for fossil zones according to Watkins et al. (1998), linear sedimentation rates (LSR) calculated from ages dates provided by Hardenbol et al. (1998). Recovery of the presented interval was 100% (Mascle et al. 1996).

shifting from average values around 25% at 1037 mbsf to 15% at the top of biozone CC15b. The amplitudes of the cyclicity, however, are larger for OC, leaving a much more distinct pattern. Whether the "missing OC peaks" between cycles 8/9, 10/11, and 12/13 are caused by postdepositional oxidation of OC comparable to the "sapropel burn down effects" described for the Pliocene-Pleistocene Mediterranean Sea (e.g., Wehausen and Brumsack, 1999) or reflect periods of reduced OC deposition cannot be determined from the present data.

The fluctuations in bulk geochemical data are often but not always reflected in the succession of laminated and bioturbated beds (Fig. 4). As shown in the detailed section in Figure 5, geochemical proxies for productivity (carbonate and OC), identification of continental source area (Si/Al), and preservation (HI, OI, and Zn/Al) in this case closely follow the succession of homogeneous and laminated beds. The laminated interval is characterized by enhanced OC burial, reduced carbonate productivity, and continental

supply from tropical source areas (Si/Al), better preservation of hydrogen-rich OM (OI and HI) and the development of anoxic bottom-water conditions (Zn/Al).

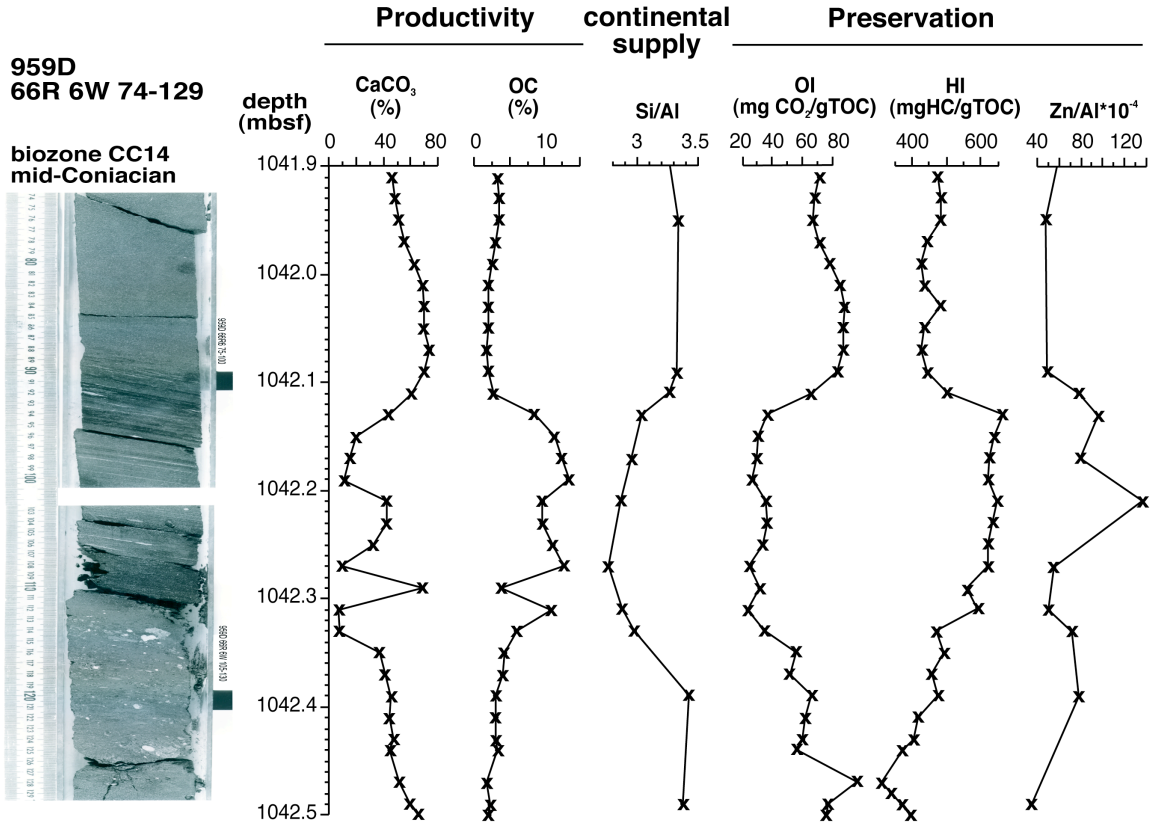

Fig. 5: Close up photograph of the sample interval 66R6W74-129 (1041.9 – 1042.5 mbsf) and selected associated results from geochemical and pyrolytic analyses. Carbonate ($CaCO_3$) and organic carbon (OC) content as indicators for productivity, Si/Al ratio (indicator for terrigenous supply), Oxygen Index (OI; $mgCO_2$/gTOC), Hydrogen Index (HI; mgHC/gTOC), and Zn/Al ratio as proxies for preservation. Elevated OC is almost exclusively restricted to the laminated intervals, HI and Zn/Al follow the OC signal. Carbonate shows a reverse trend to OC, as does OI and Si/Al.

3.5.1.1 Organic-matter composition

In order to assess the type of OM, we used a multi-method approach (maceral analysis, stable-isotope analysis of OC, and Rock-Eval pyrolysis). Optical analysis reveals that finely disseminated, brightly fluorescing OM, algae, and amorphous organic matter (AOM) are the main organic constituents in all samples studied (Figs. 6A, B). AOM occurs either as reddish bodies or nebulous/blurry structures with a moderate yellowish-green fluorescence. Because of the lack of characteristic structures, the origin of AOM cannot be determined by optical means. It is most likely derived from marine and bacterial sources because hopanoid biomarkers are abundant (Wagner, unpublished data). Another distinct optical feature of OC-rich black shales is layers with brownish-fluorescing fecal pellets in high concentration (Figs. 6A, B). These layers probably record short-term events of enhanced zooplankton productivity

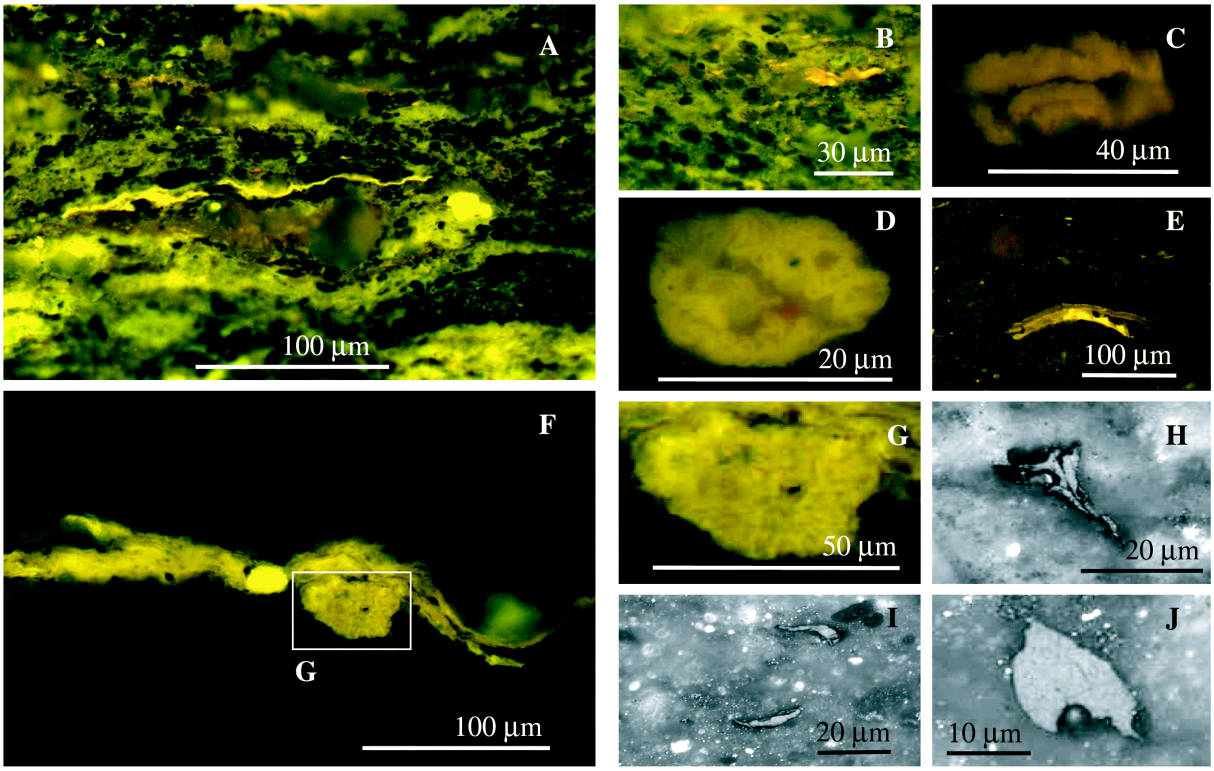

Fig. 6: Photomicrographs illustrating the typical organic matter (OM) composition in sediments from CC15b. **(a)** strongly fluorescing, finely disseminated OM, laminated algae, amorphous organic matter (AOM), and distinct layers of brownish-fluorescing fecal pellets. **(b)** AOM with moderate yellowish-green fluorescence, detrital fragments (liptodetrinite), layers of fecal pellets, and reddish-orange fluorescing spore. **(c)** Moderately, reddish fluorescing spore. **(d)** Moderately yellowish-green fluorescing colonizing algae of *botryoccocus* type. **(e)** Sporangium with strongly fluorescing spores inside, detrital liptinitic fragments (liptidetrinite), and weakly fluorescing AOM. **(f, g)** Strong yellowish-green fluorescing colonizing algae, type *botryoccocus*, partly overgrown by microbial mat. **(h-j)** Detrital vitrinite and inertinite.

and may be related to seasonal plankton cycles. Admixture of OM from terrestrial sources is generally moderate, and the terrigenous to marine OM ratios remains fairly constant regardless of the organic matter content of the samples. Terrigenous OM consists of spores and organic particles from woody material including detrital vitrinite and inertinite (Figs. 6B, C, D, H-J). Colonizing freshwater algae of the *botryococcus* type (Figs. 6D, F, G) can be recognized (e.g., Stach et al., 1982; Tissot and Welte, 1984). The occurrence of this type of algae in deepwater sediments more than 200 km away from the nearest continental margin indicates at least temporary freshwater input to the DIB.

Stable carbon isotope ratios of bulk OM show only minor fluctuations over the studied interval and vary from –28 to –26.5‰ (Fig. 7). These $\delta^{13}C_{org}$ values are similar to data compiled by Dean et al. (1986), Dean and Arthur (1999), and Hofmann et al. (2000). These authors report $\delta^{13}C$ values of –29 to –27‰ for Cretaceous marine-dominated OM. Terrigenous OM from Cretaceous coals, for comparison, range from –24 to –26‰ (Dean and Arthur, 1999). The latter range in $\delta^{13}C_{org}$ is supported by isotopic studies on OC-rich

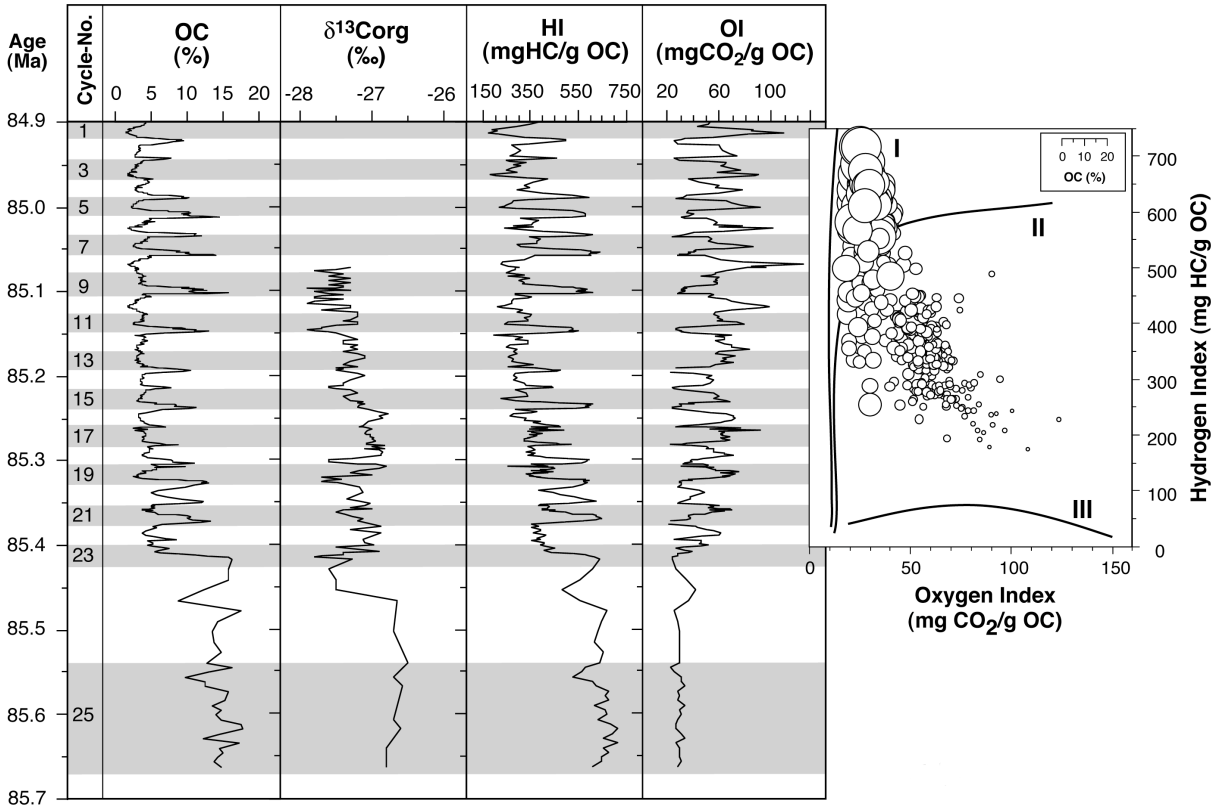

Fig. 7: Records of Hydrogen Indices (HI; mgHC/gTOC) and Oxygen Indices (OI; $mgCO_2$/gTOC) obtained from Rock Eval pyrolysis, and bulk $\delta^{13}C_{org}$ (‰) for biozone CC15. HI and OI show high amplitude fluctuations that closely follow OC accumulation. Isotopic signatures display minor variability and no or only a weak negative co-variation with OC accumulation suggesting little fluctuations in OM composition. Insert: Plot of HI versus OI and OC in a modified "Van Krevelen" type diagram for samples from Biozone CC15 displaying gradual changes in OM preservation between two endmembers, i.e. kerogen type I OM representing black shales and mixed kerogen type II/III representing TOC-lean background sediments.

Cenomanian strata that exclusively contain terrestrial plant material providing average values of –23.4‰ (Nguyen Tu et al., 1999). The $\delta^{13}C$ values of the OM in CC15 suggest a mixture of terrigenous and marine derived OM, with a dominant marine component. A quantitative estimate of the marine versus terrigenous component can be reached by applying an isotope mixing model. Assuming –24‰ and –29‰ as end-member values for Cretaceous terrigenous and marine OM, $\delta^{13}C_{org}$ signatures at Site 959 suggest marine proportions in the order of 55-80% of the bulk OM. This first-order estimate is supported by the results from maceral analysis. It is important to note that the isotopic composition of the organic matter changes only slightly (less than 1‰) within each depositional cycle, even though the OC content fluctuates considerably (from ~ 2% to up to 18%). This relationship implies that OM-production and the delivery and accumulation of terrigenous OM are linked in the DIB.

HI and OI records also reveal pronounced fluctuations which closely follow OC concentration cycles (Fig. 7). OM-rich samples reach HI values of up to 720 mg HC/g OC and lowest OI of 20 mg CO_2/g OC, whereas low HI and OC, but high OI values characterize

samples with low OC content. This pattern is distinct and consistent and reflects fluctuating preservation conditions for the OM rather than source fluctuations, because both maceral analysis and $\delta^{13}C_{org}$ values show only minor shifts in OM composition from OC-rich to OC-poor samples. The HI/OI plot (Fig. 7) illustrates the gradational transition between the two opposing depositional modes, i.e., excellent preservation conditions with type I kerogen (oil-prone algal material), not related to a lacustrine source of OM but characterizing lipid-rich material of algal origin, associated with the black-shale mode and moderate to poor preservation indicated by mixed type II/III kerogen (hydrogen-depleted OM) representing the background mode. The fluctuating preservation conditions suggested by the HI and OI records can be also traced by proxy data based on inorganic parameters.

3.5.1.2 Preservation conditions

Carbon-sulfur relationships are controlled by sulfate reduction processes and are frequently used to assess the degree of oxygenation during the deposition of fine-grained marine sediments (e.g., Berner and Raiswell, 1983; Leventhal, 1983). The OC and sulfur data for CC15 are clearly characterized by a moderate to high sulfur content ranging from 2 to 4% regardless of OC content (Fig. 8A). Similar C/S relationships have been interpreted as indicative for euxinic environments in general (Leventhal, 1983) and have been reported from euxinic sediments underlying areas with high primary productivity (e.g., Morse and Emeis, 1992; Emeis and Morse, 1993). Microscopic examination showed that pyrite is the dominant sulfur-bearing mineral in the sample set. Sulfates, e.g., barite and gypsum, are absent or occur in trace amounts only.

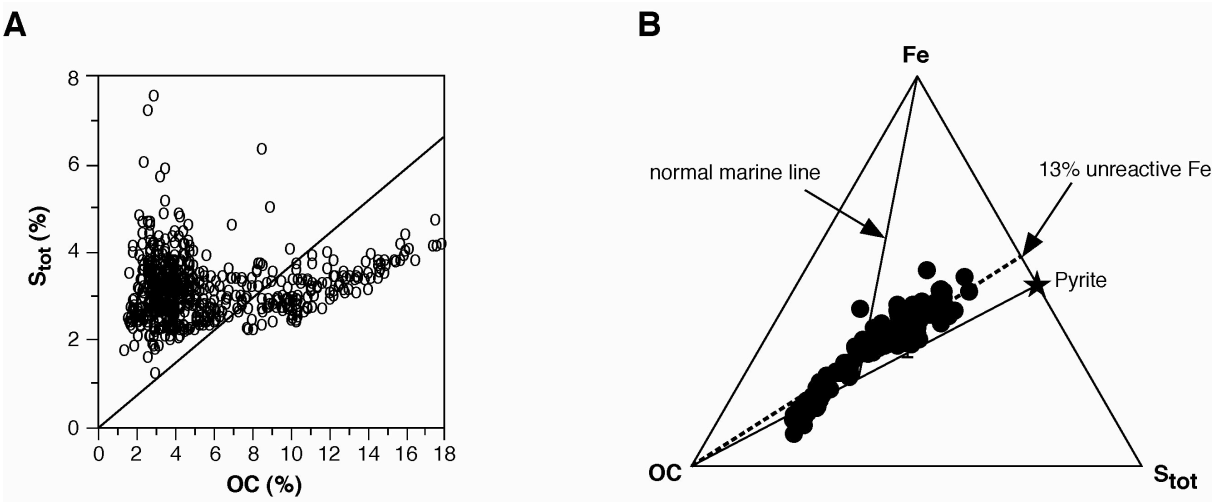

Fig. 8: (a) Organic carbon-total sulfur cross-plot from the investigated interval. The normal marine line for sediments deposited in oxygenated environments (C/S=2.8) according to Berner and Raiswell (1983). **(b)** Fe-TOC-S ternary diagram for recognition of limitations of pyrite formation in marine sediments (following Dean and Arthur 1989). The normal marine line (C/S=2.8) and the pyrite line (TOC corner to pyrite point, marked by asterisk) are shown.

In order to understand sulfur fixation at Site 959, pyrite formation is examined in more detail. In the ternary Fe-OC-S diagram, samples from CC15 plot along a line extending from the OC corner to the Fe / S line of the diagram (Fig. 8B), indicating a constant Fe / S ratio and variable OC content. This relationship is typical for sample populations where pyrite formation is limited by the availability of reactive iron (Dean and Arthur, 1989; Arthur and Sageman, 1994; Hofmann et al., 2000). Iron limitation has been reported for modern oxygen-depleted environments such as the Black Sea (Raiswell and Berner, 1985; Dean and Arthur, 1989; Arthur and Sageman, 1994), the Californian (e.g., Hutchins and Bruland, 1998) and Peruvian (e.g., Hutchins et al., 2002) continental upwelling areas, and has also been inferred for OC-rich Cretaceous strata (e.g., Dean and Arthur, 1989; Hofmann et al., 1999; 2000; 2001). The systematic deviation of most of the samples from the pyrite line indicates the presence of nonreactive iron, which is probably fixed to iron-containing clay minerals, such as smectite. Samples plotting below the OC-pyrite line derive from OM-rich (OC > 7%) black shales and contain sulfur not bound in pyrite. This excess sulfur can, in the absence of sulfates, occur either as native sulfur or as sulfur bound in OM. The high abundance of sulfur-containing biomarkers in these sediments suggests that early sulfurization processes played an important role in the preservation of OM and supports the conclusion that a considerable portion of sulfur is organically bound (Wagner, personal communication).

Redox-sensitive trace elements are known to accumulate in concentrations above crustal abundance in sediments deposited under anoxic conditions (e.g., Vine and Tourtelot, 1970; Brumsack, 1986; Arthur et al., 1990). In order to assess trace metal enrichment, aluminum-normalized metal ratios are compared with average shale values (ASV, Fig. 9; Wedepohl, 1971). At Site 959, aluminum-normalized trace-metal ratios from CC15 are significantly higher than their respective ASV. Notably, trace-metal/Al profiles follow the OC record (r^2=0.51 for Zn/Al, 0.6 for V/Al, and 0.67 for Ni/Al). V/Al ratios range from almost $600x10^{-4}$ during peak OC concentration to approximately $30x10^{-4}$ in low OC samples. Ni/Al and Zn/Al show a pattern similar to that of V/Al, with Ni/Al fluctuating between 15 and $80x10^{-4}$, and Zn/Al between approximately 20 and $500x10^{-4}$.

A better positive correlation with OC is observed if trace-metal concentrations are considered (r^2=0.79 for Zn and V, and 0.89 for Ni). These trace metals are bound to OM (Ni and V are enriched in porphyrins, e.g., Arthur et al., 1990; Calvert and Pedersen, 1993; Jones and Manning, 1994) and/or form insoluble sulfides in the presence of H_2S (Ni and Zn; e.g., Calvert and Pedersen, 1993) and thus might be enriched in organically bound sulphur. Trace-metal content of the OC-rich black shales from Site 959 is generally comparable to the one reported for sapropels of the Mediterranean Sea (e.g., Nijenhuis et al., 1999; Wehausen and Brumsack, 1999), values fluctuate between 200 and 2500 µg/g V, 200 and 2000 µg/g Zn, and 50 and 350 µg/g Ni. Cycles with maximum OC deposition approach values comparable to those reported as average values for the Cenomanian-Turonian OAE2 from deposits in both deep and shallow marine settings (Brumsack, 1988; 1991). Whether the trace metals in the

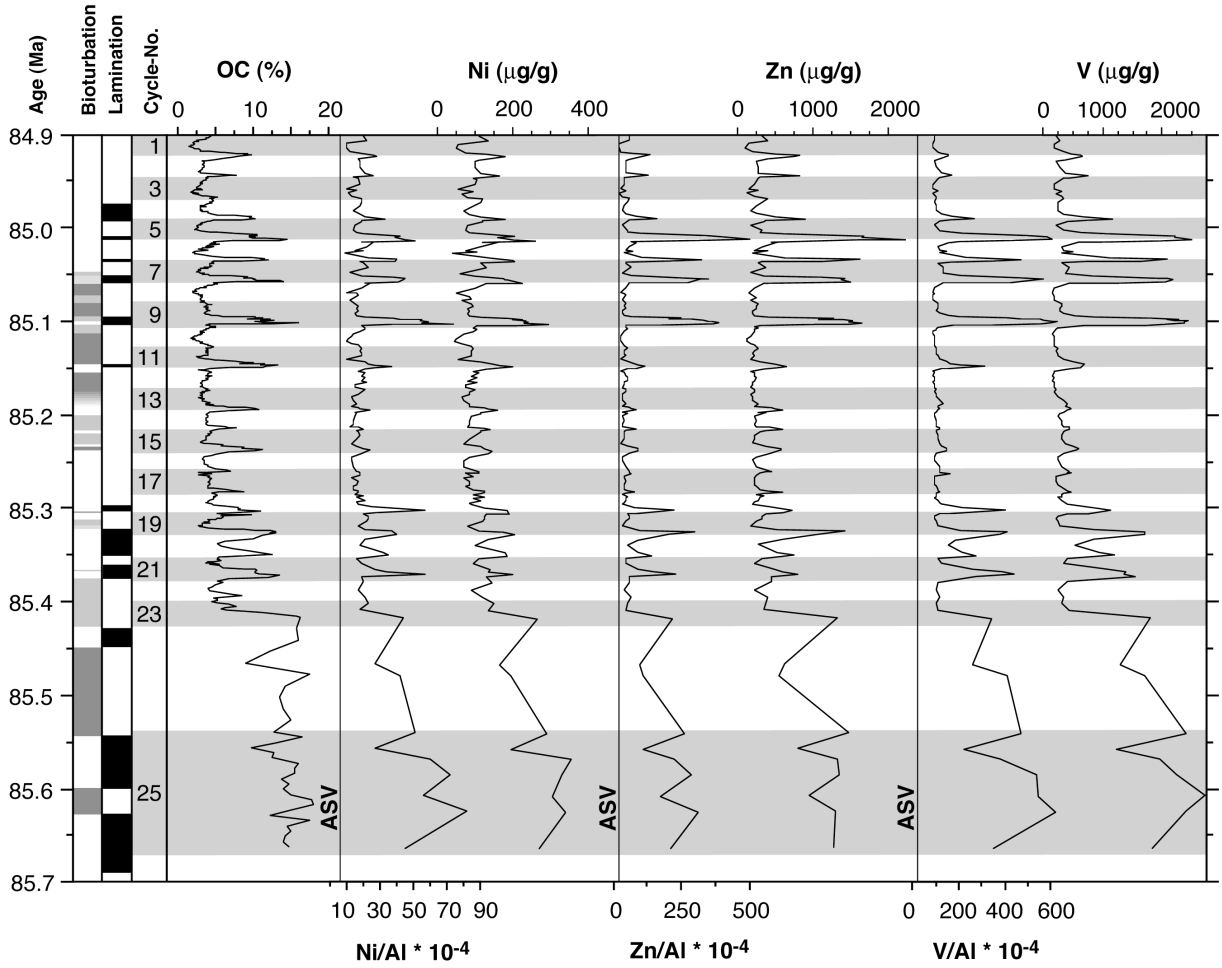

Fig. 9: Records of Aluminum normalized ratios of redox-sensitive trace-metals (Ni, Zn, V) and concentrations of OC, Ni, V, and Zn (μg/g) for CC15. Vertical lines represent average shale values (ASV) for Ni/Al (7.7), Zn/Al (10.7), and V/Al (14.7) from Wedepohl (1971). Cycle numbers and absolute ages from Hofmann et al. (2003), bioturbation and lamination transferred from figure 3.

Site 959 samples derived from hydrothermal activity connected to the Cretaceous opening of the Equatorial Atlantic Ocean or are related to delivery via continental runoff cannot be finally decided on the basis of the data present. Fluctuations in trace-metals therefore do not necessarily reflect variations in sources but rather mark periods of enhanced fixation of these metals, probably fostered by reducing bottom-water conditions.

The observed enrichment in redox-sensitive trace metals, as well as Fe-OC-S relationships, support the conclusion that sediment pore water at Site 959 was anoxic for most of CC15. These anoxic conditions probably extended episodically into the bottom-water when highest OC and trace-metal deposition took place (e.g., during cycles 5, 6, 7, 9 and 18, 19, 21; Fig. 9). Laminated sediments commonly characterize these short time intervals of most severe anoxia (Fig. 9). During background sedimentation the depositional environment changed drastically to suboxic and maybe at times even oxic bottom-water conditions, allowing bottom-dwelling organisms to recolonize the sea floor and bioturbate the uppermost sediment layers.

3.5.1.3 OC and carbonate relationships

As already noted, both carbonate and OC display distinct cyclic patterns. In the lowermost two cycles (24 and 25), carbonate and OC content do not correlate, whereas starting from cycle 23, two general patterns emerge. First, cycles 23, 22, 17-10, 8, and -1 (Fig. 4; see Fig. 10A for details) show a generally reverse trend, where drops in carbonate mirror peaks in OC. To identify the influence of dilution (e.g., by terrestrial material derived from continental runoff or eolian input), productivity, and diagenesis on the depositional environment and later the sedimentary record, we consider OC and carbonate as proxies for marine productivity and Al_2O_3 as a proxy for supply of terrigenous clay. The depositional model introduced by Hofmann et al. (2003) proposes that OC and continental supply from a tropical source are in phase. The relationship between OC + Al_2O_3 versus carbonate (Fig. 10B) shows an overall negative trend, consistent with the assumption that dilution is the principal mechanism controlling the observed cyclicity (dilution pattern, DP).

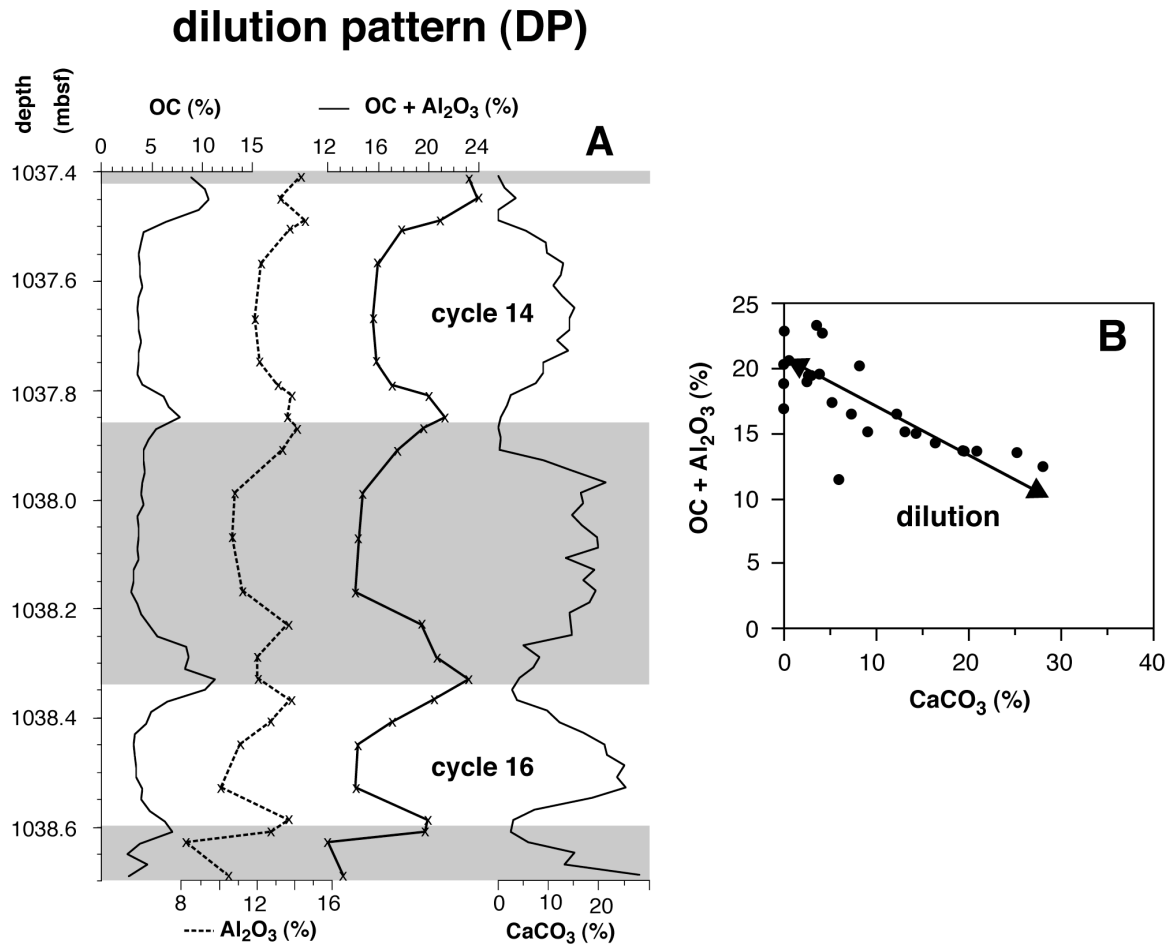

Fig. 10: (a) Detailed cycle pattern of cycles 16 to 14 showing organic carbon (OC) and carbonate ($CaCO_3$) as proxies for marine productivity, and Al_2O_3 as a proxy for supply of terrigenous clay. OC and Al_2O_3 display a general reverse trend to carbonate indicating a Dilution Pattern (DP) for most cycles. XRF-samples are marked with (X). **(b)** Relationship between OC + Al_2O_3 versus carbonate for cycles 16 to 14 revealing an overall negative trend between organic-walled productivity plus supply of terrigenous clay versus carbonate productivity.

A second pattern is recognized in cycles 21-18, 9, and 7-4 by distinct double peak in both OC and carbonate (Fig. 4; detail in Fig. 11A). Notably the initial OC peak is slightly preceding a pronounced but narrow carbonate maximum, whereas the second carbonate peak is typically not reflected by OC. For the second pattern, the relationship between OC + Al_2O_3

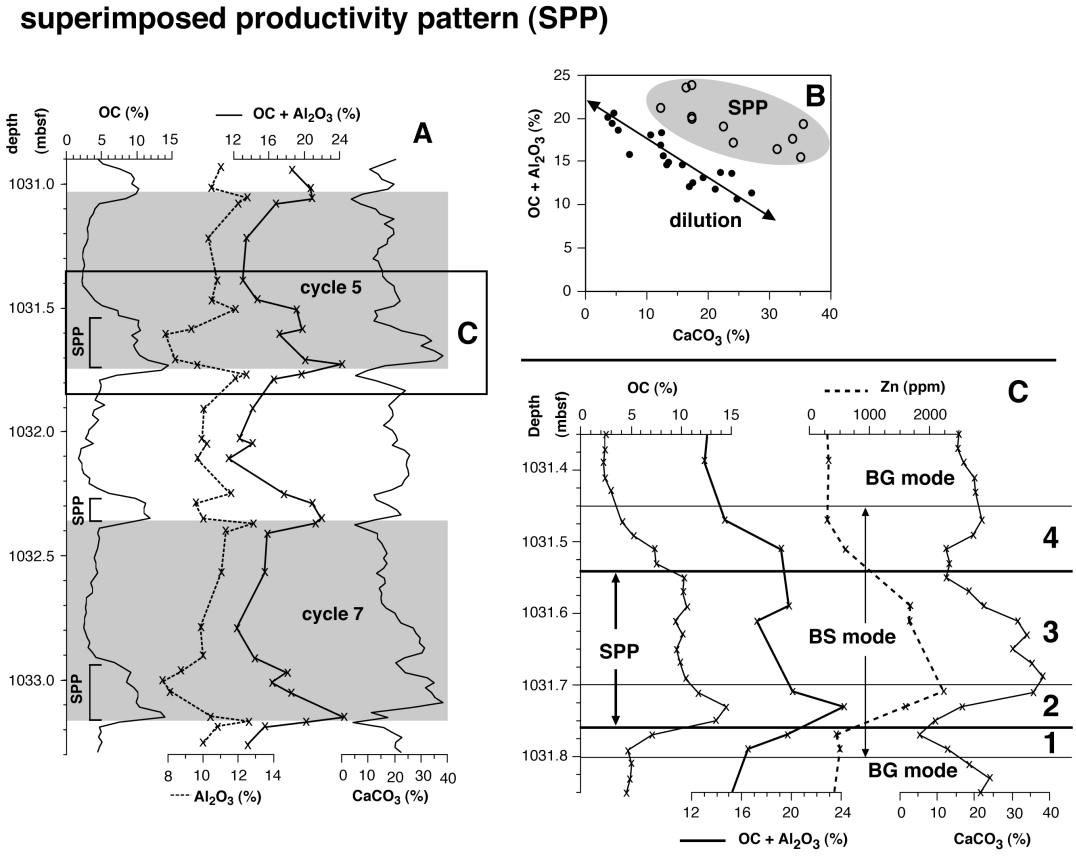

Fig. 11: (a) Detailed cycle pattern of cycles 7 to 5 showing organic carbon (OC) and carbonate ($CaCO_3$) as proxies for marine productivity, and Al_2O_3 as a proxy for supply of terrigenous clay. A pronounced but narrow carbonate peak follows the initial OC maximum, the second carbonate peak is not followed by the OC signal which gradually returns into its background signal. SPP indicates samples being related to the Superimposed Productivity Pattern during maximum OC deposition. Box marks the focus shown in figure 7C, XRF-samples are marked with (X). **(b)** Relationship between OC + Al_2O_3 versus carbonate for cycles 7 to 5 revealing two populations: dilution that persists throughout the entire record and a SPP that is related to maximum black shale deposition clearly deviating from the DP (shaded area). **(c)** Detail of cycle 5 illustrating the proposed 4 phases of carbonate and OC accumulation in cycles displaying the superimposed productivity pattern (SPP). Organic carbon (OC), carbonate ($CaCO_3$), and OC + Al_2O_3 from figure 7A, Zn content illustrating reducing bottom water conditions. Numbers 1 to 4 relate to phases described in the text, thick bars indicate borders of phases related to SPP, light bars those of individual phases. (BS mode = black shale mode; BG mode = background mode).

versus carbonate reveals two populations (Fig. 11B), one reflecting dilution that persists throughout the entire record and the other indicating a modulation of the dilution pattern due to carbonate and OC productivity as revealed by an offset of OC + Al_2O_3 towards higher values compared to the dilution trend (superimposed productivity pattern, SPP). The superimposed productivity pattern can be distinguished into four phases (Fig. 11C), which are

attributed to changes in nutrient availability, biotic response, the development of bottom water anoxia, and black-shale formation. Phase 1 marks the transition from the background mode to the black-shale depositional mode, which is characterized by a rapid increase in OC production and burial in phase with continental supply from tropical source areas (Fig. 11A). During this period, huge amounts of (mainly continental) nutrients were introduced into the DIB, stimulating enhanced primary productivity of organic-walled plankton. This initial period is followed by peak trophic levels with maximum OC production and the development of bottom-water anoxia (phase 2). Because of extensive nutrient leaching during that phase, the trophic level decreased and productivity shifted from mainly organic-walled plankton towards a carbonate-dominated community of primary producers in phase 3 (see, e.g., explanation on Cretaceous paleoceanography deduced from planktonic foraminifera by Premoli-Silva and Sliter, 1999). This is indicated by a plateau of elevated OC and initially very high carbonate concentrations that progressively decreased. Phase 4 marks the return from the black-shale mode to the background mode with the re-oxygenation of deep waters and reduced OC burial.

3.5.2 Controls on OM deposition in the DIB

The cycle pattern defined by the OC, HI, OI, and trace-metal concentration curves allows to distinguish two general modes of deposition which repetitively occurred during CC15. A background mode, characterized by moderate OC concentrations (between 2 and 4%), low hydrogen indices (200 to 300 mg HC/g OC), moderate oxygen indices (50 to 100 mg CO_2/g OC), and low trace-metal concentrations (50 to 100 µg/g Ni, 200 to 250 µg/g Zn, and 200 to 300 µg/g V). During the black-shale mode, on the other hand, OC content can reach up to 18%, HI and trace-metal concentration are high (up to 720 mg HC/g OC, 150 to 300 µg/g Ni, 700 to 2300 µg/g Zn, and 500 to 2500 µg/g V), OI are low. The relative contribution of OM from marine and terrigenous sources remains fairly constant throughout both modes, as indicated by first results from microscopic evaluation of the OM composition and by the isotopic composition of the OC. This implies an overall co-fluctuating supply of terrigenous OM (vitrinite, inertinite, sporinite, and *botryococcus*-type algae) from the African continent and the production of organic matter in the DIB. Extreme shifts in OC from on average 3% during the background mode to up to 18% during the peak mode, therefore, suggest either an up to six-fold increase in OM production and in the delivery of terrigenous OM to the DIB and/or significantly better preservation conditions. Co-variation of the OC record and proxy data for preservation conditions (trace-metal concentrations, HI and OI curves) clearly show improving preservation conditions for OM from background mode to peak OM sedimentation mode that could be a consequence of enhanced productivity. Whether improved preservation was a consequence of high productivity or related to the onset of estuarine circulation and the consequent upwelling of oxygen-depleted subsurface water

cannot be determined from this data set. The preferential occurrence of high concentrations of fecal pellets from zooplankton in the OC-rich intervals of the depositional cycle indicates strongly that productivity levels increased during the peak mode. It is, however, to be expected, inasmuch as productivity and preservation conditions are connected to some extent, that both mechanisms determined the organic-matter deposition in the DIB. Changing rates of productivity in the DIB imply varying degrees of nutrient supply. The delivery of nutrients to the DIB is probably controlled by continental runoff from the African continent. Fluctuating levels of runoff can be traced by shifts in the accumulation of terrigenous OM. This type of OM is generally thought to be more resistant to degradation processes than marine OM (e.g., Tyson, 1995). The fairly constant ratio of marine to terrigenous OM throughout each depositional cycle implies that peak accumulation of terrigenous OM occurred during peak OC accumulation and, hence, periods with the highest amounts of continental runoff correspond to periods with the highest productivity of OM in the DIB.

This interpretation is in good agreement with data presented by Hofmann et al. (2003), who showed that the maximum input of kaolinite and smectite to the DIB occurred during the peak OC deposition mode. Both minerals were delivered to the DIB from intensely weathered areas in tropical West Africa (Wagner and Pletsch, 1999; Pletsch et al., 2001) probably via continental runoff. Whether or not the increased supply of nutrients to the DIB via runoff was sufficient to stimulate the observed fluctuations in productivity from background to peak mode is difficult to assess. Climate simulation and chemical weathering models suggest that precession-controlled differences in precipitation over Western Africa are insufficient to explain more than a 40% increase in nutrient supply to the DIB (Flögel 2001; Flögel, unpublished data). Hence, differences in preservation condition, or changes in oceanic circulation which can supply nutrients to the DIB, must be considered. Hofmann et al. (2003) related the black-shale depositional mode to a strong African monsoonal system that promoted periods of high precipitation and continental runoff from extensive laterite deposits of equatorial Africa (Fig. 2). At times of intense precipitation this continental runoff may have caused a freshwater cap, which induced estuarine circulation conditions in the semi-enclosed DIB. The development of an estuarine circulation may have sustained high productivity levels and zooplankton blooms. The occurrence of the freshwater alga *Botryococcus* and the relatively high amounts of terrigenous OM in sediments from Site 959 may serve as arguments for the presence of a fresh-water cap.

3.5.3 Marine-continental phase relationships

The temporal relationships between the delivery of continental matter and input from marine sources to the DIB can be assessed using the detailed time model of Site 959. The time model assumes that each depositional cycle reflects the same length of time. We follow Hofmann et al. (2003) in assuming that each depositional cycle corresponds to one precession

cycle and assign a duration of 22.5 kyr to each cycle. Each cycle is treated as if sedimentation rates were constant throughout the cycle, owing to the fact that variable sedimentation rates within individual cycles can currently not be determined. Following these basic assumptions an ideal depositional cycle was generated on the basis of data from cycles 1-21 and the relative position of peak concentrations of (1) Al as a proxy for kaolinite and smectite, (2) Si for quartz, (3) Ni, V, Zn as indicators for preservation conditions, and (4) OC and $CaCO_3$ as a proxies for marine organic and inorganic productivity. In addition, (5) the onset of OC accumulation above background level, (6) the point of peak OC sedimentation, and (7) the return to background OC levels were determined.

The results for this idealized cycle pattern show a distinct asymmetry in the OC peaks (Fig. 12). The average time required to switch from background to peak OC sedimentation and to return to background levels took about 7.2 kyr . Depositional conditions commenced to change from background to peak OC accumulation in about 2.4 kyr which was followed by a

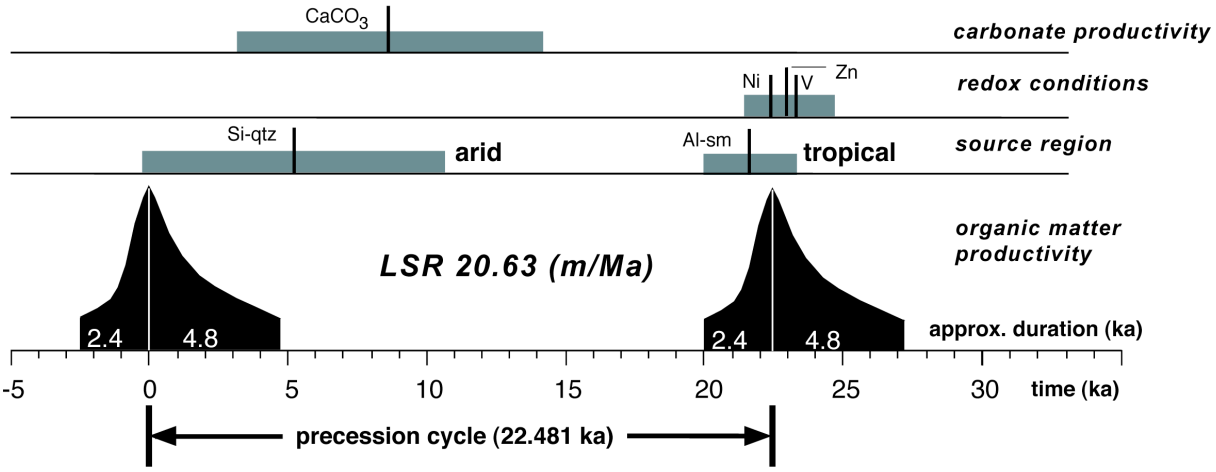

Fig. 12: Idealized, average precession cycle representing all cycles from CC15b with average linear sedimentation rate (LSR; m/Ma) and approximate transition times (ka) for the onset and decay of peak OC accumulation, i.e. the change from background to black shale depositional modes. The timing of peak accumulation of parameters indicative of carbonate productivity ($CaCO_3$), redox conditions (Ni, V, Zn), input from arid source regions (Silicium, attributed to quartz deposition, "Si-qtz"), and tropical source areas (Aluminum, attributed to smectite deposition "Al-sm") in respect to peak OC accumulation are shown. Solid lines mark average peak values, shaded bars indicate standard deviation of each individual proxy; black areas indicate phases of enhanced OM productivity in contrast to background depositional mode; duration of a precession cycle according to Berger et al. (1992).

more gradual return to background conditions taking about 4.8 kyr (Fig. 12). In some of the studied cycles the transition time from background to black shale conditions was much shorter, i.e., less than 1 kyr (e.g., cycles 3 and 16). Peak concentrations for Ni, V, and Zn coincide with maximum OC, suggesting that the development of low-oxygen or oxygen-free bottom-water conditions were directly linked to OC accumulation. The highest Al concentrations are encountered during the transition from background to peak TOC

sedimentation. Because the supply of Al to the DIB was mainly as smectite and kaolinite from tropical source regions (Wagner and Pletsch, 1999; Pletsch et al., 2001; Hofmann et al., 2003), a link between continental runoff from western Africa and marine black-shale sedimentation is therefore highly probable. Peak Si concentrations, on the other hand, follow the OC peak by approximately 5 kyr in this time model. Si input is from quartz of arid regions of southern Africa (Hofmann et al., 2003) and generally overlaps with peak $CaCO_3$ concentrations in each depositional cycle (Fig. 12). Independently of the assigned time model, the phase relationships recorded by the depositional cycles at Site 959 show the direct link between climate conditions and the response of the oceanic system.

3.5.4 OAE 3 in tropical regions

Most known OC-rich OAE3 sites were located in intermediate and shallow water depths along the continental margins of many late Cretaceous ocean basins and intercontinental connections between them (e.g., Mello et al., 1995; Erlich et al., 1996; Erlich et al., 1999; Vergara ,1997; Dean and Arthur, 1998; Davis et al., 1999; Holbourn et al., 1999; Wagner and Pletsch, 1999). The proposed mechanisms that led to the deposition of these OC-rich marine sediments were generally similar, but depending on the geographical position and local effects, they differ to some extent from those proposed for Site 959. As stated earlier, Hofmann et al. (2003) related shifts in the atmospheric circulation pattern (variation of the ITCZ) which resulted in alternations of influence from arid and humid source regions, to the mainly precessional cycles in the sedimentary record of Site 959. Continental runoff as stimulus for OM productivity in equatorial regions of the Cretaceous hothouse has been shown for the DIB on the basis of the data presented here; enhanced preservation was connected to recurrent episodes of anoxia. Because both continental runoff and hydrological cycling are key elements of the larger-scale atmospheric circulation, which determines continental climate over a range of latitudes, it appears reasonable to expect that other continental margins along the tropical ocean experienced conditions comparable to those of the DIB, making the low-latitude ocean a key site for short-term but massive OC burial during the OAE3 and, consequently, a sink for atmospheric CO_2.

Related to their geographic position in the tropics on the conjugate South American margin, the La Luna and Querecual Formations in Venezuela represent the closest similarities with the DIB deposits, in terms of both mechanisms and sedimentary facies. In the South American sections, several authors have recognized a cyclic pattern of Turonian to Santonian marine shales and identified intense primary production coupled with enhanced preservation as the main triggers for their formation (e.g., Mongenot et al., 1996; Perez-Infante et al., 1996; Alberdi-Genolet and Tocco, 1999; Davis et al., 1999; Erlich et al., 1999; Cotillon et al., 2000). Similarly to the DIB, enhanced preservation was connected to recurrent episodes of anoxia (e.g., Alberdi-Genolet and Tocco, 1999; Erlich et al., 1999) and a thick layer of

sulfidic bottom water (e.g., Mongenot et al., 1996; Davis et al., 1999). The latter phenomenon is intimately related to the paleogeographic setting of the Cretaceous Equatorial Atlantic Gateway and its associated atmospheric and oceanic circulation patterns (Wagner, 2002). According to Erlich et al. (1999), the presence of paleobathymetric barriers related to basement uplift in the Maracaibo and Barinas-Apure Basins resulted in stagnation and poor circulation, which, in combination with high evaporation rates and salinity stratification, lead to low-oxygen water mass in shallow shelf areas that acted as a local source of bottom waters.

In order to compare the OC record of the DIB at Site 959 with other depositional settings, we applied the cycle-based time model for CC15 by Hofmann et al. (2003) to calculate LSR and AR of selected proxies. Accordingly, LSR fluctuate between 39 m/Myr in cycle 9 and 7.1 m/Myr in cycle 20 (Fig. 13). Cycles 24 and 25, assigned to the eccentricity frequency, display LSR of approx. 1.6 m/Myr and 3.5 m/Myr, respectively. Carbonate accumulation displays high-amplitude fluctuations throughout CC15, with AR that vary between 30 g/m^2/year in cycle 9 and less than 0.1 g/m^2/year in cycle 24 (Fig. 13). The

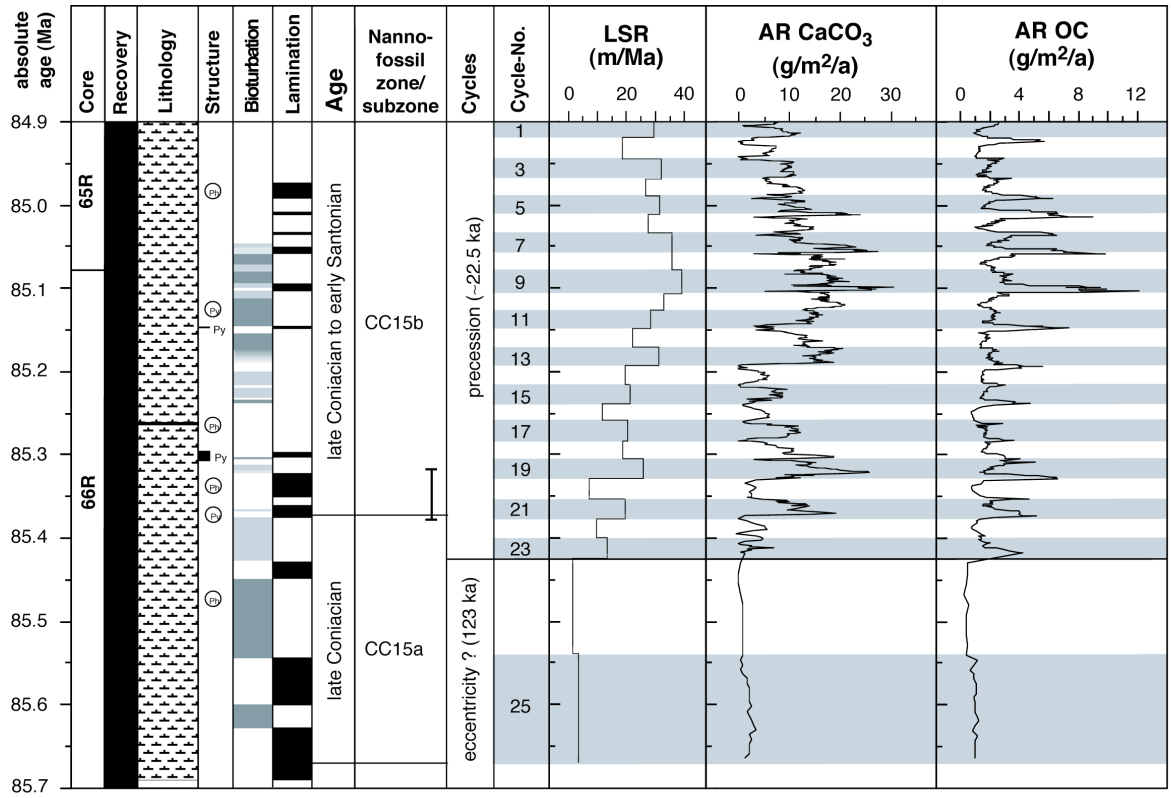

Fig. 13: Linear sedimentation rates (m/Ma), carbonate, and organic carbon accumulation rates (AR; g/m^2/a), for nannofossil zone CC15. CC15 is interpreted to represent 23 precession cycles of 22.5 ka each (Berger et al. 1992) and 2 cycles that are tentatively assigned to eccentricity (123 ka). Generalized Lithology, structures, bioturbation and lamination from Figure 3, nannofossil sub-zones, age, and error bar from Watkins et al. (1998); absolute age (Ma), cycles, and linear sedimentation rates (LSR; m/Ma) according to Hofmann et al. (2003).

condensed lower section at the base of cycles 24 and 25 generally exhibit very low carbonate AR (below 1 g/m^2/year). In general, two overlying cycles of enhanced carbonate accumulation are recognizable which are not as evident in carbonate content. These cycles suggest longer-term fluctuations in carbonate productivity, probably related to the bands of longer eccentricity. The first overlying cycle covers precessional cycles 14-23 (85.43 to 85.2 Ma) equivalent to about 230 kyr and is followed by a second cycle of approximately the same duration (cycles 2-13, about 250 kyr).

A comparable but more distinct cyclic pattern characterizes OC accumulation (Fig. 13). As with carbonate accumulation, maximum AR of OC occurred during periods of highest bulk sedimentation rates, approaching maximum values at the base of cycle 9. Amplitudes in OC accumulation are large and vary by about two orders of magnitude from 0.1 to about 12 g/m^2/yr. Accumulation rates calculated for the Venezuelan Coniacian-Santonian La Luna Formation vary between 0.08 and 2.56 g/m^2/yr (Davis et al., 1999), one order of magnitude lower than the AR reported from the DIB in this study, whereas samples from the Cenomanian-Turonian black shales from DSDP Site 367 off Cape Blanc (9 g/m^2/yr, Kuypers et al., 2002) exhibit comparable values. DIB samples are in the range of some Holocene sites with oxygen-deficient bottom waters, such as the Arabian Sea (between 6.1 and 10 g/m^2/yr, van der Weijden et al., 1999), the Black Sea (between 3.1 and 4.8 g/m^2/yr, Arthur et al., 1994), and the Pleistocene sapropels of the eastern Mediterranean (between 1.5 and 3.7 g/m^2/yr, Nijenhuis et al., 2001). However, the most extreme Holocene upwelling setting along the Peruvian margin exhibits three times higher AR (average of 39 g/m^2/yr, Bralower and Thierstein, 1987), similar to Cenomanian-Turonian black-shale sites in southern Morocco (Tarfaya, between 9 and 40 g/m^2/yr, Kuypers et al., 2002; Kolonic, personal communication).

There is evidence from both geological data and computer simulations that marine sedimentation has been strongly influenced by orbital forcing on both sides of the upper Cretaceous Equatorial Atlantic. On the basis of analysis of thin sections from cores drilled from La Luna and Querecual Formations as well as field observations, Cotillon et al. (2000) identified several high-frequency sedimentary cycles (varves, El Niño cycles, and cycles of solar activity) that they interpret result from very short-term fluctuations in continental upwelling. On a longer time scale, Erlich et al. (1999) describe episodes of regional aridity in South America during the Turonian to early Santonian. Similar to our conclusions drawn for Site 959, they interpret low OC content coinciding with sharp increases in Si, quartz, and clay content to result from dilution by eolian siliciclastics. They further conclude that high fluvial outflow and decreasing stratification of the water column due to seasonal upwelling were common features along the northern South American margin characterizing late Santonian to Maastrichtian marine sedimentation.

Several studies have addressed the development of precipitation during the upper Cretaceous in global climate models (GCMs), supporting observations from the upper Cretaceous equatorial Atlantic that indicate a strong influence of continental runoff on the

deposition of OAE3 black-shales. DeConto et al. (1999) simulated an overall wetter Campanian (80 Ma), with zonal average precipitation approximately 25% higher at all latitudes than present-day values, whereas Bush and Philander (1997) found evidence for an increase in precipitation in tropical convergence zones during the late Cretaceous (75-65 Ma). According to Otto-Bliesner et al. (2002), maximum precipitation occurred along the equator during the Campanian. Numerical climate modeling for the Cenomanian-Turonian boundary investigating climate sensitivity to precessional changes (Flögel, 2001) further supports these findings in identifying equatorial regions as highly sensitive to precession-forced changes in mean annual precipitation.

3.6 Summary and conclusions

Organic sedimentation during the Coniacian-Santonian OAE 3 in the DIB was intimately linked to the climate conditions over equatorial Africa through the hydrological cycle. Inversely correlated (OC + Al_2O_3) and carbonate records point towards dilution as a prominent mechanism. This general pattern is modulated during periods of maximum productivity, i.e., black-shale sedimentation, in response to short-term fluctuations in nutrient availability and trophic levels. The temporal relationships between OC and carbonate records suggest a systematic succession of primary producers, starting with mainly organic-walled plankton (maximum nutrition, initial peak black-shale formation) followed by carbonate producers (moderate to low nutrition, declining black-shale formation and background depositional mode). Periods of maximum marine OM productivity must have stimulated oxygen deficiency in the water column providing excellent preservation conditions for marine OM settling to the sea floor. We infer that both mechanisms of continental runoff, i.e., riverine nutrient supply and the periodic development of an estuarine circulation generating a freshwater cap and the associated upwelling of subsurface waters, were main triggers for productivity cycles in the DIB. The data from nannofossil biozone CC15 further suggest that the coupled productivity-redox-dilution cycles in the DIB were orbitally forced. A link between the long-term climate development of equatorial Africa and periodically fluctuating insolation intensities caused by the Earth's precession is reasonably supported by the geological record. Recent climate modeling emphasizes the development of orbitally forced fluctuations in the hydrological cycle over Africa and South America (Flögel, 2001). The millenial-scale records from the DIB presented here provide evidence that the response time of the oceanic system to climate fluctuations was rapid, on the order of a few thousand years or even less, and dramatic with respect to redox conditions, i.e., the development of anoxia. Literature data from the conjugate South American continental margin (e.g., the Venezuelan Maracaibo Basin) suggests that the mechanism of OM sequestration characteristic of the DIB also operated in other equatorial regions during Cretaceous hothouse conditions.

3.7 Acknowledgments

This study was funded by the Deutsche Forschungsgemeinschaft (Ocean Drilling Program, grant Wa1036/7 and 8, and Ho2188/1). We especially thank the technical staff of the Geoscience Departments at Bremen and Cologne and the Bremen ODP Core Repository for assistance. Rock-Eval data were kindly provided by H. Wehner and G. Scheeder (BGR-Hannover, Germany). We thank Walter Dean and Tim Lowenstein for helpful and instructive comments on a previous version of this manuscript. Nick Harris is thanked for his thoughtful remarks and suggestions, which helped to improve an earlier version of this manuscript.

Chapter 4.

Euxinia and primary production in Late Cretaceous eastern equatorial Atlantic surface waters fostered orbitally driven formation of marine black shales

Thomas Wagner[1], Jaap S. Sinninghe Damsté[2], Peter Hofmann[3], and Britta Beckmann[1]

[1] *University of Bremen, Department of Geosciences, Bremen, Germany*

[2] *Royal Netherlands Institute for Sea Research, Department of Marine Biogeochemistry and Toxicology, Den Burg, the Netherlands*

[3] *University of Cologne, Department of Geosciences, Cologne, Germany*

Status: published Paleoceanography, vol. 19 (3), PA 3009, p. 1-13

4.1 Abstract

Oceanic Anoxic Events (OAE) in the Cretaceous represent major perturbations in the global climate and ocean system characterized by widespread deposition of organic carbon in the ocean. The causes and effects of these events are poorly constrained, mainly because of the lack of high-resolution marine records. Here we report the distribution of molecular markers from a millennial-scale record of Coniacian-Santonian black shale (OAE-3) from Ocean Drilling Program Site 959 in the Deep Ivorian Basin (DIB) in the eastern Equatorial Atlantic. Highly-branched isoprenoids (HBIs) and alkenone-derived organic compounds indicate that diatoms and calcareous nanoplankton were important primary producers. Changes in redox sensitive trace metal accumulation and biomarkers of green sulfur bacteria provide evidence for extreme variations in redox conditions, with intervals of lower photic zone euxinia (PZE). Accordingly, oxygen in the Coniacian-Santonian tropical Atlantic was absent as during the Cenomanian-Turonian boundary OAE-2, but over more restricted geographic area and more limited time intervals. We hypothesize that PZE was a common phenomenon typical in large areas of tropical continental margins. These conditions fostered sequestration of atmospheric CO_2 and thus helped cause the positive excursion in $\delta^{13}C$ of carbonate documented in higher latitude marine records.

4.2 Introduction

The Cretaceous climate and ocean system had striking similarities in pacing and variability to the Quaternary system (Arthur and Dean, 1991; Oglesby and Park, 1992; van Buchem et al., 1995; Kuhnt et al., 1997; Dean and Arthur, 1999a; Kuhnt et al., 2001; Meyers et al., 2001; Kuypers et al., 2002; Hofmann et al., 2003) despite distinct differences in ocean and atmosphere circulation, temperature distribution, continental climate and vegetation, and ocean chemistry (DeConto et al., 1999; Hay et al., 1999; Larson and Erba, 1999; Parrish, 1995; Poulsen et al., 2001; Wilson et al., 2002; Poulsen et al., 2003). Evidence for the unusual ocean chemistry comes from the widespread deposition of sediments enriched in marine organic carbon.

Several periods of organic carbon-rich marine black shale formation, termed Oceanic Anoxic Events (OAEs), occurred in the Cretaceous (Jenkyns, 1980) and apparently were restricted to relatively short time intervals on the order of a few million years or less (see Leckie et al., 2002 for review). OAEs represent major perturbations in the global climate-ocean system that led to diagnostic shifts in the global carbon isotopic signature of sedimentary carbon and subsequent cooling of the atmosphere via extensive CO_2 draw down in response to massive burial of marine organic carbon (Arthur et al., 1988; Jenkyns, 1997; Kuypers et al., 1999). Despite their fundamental role in rapid climate change, the causes and effects of these events are still not well understood, mainly because high-resolution and multi-proxy paleoceanographic are still rare (Norris et al., 2002; Wilson et al., 2002. Recent data emphasize the significance of the low latitudes in driving the mid-Cretaceous global ocean-atmospheric circulation due to extreme surface water temperatures in the range of 32-36°C (Huber et al., 2002; Schouten et al., in press) and a strongly enhanced hydrological cycle (Wilson et al., 2002; Hofmann et al., 2003).

Compared to the extensive research on the two global OAEs in the Cretaceous, the early Aptian Selli Event (OAE-1a; ~120 Ma) and the Cenomanian-Turonian boundary Bonarelli Event (OAE-2; ~93.5 Ma) (Arthur et al., 1990; Thurow et al., 1992; Bralower et al., 1994), few studies have addressed the other OAEs. These are generally considered to be more local in character, and less extreme in terms of global environmental impact. Little is known about the youngest event, the Coniacian-Santonian OAE-3. With a total duration of ~2.3 My (87.3-84.6 Ma) the OAE-3 is not a short-lived event like the Aptian OAE-1a or the Cenomanian-Turonian boundary OAE-2 but more as the protracted Albian OAE-1b (e.g., Leckie et al., 2002). The OAE-3 also marks an important transition in long-term global climate evolution from Cretaceous greenhouse/hothouse conditions, characterized by extremely high temperatures and a small thermal equator-to-pole gradient, to the Late Cretaceous-Paleogene cooling. During OAE-3 time, several marginal basins along the Atlantic margin maintained an expanded oxygen minimum zone (OMZ) while the deep basins were already well oxygenated (Figure 1; Table 1) (Thiede and van Andel, 1977; van Andel et

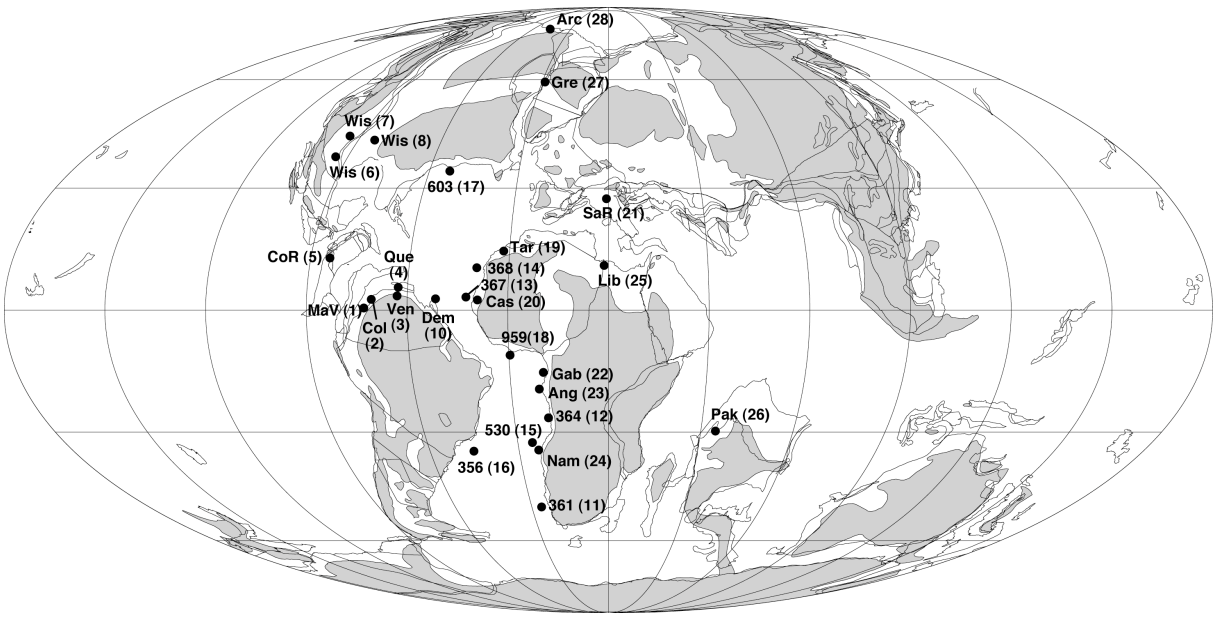

Fig. 1: Reported organic carbon-rich marine sites (see Table 1 for locations and references) of Coniacian to early Campanian age superimposed on the paleogeographic map of the mid-Cretaceous at ~80 Ma (from Hay et al., 1999).

al., 1977; Dean et al., 1984; Arthur et al., 1990; Ly and Kuhnt, 1994; Mello et al., 1995; Holbourn et al., 1999; Wagner and Pletsch, 1999; Davis et al., 1999; Erlich et al., 1999). Organic carbon-rich marine sediments of the same age are reported from as far north as Greenland (Dam et al., 1998) and the Canadian Arctic (Leith et al., 1992). Even though many of these Coniacian-Santonian age black shales are less widespread and stratigraphically less constrained, they were attributed to the OAE-3 (Arthur et al., 1990). A single correlative event, evident by a moderate, broad positive excursion in $\delta^{13}C$ profiles of carbonates, from the Western Interior Basin, the English Chalks, the Italian Scaglia (Jenkyns et al., 1994), and the Venezuelan La Luna Formation (DeRomero et al., 2003). has been used to propose the existence of a less pronounced OAE during the Coniacian-Santonian. The resolution of most deep marine records, however, is insufficient to determine the response of that event in the Atlantic Ocean (Jenkyns et al., 1994). Given the limited data available at present, an improved and precise definition of the OAE-3 is still lacking.

In this study we present biomarker records from Coniacian-Santonian (OAE-3) sections of Ocean Drilling Program (ODP) Site 959 from the Deep Ivorian Basin (DIB) about 200 km offshore equatorial west Africa. We propose the development of euxinic, i.e. H_2S bearing, conditions in the lower photic zone (PZE) and discuss communities of primary producers that thrived in mid-Cretaceous tropical Atlantic surface waters. To address molecular evidence for environmental change on orbital time scales, these investigations were confined to couplets of TOC-rich black shale and TOC-lean interbeds. The biomarker data are embedded in recently published bulk geochemical records (Hofmann et al., 2003; Beckmann et al., 2005).

No	Locality	Formation	Autor
1.	Colombia, Magdalena Valley	Lomagorda	*Vergara (1997)*
2.	Colombia	La Luna	*Rangel et al. (2000)*
3.	Venezuela	La Luna	*Alberdi-Genolet and Tocco (1999), Davis et al. (1999), Erlich et al. (1999)*
4.	Venezuela	Querecual	*Crespo de Cabrera et al. (1999)*
5.	Costa Rica	Loma Chumico	*Erlich et al. (1996)*
6.	WIS, New Mexico	Niobrara	*Bottjer and Stein (1994)*
7.	WIS, Colorado	Niobrara	*Dean & Arthur (1989)*
8.	WIS, Kansas	Niobrara	*Dean & Arthur (1998)*
9.	WIS, Canada	Niobrara	*Schröder-Adams et al. (2001)*
10.	DSDP 144/ODP 1257		*Deroo et al. (1984); Erbacher (pers. Comm, 02/2003)*
11.	DSDP 361		*Stein et al. (1989)*
12.	DSDP 364		*de Graciansky et al. (1986); Stein et al. (1989)*
13.	DSDP 367		*Stein et al. (1989)*
14.	DSDP 368		*de Graciansky et al. (1986)*
15.	DSDP 530		*de Graciansky et al. (1986); Stein et al. (1989)*
16.	DSDP 356		*Stein et al. (1989)*
17.	DSDP 603		*Stein et al. (1989)*
19.	ODP 959		*Wagner and Pletsch (1999), this study*
19.	Morocco, Tarfaya		*Leine (1986); Holbourn et al. (1999)*
20.	Senegal, Casamance		*Holbourn et al. (1999)*
21.	Italy, Sasso Rosso		*Jenkyns (1980)*
22.	Gabon, offshore	Anguille	*Katz et al. (2000)*
23.	Angola, offshore	Iabe	*Schoellkopf and Patterson (2000)*
24.	Namibia, offshore		*Holtar and Forsberg (2000)*
25.	Lybia, South Ajdabiya Trough	Sirt-Rachmat	*Rusk (2001)*
26.	Pakistan	Upper Goru	*Robison et al. (1999)*
27.	W-Greenland, Umiivik-1		*Dam et al. (1998)*
28.	Canadian Arctic, Sverdrup Basin	Kanguk	*Leith et al. (1992)*

Table 1: Reports on Coniacian to lower Campanian organic-carbon-rich marine sediments representing the OAE-3 (Coniacian-Santonian) and the succeeding "biosiliceous event" (lower Campanian) as proposed by Kuhnt et al. (1998) in the Atlantic and Tethyan Ocean. WIS = Western Interior Seaway

4.3 Previous studies on OAE-3 sections of Site 959

Long-term deposition of organic-rich sediments in the Upper Cretaceous DIB was intimately linked to the plate tectonic and oceanographic evolution of the Equatorial Atlantic Gateway (Wagner and Pletsch, 1999; Pletsch et al., 2001; Wagner, 2002) and the climatic evolution on the African continent (Hofmann et al., 2003). Middle Coniacian to lower Santonian benthonic foraminiferal assemblages at ODP Site 959 (Mascle et al., 1996) in the southern DIB are dominated by buliminid associations, suggesting poorly oxygenated bottom waters in an outer shelf or upper slope environment (Holbourn et al., 1999) while nutrient levels in surface waters apparently were low as suggested by calcareous nannofossils (Watkins et al., 1998).

Recently, millennial-time scale records of marine and continental proxies have been presented for the Late Coniacian-Early Santonian part of OAE-3 from Site 959 (Hofmann et al., 2003; Beckmann et al., 2005). The data presented cover the depth interval between 1046 mbsf (nannofossil zone CC13) and 1029 mbsf (boundary between nannofossil zones CC15/CC16, ~84.9 Ma) and include TOC, $CaCO_3$, K/Al, Si/Al, Rock-Eval properties, bulk $\delta^{13}C_{org}$, and concentrations of the redox-sensitive elements V, Zn, and Ni. One distinct feature of all of these records is a well expressed cyclicity on a cm- to meter-scale that has been attributed to orbital-forced (mainly precessional) fluctuations in continental supply from different African source areas and deep water redox conditions associated with pronounced changes in the rate of organic carbon burial. Cycle boundaries were defined by minima in Si/Al and K/Al that generally correspond to maxima in TOC (Hofmann et al., 2003). Based on the assignment of individual cycles orbital tuning provided a high-resolution cyclostratigraphic model that was used to determine organic and inorganic carbon accumulation rates, the recognition of lead-lag relationships of marine and continental proxies, and provide precise estimates for average transient times from oxygenated to oxygen-depleted environmental conditions (Beckmann et al., 2005).

Hofmann et al. (2003) demonstrated that the terrigenous fraction records fluctuating supply of illite and quartz (Si/Al and K/Al proxy) and smectite and kaolinite (K/Al proxy). This was interpreted to document aeolian dust supply from southern Africa and continental run–off from tropical northern Africa. Input from the two African source areas to the DIB was interpreted to document repetitive shifts in the position of the Inter-Tropical–Convergence Zone (ITCZ) leading to a succession of drier and wetter climate periods over western Africa. Following that depositional model, wet periods of the climate cycle were intimately linked to black shale deposition in the DIB, slightly preceding maximum organic carbon burial rates by less than 1000 years (Beckmann et al., 2005). This time relation suggests that marine sedimentation reacted to rather than triggered atmospheric circulation and hydrologic cycling, at least in the tropical Atlantic.

The bulk composition of organic matter (OM) was studied by Oboh-Ikuenobe et al. (1998), Wagner and Pletsch (1999), and Beckmann et al. (2005) using palynology, carbon isotopes of bulk OM, Hydrogen Index (HI) and Oxygen Index (OI) from Rock-Eval Pyrolysis, and organic petrology (maceral distribution). Accordingly, bulk OM is of hydrogen-rich type I/II kerogen in the TOC-rich black shale with fluorescent, amorphous OM and some contribution of structured alginite. In sediments with baseline TOC more oxygen-enriched but hydrogen-depleted type II/III kerogen dominates. Generally, there is no indication for a substantial contribution of terrigenous OM. The observed changes in OM composition are cyclic and seem to relate more to gradual fluctuations in OM preservation (anoxia to weak dysoxia) rather than terrigenous dilution.

4.4 Materials and Methods

High-resolution sampling was performed continuously at one cm spacing. To accommodate the higher amount of sample material required for biomarker investigations, samples used in this study were taken from two types of lithology, laminated black shale or more homogenous interbeds. Biomarker samples in the section below 1037 mbsf integrate over 8-22 cm, equivalent to ~4-163 kyrs. Above, biomarker samples represent 10-40 cm, equivalent to about ~2.8-7.7 kyrs. Biomarkers were studied in 23 sediment samples.

To accommodate the new biomarker data from sections above those introduced in the previous publications, this study presents new bulk geochemical records (TOC, K/Al, Si/Al, redox-sensitive elements) from the transition between nannofossil zones CC15/CC16 at 1029 mbsf up to 1024 mbsf, well in the Late Santonian nannofossil zone CC16.

Analyses of bulk parameters [TOC, T_{max}] were performed on freeze-dried and homogenized material from both sets of samples using Leco CS 300 and Rock Eval 6 instruments, employing duplicate measurements every fifth sample. Precision is ±3% for the Leco analysis and ±4% for Rock Eval Pyrolysis. Extraction and further processing of sediment samples for biomarker analyses was conducted on about 10g of freeze-dried and homogenized sample material at the MBT Department of the NIOZ (Netherlands) following standard laboratory procedures. Samples were extracted with an Accelerated Solvent Extractor, ASE [temperature: 100°C; pressure: 100psi; solvent: dichloromethane (DCM):MeOH: 9:1v/v]. A weighed aliquot of the extract (6-86 mg) was separated by column chromatography (Al_2O_3) into an apolar and a polar fraction by elution of *n*-hexane/DCM (9:1 v/v) and DCM/methanol (1:1v/v), respectively. A known amount of standard (2,3-dimethyl-5-[1',1'-d2-hexadecyl] thiophene) was added to both fractions enabling quantitative analysis of biomarkers. Polar fractions were desulfurized with Raney Ni (Sinninghe Damsté et al., 1990b). The released hydrocarbons were isolated from the desulfurized polar fraction by column chromatography using activated alumina and hexane/DCM (9:1v/v) as the eluent and the apolar fractions obtained were subsequently hydrogenated (Sinninghe Damsté et al.,

1990a). Analyses of the apolar fractions and desulfurized polar fractions were conducted using gas chromatography (GC, HP 5890 equipped with an on-column injector, and flame ionisation [FID]) and sulfur-selective flame photometric [FPD] detectors) followed by gas chromatography-mass spectrometry (GC-MS, HP 5890 interfaced to a VG Autospec Ultima mass spectrometer operated at 70 eV with a mass range m/z 50-800 and a cycle time of 1.8s). Biomarkers were quantified by integration of peaks in mass chromatograms of characteristic major fragment ions (*m/z* 57 for saturated hydrocarbons; *m/z* 217 for steranes; *m/z* 191 for hopanes; *m/z* 367 for hopenes; *m/z* 133+134 for isorenieratene derivatives). Corrections were made to account for the individual intensity of the fragment ions used in their mass spectra relative to that of the internal standard.

Taking advantage of the orbitally-tuned cyclostratigraphic age model for Site 959 presented by Hofmann et al. (2003), bulk TOC, redox-sensitive element, and biomarker data are presented as accumulation rates of individual compounds in $g.m^{-2}.yr^{-1}$ and $\mu g.m^{-2}.yr^{-1}$, respectively. Corresponding percentages of organic carbon and absolute concentrations of organic compounds relative to TOC (µg/TOC) are available as supplementary information at www.pangaea.de.

4.5 Results

4.5.1 Cycle pattern of bulk parameters and continuation of cyclostratigraphy

K/Al and total organic carbon (TOC) profiles maintain their cyclicity between 1029 mbsf and 1024 mbsf, similar to the previously reported early Coniacian through late Santonian nannofossil zones CC13-CC15 (Hofmann et al., 2003) (Figure 2a-c). Si/Al, in contrast steeply increases in nannofossil zone CC16, thereby losing its distinct cyclic pattern. Maxima in TOC concentrations gradually decrease below 4% at 1027-1026 mbsf in nannofossil zone CC16. Highest concentrations of up to 18% have been described from the lower part of nannofossil subzone CC15a by Hofmann et al. (2003) (Figure 2a). Notably, TOC peaks increase in the uppermost part of the profile approaching values as high as 10% between 1025 and 1025.7 mbsf. Baseline TOC values are <1% in nannofossil zone CC16. They gradually increase up to ~4% in nannofossil subzone CC15a with depth. Integrated biomarker samples reveal TOC values that range from 13% to 3% and are thus representative samples for peak and background sedimentation. Spacing of TOC cycles varies due to a gradual but large change in linear sedimentation rates (LSR, Figure 2d). LSR in nannofossil zone CC16 remain moderate at ~2cm/ky except for minor excursions. These data are part of a long-term cycle with highest rates of ~4cm/ky in cycle 15 at ~1043 mbsf that generally decrease toward the base of nannofossil zone CC15 at ~1042 mbsf.

To assign ages and accumulation rates to the new bulk data we applied a similar tuning approach as used by Hofmann et al. (2003), defining cycle boundaries based on minimum

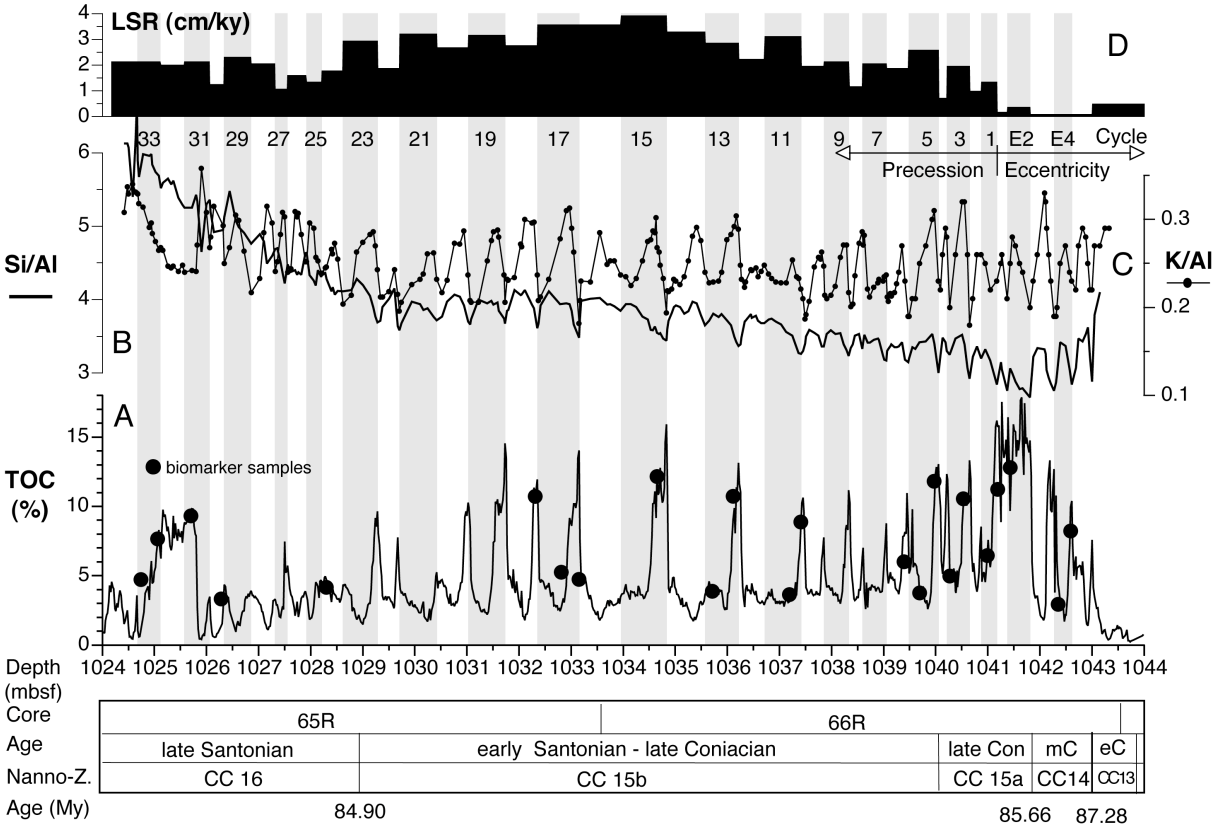

Fig. 2: Cyclic fluctuations of **(a)** the total organic carbon (TOC) content, **(b)** the Si/Al and **(c)** the K/Al ratios with depth for middle Coniacian through late Santonian nannofossil zones CC 14, CC 15 and partly CC 16 at ODP Site 959. Filled circles in (A) indicate position and TOC content of integrated samples selected for biomarker studies presented in this study. All data from nannofossil zone CC 15 were adapted from Hofmann et al. (2003). Ages and nannofossil zones and subzones from Watkins et al. (1998); age dates provided by Hardenbol et al. (1998). The age model, indicated by grey bars representing orbital cycles, is based on the approach proposed by Hofmann et al. (2003) using orbital tuning of the proxy records and subsequent calculation of linear sedimentation rates (D). Sedimentation rates are calculated linear over each orbital cycle, with (?) three long eccentricity cycles of 421 kry each (E3-E5) at the base followed by two short eccentricity cycles of 123 kyrs (E1-E2) and 34 precession cycles of 22.5 kyrs each (1-34). Note that biomarker samples in most cases were taken from adjacent TOC-rich and TOC-lean beds, both belonging to one orbital cycle.

values of continental proxies (K/Al, Si/Al) and assigning chronological ages to the respective nannofossil zonal boundaries following the absolute age dates of Hardenbol et al. (1998). The assignment of cycle boundaries and subsequent orbital tuning in nannofossil zone CC16 is primarily based on K/Al due to its clear cyclic pattern (Figure 2c). Apart from an average thinning of cycles in nannofossil zone CC16 orbital pacing is assumed to remain similar as in nannofossil zone CC15. Consequently, 33 precessional cycles of 22.5 ky each (Berger et al., 1992) were identified in nannofossil zones CC15 and CC16. Hofmann et al. (2003) did not specify orbital frequencies below two short eccentricity cycles at the base of nannofossil subzone accumulation section of nannofossil zones CC13 and CC14. The definition of cycles in these zones is problematic and preliminary, taking three sedimentary cycles (E3-E5) and a total duration of ~1.62 My for nannofossil zone CC14 (Hardenbol et al., 1998; Watkins et al., 1998) into account. We speculate that E3-E5 represent long eccentricity cycles. The

geological context at Site 959 (Pletsch et al., 2001) makes it reasonable to assume increasing condensation and thus lower sedimentation rates in nannofossil zones CC13 and CC14. Adding all eccentricity and precessional cycles of the record, the entire section presented covers a time span of ~2.4 Myr.

4.5.2 Bulk organic matter accumulation, composition and maturation

Accumulation rates of bulk organic carbon (AR TOC) have been presented for zone CC15 by Beckmann et al. (2005). Over the entire record (nannofossil subzone CC13b to nannofossil zone CC16) they reveal large amplitudes that range from peak values of ~12 gC.m-2.yr-1 at ~85.1 Ma in cycle 15 to almost zero at 84.75 Ma in cycle 30 (Figure 3a). Two superimposed longer cycles are recognizable, one from ~85.7 to 85.25 Ma (~450 kyr, upper nannofossil subzone CC15a to lower nannofossil subzone CC15b) and a second from 85.25 to ~84.85 (~400 Kyr, lower nannofossil subzone CC15b to lower nannofossil zone CC16) suggesting the expression of the long eccentricity band.

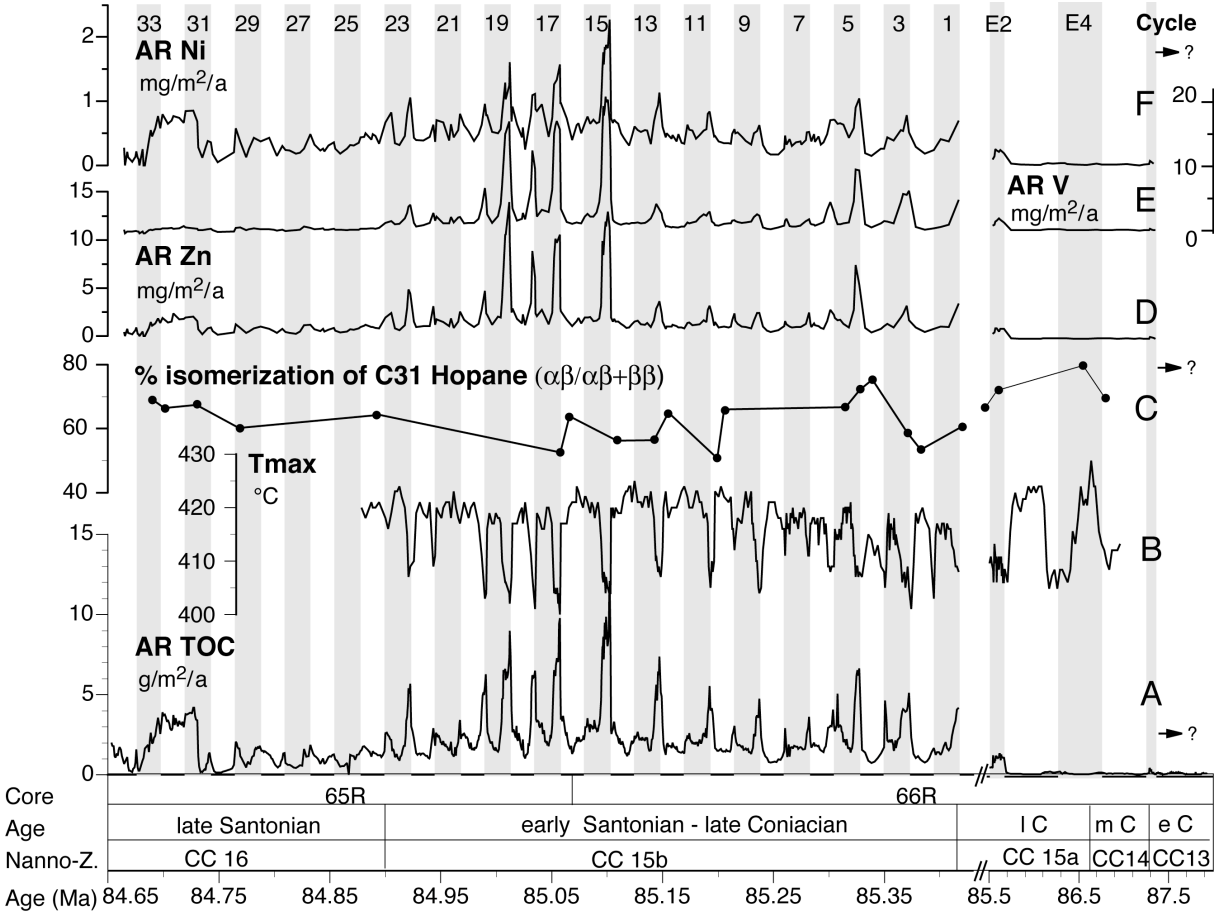

Fig. 3: Time series of total organic carbon ARs **(a)**, T_{max} obtained from Rock-Eval analysis **(b)**, degree of hopane isomerization **(c)**, and ARs of the redox-sensitive elements Zn **(d)**, V **(e)** and Ni **(f)** for nannofossil zones 14 through 16 at Site 959. Data on accumulation of OC within zone CC 15 are adopted from Beckmann et al. (2005). The assignment of orbital cycles is as in figure 1.

Biomarkers support a primary marine origin of sedimentary OM at Site 959 as concluded from previous bulk palynological (Oboh-Ikuenobe et al., 1998) and geochemical studies (Wagner and Pletsch, 1999; Beckmann et al., 2005). Diagnostic terrestrial biomarkers are absent and generally a low odd-over-even carbon number predominance in the C_{27}-C_{32} *n*-alkane range (CPI=1-2.5) is observed, supporting a relatively low to moderate contribution of terrestrial *n*-alkanes. CPI values show little variation throughout the record and do not correlate with changes in TOC.

The thermal maturity of the OM as determined by Rock Eval pyrolysis derived T_{max} reveals immature conditions with respect to hydrocarbon generation [T_{max} <425°C, Figure 3b). T_{max} is drastically depressed to values between 400-410°C in kerogen-type I/II black shales deposited at peak TOC ARs, a feature that is well known in the presence of high amounts of labile, marine OM (Tyson, 1995) but may also be an expression of the interaction of the kerogen fraction with the fine-grained mineral phase (Espitalié et al., 1984; Whelan and Thompson-Rizer, 1993), the increasing cross-link density of kerogen with increasing maturity (Larsen et al., 2002), or the sulfur-richness of the kerogen (Eglinton et al., 1990). Slightly more advanced levels of isomerization of 17ß, 21ß(H)-hopanoids (50-70 for %ßß for the C_{31} hopanes, Figure 3c) than reported for most OAE-2 black shales from the low latitude Atlantic (73-93 for %ßß C_{31}) (Sinninghe Damsté and Köster, 1998) is observed at Site 959. This is consistent with T_{max} data. The OAE-2 black shales biomarker records have been shown to provide excellent results (Kuypers et al., 2002).

4.5.3 Inorganic geochemistry

In order to assess the trace-metal enrichment as a proxy for bottom water anoxia at Site 959 accumulation of Zn, V, and Ni is considered (Figure 3d-f). These records use element data that have been reported for nannofossil zone CC15 by Beckmann et al. (2005). Accumulation of Zn, V, and Ni range from almost zero in background sediments to ~14, 20 and 2.5 $mg.m^{-2}.yr^{-1}$ at peak TOC AR and show almost identical records that match well with that of TOC in cycles 3-5 and 13-19 (Figure 3a). In contrast to patterns in nannofossil zone CC15, accumulation of V does not follow the positive trend of Z, Ni, and TOC in cycles 31-33 at the top of the record.

4.5.4 Biomarkers

The abundance of the C_{40} tail-to-tail isoprenoid lycopane (Brassell et al., 1981; McCaffrey et al., 1990; Freeman et al., 1994; Schouten et al., 2000a) relative to the series of *n*-alkanes is a characteristic feature of the saturated HC fractions of Site 959 sediments, especially those intervals of peak TOC accumulation rates. In a recent study, Sinninghe Damsté et al. (2003) reevaluated the origin of lycopane and advocated the use of the

lycopane/C_{31} *n*-alkane ratio as a proxy to assess redox conditions in ancient sediments. Analyses of the OAE-3 samples from Site 959 did not achieve quantitative gas chromatographic separation of lycopane and the C_{35} *n*-alkane as recognized previously (Farrington et al., 1988). We therefore developed a minimum approximation of the lycopane/*n*-C_{31} ratio by estimating the relative abundance of the C_{35} *n*-alkane and calculating the relative abundance of lycopane by quantifying the peak representing the co-eluting lycopane and *n*-C_{35} and subtracting the contribution of *n*-C_{35}. The relative abundance of *n*-C_{35} in a typical distribution of *n*-alkanes is <50% of the abundance of the n-C_{33}. Therefore, the amount equivalent to 50% of the *n*-C_{33} was substracted from the lycopane/*n*-C_{35} peak. At Site 959 the lycopane/*n*-C_{31} ratios vary from 0-2.3 (Figure 4b), comparable to values reported for the Holocene NE-Arabian Sea. Notably, in cycles 3-5 and 15-17 there is a clear positive relation between this ratio and AR TOC. In the TOC-rich sections of cycles E1-E4 and 29-33 the amplitude in the lycopane/C_{31} *n*-alkane record decreases but remains recognizable.

The position of the chemocline in the lower photic zone can be reconstructed from the presence of highly specific biomarkers, isorenieratene derivatives, in the sedimentary record (Sinninghe Damsté et al., 1993; 2001). The aromatic carotenoids, isorenieratene and chlorobactene originate from different strains of photosynthetic green sulfur bacteria (Chlorobiaceae) that thrive near the sulfide-oxygen interface of the chemocline at light levels of less than 1% of surface irradiance (van Gemerden and Mas, 1995) in the lower photic zone (Madigan et al., 2000) and are most sensitive to oxic exposure (Koopmans et al., 1996). Isorenieratane and chlorobactane were both identified in desulfurised polar fractions of OAE-3 black shales at Site 959. At Site 959, the highest ARs approaching 3.4 $\mu g.m^{-2}.yr^{-1}$ for isorenieratane and 5.3 $\mu g.m^{-2}.yr^{-1}$ for chlorobactane were found in cycles 13 and 15, parallel to highest accumulation of TOC (Figure 4C). ARs are almost half of these maximum values in black shale units from cycles 3 and 5 that mark the center of the first period of enhanced AR TOC. Notably, these diagnostic biomarkers were neither found in any of the studied sediments with low, background TOC ARs nor in the TOC-rich black shales of cycles 29-33 in nannofossil zone CC16.

C_{25} and C_{30} highly branched isoprenoid (HBI) alkanes and alkenes serve as diagnostic biomarkers for their marine precursors, i.e. diatoms (e.g., Rowland and Robson, 1990; Volkman et al., 1994; Sinninghe Damsté et al., 1999). They are known to be biomarkers produced in the upwelling season in the modern Arabian Sea (Prahl et al., 2000; Wakeham et al., 2002) and, therefore, are likely to be indicators of high nutrient levels that favor siliceous plankton. In the geological record, HBIs are reported from the Holocene back to Upper Cretaceous, both in sediments (Kohnen et al., 1990; Köster et al., 1998) and crude oils (Sinninghe Damsté et al., 1989). At Site 959 highest ARs of C_{25} HBI were detected in the apolar fractions. ARs vary from 8-813 $\mu g.m^{-2}.yr^{-1}$ with the highest values co-occurring with the peak in AR TOC in cycle 15, followed by two minor increases in cycle 17 and cycle 31 (Figure 4d). The C_{25} HBI alkane is almost absent in the desulfurized polar fraction.

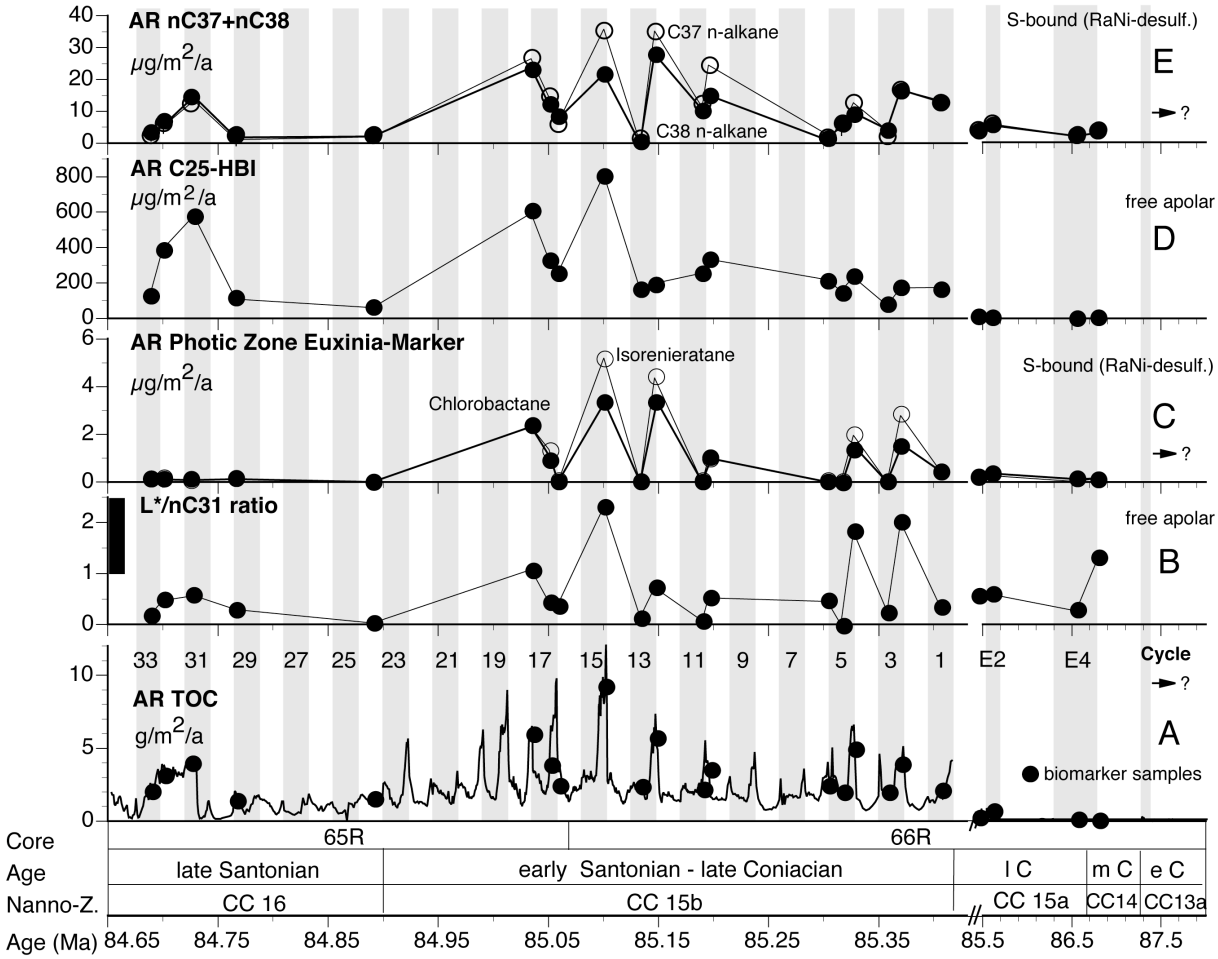

Fig. 4: Time series of TOC **(a)** and biomarker accumulation for nannofossil zones CC14-16 at Site 959 providing information about the degree of oxygen depletion in the water column (b, c) and the community of primary producers that thrived in the oxic photic zone (d, e). **(b)** Profile of the bottom water redox proxy, the lycopane/n-C_{31} ratio (for estimation of lycopane see explanations in the text). Black bar indicates range of values reported for the low-oxygenated Holocene Arabian Sea (Sinninghe Damsté et al., 2003). **(c)** ARs of biomarkers for photic zone euxinia, i.e. Isorenieratane and Chlocobactane, both derived from photosynthetic green sulfur bacteria, suggesting repetitive penetration of sulfidic conditions in the lower photic zone. Note the close relation of PZE-markers in cycles 3-5 and 15-17 to peaks in OC accumulation and elevated lycopane/n-C_{31} ratios supporting the conclusion of deep-water anoxia during black shale conditions. **(d)** AR of the C_{25} highly branched isoprenoid HBI alkane, likely originating from biosiliceous primary producers, i.e. diatoms, and **(e)** AR of sulfur-bound saturated C_{37}/C_{38} *n*-alkanes, probably derived from unsaturated alkenones and thus representing a calcareous nannoplankton record from the upper Creatceous upper water column. The assignment of orbital cycles is as in figure 1.

At Site 959, C_{37} and C_{38} *n*-alkanes were found in desulfurized polar fraction with ARs ranging from 0-36 $\mu g.m^{-2}.yr^{-1}$ (Figure 4e). These values were substantially higher than for the other n-alkanes in the C_{35}-C_{40} range, suggesting an origin from S-bound alkenones (e.g., Koopmans et al.,1997; Grice et al., 1998). ARs of C_{37}/C_{38} *n*-alkanes follow the general pattern of TOC AR (Figure 4a) with highest rates during peak black shale deposition in cycles 10 through 17, and almost parallel the C_{25} HBI alkane profile (Figure 4d). Many studies have proven that natural sulfurization, the reaction of reduced inorganic sulfur with functionalised lipids, may result in sequestration of carbon skeletons into macromolecular fractions (e.g.,

Sinninghe Damsté and de Leeuw, 1990). To support the idea that sulfur-bound C_{37} and C_{38} aliphatic skeletons in sediments at Site 959 originally derived from unsaturated alkenones and thus represent a calcareous nannoplankton record we consider the absolute abundance normalized to TOC of both components (Figure 5a). These TOC-normalized abundances are highly correlated (r^2=0.93) as would be expected if both were biosynthesized by one algal species. This correlation, however, may well be an effect of sulfurization itself. Indeed, correlation of the ARs of S-bound n-C_{37} to other S-bound biomarkers, e.g. phytane and the C_{35} hopane, reveal fairly high covariation (r^2 = 0.71 and 0.54, respectively; Figures 5b-c) that may not be expected in view of their different origins. To compensate for the effect of early sulfurization these four components normalized to the sum of all components from the desulfurized fraction were assessed and compared in terms of their remaining relationships. Notably, the relation between C_{37} and C_{38} *n*-alkanes remains high (r^2=0.74; Figure 5d), thereby supporting a common origin, whereas there is no significant correlation with phytane and the C_{35} hopane (Figure 5e-f). The observed C_{37} and C_{38} *n*-alkanes at Site 959 thus most likely originate from calcareous nannoplankton that grew in the oxic upper part of the photic zone.

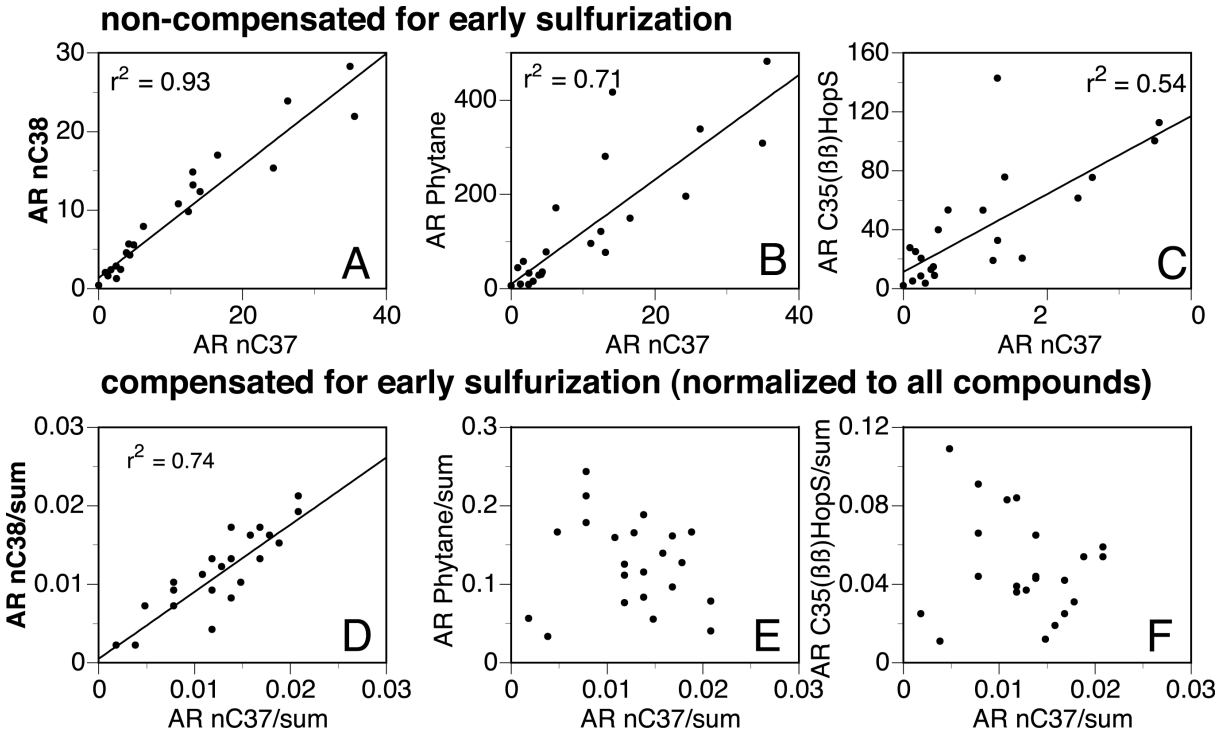

Fig. 5: Relationships of C_{37} and C_{38} *n*-alkanes of probable alkenone origin with two other prominent organic compounds of the desulfurized fractions, i.e. phytane and C_{35} hopane.

4.6 Discussion

4.6.1 Bottom water redox conditions in the Coniacian-Santonian DIB

In view that regional Cretaceous OAEs (OAE 1b, OAE 1d, OAE 1c, OAE 3) have been less widespread and therefore less extreme in global environmental impact than their global counterparts (OAE 1a, OAE 2) (e.g. Jenkyns, 2003; Leckie et al., 2002), the biomarker records from OAE 3 black shale at Site 959 provide new insights. At Site 959, lycopane/ *n*-C_{31} ratios approach the highest values parallel to maxima in the accumulation of OC, V, Zn and Ni. Accordingly, bottom water anoxia supported better preservation of labile OM, similar to many other OAE black shale settings (Brumsack, 1986; Kuypers et al., 2002). The highest trace metal contents at Site 959 generally exceed those of sapropels from the Black Sea and in cycles 15-19 with highest OC accumulation the trace metal concentrations are comparable to those reported from "average CT OAE-2 black shales" (Brumsack, 1991, 1988) and Pliocene Mediterranean Sapropels (Passier et al., 1999). The observed enrichment in redox-sensitive trace metals in combination with Fe-TOC-S relationships have been used to propose that sediment pore waters at Site 959 were anaerobic for most of nannofossil zones CC15, e.g., cycles 5-23 (Beckmann et al., 2005) and CC16. Strictly anoxic conditions probably extended periodically into the bottom water when highest TOC and trace-metal AR took place leading to the formation of laminated sediments. During background TOC AR depositional conditions changed drastically to suboxic and maybe occasionally even oxic bottom water conditions allowing bottom dwelling organisms to recolonize the seafloor and bioturbate the uppermost sediment layers. This interpretation is supported by PZE markers from the upper water column.

4.6.2 Surface water redox conditions and primary producers

Isorenieratane and Chlorobactane in Site 959 black shales define the most extreme redox end-member in the DIB that likely repeatedly graded to more ventilated conditions on orbital (precessional) time scale. These records suggest for an upward migration of the chemocline into the lower photic zone (~50-120 m water depth), at least temporary, if modern Black Sea conditions are considered to be representative of partly restricted Cretaceous ocean basins. Notably, modern high productivity areas along continental margins rarely contain free sulfide and thus do not support habitats for green sulfur bacteria. Free sulfide has in a few exceptional cases been reported from intermediate waters of the expanded OMZs of the Arabian Sea (Brumsack, 1986), the Pakistan shelf (Naqvi et al., 2001), and the Namibian high productive area (Brüchert et al., 2003). However, PZE markers have so far not been reported for these sites.

Comparison of maximum ARs of 3.4 $\mu g.m^{-2}.yr^{-1}$ for isorenieratane and 5.3 $\mu g.m^{-2}.yr^{-1}$ for chlorobactane, respectively, at Site 959 with other OAE-2 black shale sites reveal that they are in the same order of magnitude as those reported from N Atlantic deep-sea sections, e.g. ~9 $\mu g.m^{-2}.yr^{-1}$ at DSDP Site 603B off North America (Sinninghe Damsté and Köster, 1998; Kuypers et al., 2002), but considerably lower than those estimated for the southern N Atlantic, e.g., ~1000 $\mu g.m^{-2}.yr^{-1}$ at DSDP 367 from the Cape Verde area (Sinninghe Damsté and Köster, 1998; Kuypers et al., 2002) and up to 6000 $\mu g.m^{-2}.yr^{-1}$ in the central part of the Tarfaya shelf basin at exploration well S13 (Kolonic et al., subm.), and the Pliocene Mediterranean sapropels (3000 $\mu g.m^{-2}.yr^{-1}$) (Menzel et al., 2002). Direct comparison with ARs from the Mediterranean sapropels, however, is hardly possible due to the effect of diagenesis on intact carotenoids.

Euxinic conditions in the Coniacian-Santonian DIB must have been highly unstable and sensitive to any admixture of oxygenated water from the open Equatorial Atlantic south of the marginal ridge. Given the broad spectrum of time estimates for the duration of PZE between ~2.8 kyr to 163 kyr, it is not possible to assess the relative timing of calcareous and siliceous primary production as evidenced by the presence of highly branched isoprenoids (HBIs) and and alkenone-derived organic compounds. Both, however, support a more ventilated oxic photic zone relative to periods of euxinia in the lower photic zone. From a modern oceanographic perspective they may represent repetitive (seasonal?) successions of more oligotrophic mainly calcareous production that change into peak siliceous production, perhaps stimulated by enhanced riverine nutrient supply during more humid conditions in tropical West Africa. Both freshwater supply and enhanced oxygen consumption from degradation of settling labile OM should have fostered expansion of an OMZ, stratification of the water column and progressive upward poisoning of the water column by free sulfide, finally leading to optimal conditions for black shale formation.

Deposition of OAE-3 black shales in the Cretaceous DIB was fostered by, but not restricted to, euxinic conditions. Notably, black shales are well documented in the late Santonian zone CC16 (cycles 23-33), a period when the marginal ridge progressively subsided from middle to lower bathyal to its modern water depth (Holbourn et al., 1999) and where no isorenieratane derivatives were found. Bottom waters were likely oxygen depleted during this late period but not as severe as in nannofossil subzone CC15b, as suggested by moderately elevated lycopane/n-C_{31} ratios and slightly enhanced accumulation of Zn and Ni in nannofossil zone CC16. Both elements were probably precipitated in the presence of free dissolved sulphide (Calvert and Pedersen, 1993). Redox conditions still supported sulfur-linked sequestration of organic compounds based on the presence of sulfur-bound C_{37}/C_{38} *n*-alkanes but apparently inhibited substantial fixation of V to organic matter, e.g. by complexation to porphyrines (Lewan and Maynard, 1982; Breit and Wanty, 1991).

4.6.3 Paleoceanographic implications

The deposition of black shales during the OAE-3 likely occurred in areas with restricted circulation such as sheltered sub-basins along the upper continental margin where redox conditions and primary productivity were suitable to sustain enhanced OC burial over longer time periods. Due to its tectono-sedimentary position the DIB serves as an excellent example of such a preconditioned setting (Wagner and Pletsch, 1999). We hypothesize that short-term photic zone euxinia was not a local phenomenon confined to the position of Site 959 but periodically affected larger areas of the tropical West African continental margin and may also have existed along the conjugate tropical South American margin. This hypothesis can be tested by detailed reinvestigation of time equivalent black shales from the South American marginal basins (Mello et al., 1995) and the Demerara Rise (Shipboard Scientific Party ODP Leg 207, 2002). Various studies have shown widespread anoxic conditions along the low latitude South American margin with black shales deposited during the OAE-2 and, at least locally, throughout the Santonian (e.g., the Venezuelan La Luna and Querecual Formations) (Mongenot et al., 1996; Perez-Infante et al., 1996; Alberdi-Genolet and Tocco, 1999; Davis et al., 1999; Erlich et al., 1999; Cotillon et al., 2000). The geochemical data reported from these sub-basins, though, are not sufficient in time resolution to precisely compare them with the records from Site 959. Nevertheless, if short-term photic zone euxinia was a common phenomenon in the tropical Atlantic we assume that this area was a primary sink of OC during the OAE-3 and thus a key site of CO_2 drawdown from the atmosphere.

There is no identical modern analog for the environments during deposition of black shales at Site 959. The closest match may be the Quaternary Cariaco Trench off Venezuela. This setting is tectonically isolated and repeatedly went anoxic in response to fluctuations in riverine supply (e.g. Dean et al., 1999; Haug et al., 2001). Different from Site 959, the Cariaco Trench was strongly influenced by sea level fluctuations (Peterson et al., 2000).

4.7 Conclusions

The molecular and bulk geochemical data of OAE-3 sections from Site 959 support a highly dynamic Cretaceous climate-ocean system that had a major impact on the structure and redox conditions of Equatorial Atlantic surface waters during peak greenhouse conditions. They even imply that chemical boundary conditions in the ocean have been as extreme as during the global OAE-2, although much more restricted in extent and duration.

The proposition of a short-living but larger scale belt of PZE along West-Africa may not have been expected taking into account that the opening of the Cretaceous Equatorial Atlantic Gateway was far advanced during Coniacian-Santonian times, probably as wide as ~550 km at its narrowest point between western Ivory Coast and northeastern Brazil (Jones et al., 1995). During the Coniacian-Santonian a free exchange of deep and surface water masses

between the South and North Atlantic basins has to be considered (Wagner and Pletsch, 1999; Pletsch et al., 2001), somehow comparable to the modern ocean circulation.

We suspect that the low latitude Coniacian-Santonian Atlantic acted as a prominent sink for OC, and consequently atmospheric CO_2. That way, organic carbon burial in the tropics may have been a major cause of the moderate positive excursion in $\delta^{13}C$ documented in higher latitude carbonaceous records.

4.8 Acknowledgments

This study was funded by the Deutsche Forschungsgemeinschaft [Ocean Drilling Program, grant Wa1036/7 and 8, and Ho2188/1]. We thank Mark Leckie, Timothy Bralower, and one Associate Editor as reviewers, and Marcel Kuypers for valuable comments on a former version of this manuscript and the technical staff of the MBT department at NIOZ for their assistance as well as Dr. H. Wehner and G. Scheeder from the BGR-Hanover, Germany, for providing access and technical assistance to the Rock-Eval 6 instrument.

Chapter 5.

Orbital forcing of Cretaceous river discharge in tropical Africa and ocean response

Britta Beckmann[1], Sascha Flögel[2], Peter Hofmann[3], Michael Schulz[1,4] & Thomas Wagner[5]

[1] *Department of Geosciences, University of Bremen, Klagenfurter Str, 28357 Bremen, Germany*

[2] *IFM - GEOMAR Leibniz Institute of Marine Sciences, FB 1: Ocean circulation and climate dynamics, Wischhofstr. 1-3, 24148 Kiel, Germany*

[3] *Geological Institute, University of Cologne, Zülpicher Str. 49a, 50674 Köln, Germany*

[4] *Research Center Ocean Margins, University of Bremen, Leobener Str., 28357 Bremen, Germany*

[5] *School of Civil Engineering and Geosciences, University of Newcastle, Newcastle upon Tyne NE1 RU, UK*

Status: published **Journal:** Nature, v. 437, p. 241-244

5.1 Abstract

The tropics have been suggested as the drivers of global ocean and atmosphere circulation and biogeochemical cycling during the extreme warmth of the Cretaceous period (Wilson & Norris, 2001; Norris et al., 2002); but the links between orbital forcing, freshwater runoff and the biogeochemistry of continental margins in extreme greenhouse conditions are not fully understood. Here we present Cretaceous records of geochemical tracers for freshwater runoff obtained from a sediment core off the Ivory Coast that indicate that alternating periods of arid and humid African climate were driven by orbital precession. Our simulation of the precession-driven patterns of river discharge with a global climate model suggest that ocean anoxia and black shale sedimentation were directly caused by high river discharge, and occurred specifically when the northern equinox coincided with perihelion (the minimum distance between the Sun and the Earth). We conclude that, in a warm climate, the oceans off tropical continental margins respond rapidly and sensitively to even modest changes in river discharge.

5.2 Article

Intervals of extreme warmth and enhanced sequestration of marine organic carbon (OC), termed Oceanic Anoxic Events (OAEs), are one focus of current paleoclimate research. They provide fundamental information on the functioning of biogeochemical cycles and their feedbacks during extreme conditions, especially when applied to areas expected to react sensitive to climate change, that is, continental margins and their associated sub-basins. Deposits from the eastern tropical Atlantic at ODP Site 959 off Ivory Coast were obtained from such a setting (Fig. 1), providing a unique record of Coniacian to Campanian OC-rich sedimentation that covers the last of the Cretaceous OAEs (OAE 3). OAE 3 black shales have been reported from various basins surrounding the Atlantic and Tethyan Margin (Dean et al., 1984; Erlich et al., 1999; Rusk, 2001). Millennial-scale Coniacian to Santonian records from ODP Site 959 were used to develop a model for black shale formation in the tropical Atlantic (Hofmann et al., 2003). Additionally, records of quartz and clay mineralogy document Upper Cretaceous atmospheric circulation that triggered latitudinal shifts of Africa climate belts. The records further imply that black shales formed in response to tropical continental discharge that induced stratification and reversals in oceanic circulation within the Deep Ivorian Basin (Hofmann et al., 2003). Synchronous variations in trace metals (Beckmann et al., 2005) and biomarkers of green sulfur bacteria (Wagner et al., 2004) further provide evidence for severe variations in redox conditions, with brief intervals of lower photic zone euxinia (Wagner et al., 2004). Here we present records that double the stratigraphic range of the previous profiles into the lower Campanian, allowing the deduction of long-term trends and shorter-scale variations in the tropical atmosphere-ocean system across one of the most important transitions in global climate over the past 150 Ma.

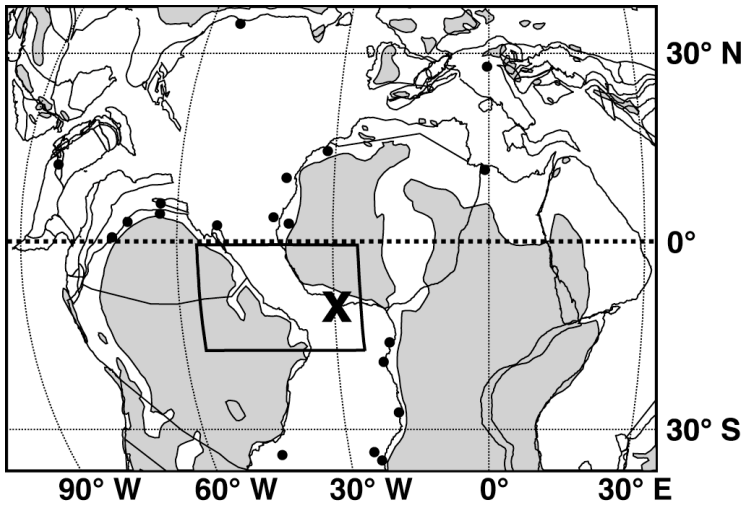

Fig. 1: Location of OAE 3 sites and investigated region for simulated river discharge. ODP Site 959 marked by **X**; dots indicate other reported OAE 3 sites (Wagner et al., 2004); black box marks investigated region for simulated river discharge. All information is superimposed on the paleogeographic map of the Upper Cretaceous at ~80 Ma (Hay et al., 1999). Grey shaded areas represent land masses.

Coniacian-Campanian African climate variability is evident from fluctuations of K/Al and Ti/Al (Fig. 2a, b). Al is mainly confined to the fine-grained aluminosilicate fraction (Calvert, 1976), typically enriched in kaolinite, smectite and iron hydroxides (Zabel et al.,

2001), and formed by intense chemical weathering under warm and humid conditions. K is associated with continental siliciclastics (that is, clay minerals and feldspar) that experienced only moderate amounts of chemical alteration (Diester-Haass & Chamley, 1993). Ti is concentrated in heavy minerals and often transported via eolian pathways into marine sediments (Yarincik et al., 2000). In agreement with vegetation simulations for the Campanian (DeConto et al., 1999), the source for Ti is assigned to desert areas of the proto-Kalahari in southern Africa, while K is associated with illite and K-feldspar derived from semi-arid tropical regions. Al from kaolinite and smectite is indicative of tropical weathering in equatorial northern Africa (Hofmann et al., 2003; Zabel et al., 2001; Yarincik et al., 2000). The persistent cyclicity of climate tracers at Site 959 documents that Upper Cretaceous climate was highly variable and modulated at different time scales. The average K/Al record exhibits a long-range increase towards the top of the profile (Fig. 2b). The progression in supply of detrital material from semi-arid regions supports a gradual aridification of Africa that started in the lower Santonian. The linearity of the complementary Ti/Al record proposes the existence of an arid proto-Kalahari in southern Africa remaining constant in extension and geographical position.

Time frequency analyses of the K/Al and Ti/Al records support the existence of one dominant period with ~1.3 m wavelength, equivalent to ~28 kyr in nannofossil biozone CC15. Given uncertainties in time control and sedimentation rate at Site 959, we conclude that this prominent periodicity lies close enough to 22 kyr to support the influence of precession. (Details of the time-frequency analysis are available as Supplementary Information.) Given the persistence of the dominant periodicity with respect to total organic carbon (TOC) burial across the core break above 1022.5 mbsf, we estimate 65 cycles for the entire section (1044-1005 mbsf), equivalent to ~1.46 Myr. Variance records of K/Al and Ti/Al reveal the evolution of African climate contrasts (Fig. 2c, d). High values document alternations between arid and humid conditions, and low values indicate more balanced climate. Above 1022.5 mbsf a robust patter consisting of 19 cycles emerges (Fig. 2c, d), corresponding to the ~400 kyr period. The variance records below 1022.5 mbsf show a frequency with a periodicity of ~315 kyrs (~14 cycles in total). This regularity is not attributable to the main orbital frequencies, and cannot easily be explained. We consider the manifestation of a 400 kyr periodicity to be the expression of a long-term drying/cooling cycle. The presence of long eccentricity and precession cycles supports Upper Cretaceous climate as having been dynamic and variable, comparable to that of the Quaternary.

A linkage of African continental climate with OC burial and oceanic productivity on a precession cycle level has been reported before (Hofmann et al., 2003; Wagner et al., 2004; Beckmann et al., 2005) and is evident when the Coniacian-Campanian OC record from Site 959 is compared to the Ti/Al and K/Al profiles. The section below 1024 mbsf displays a distinct cyclic, high-amplitude pattern (Wagner et al., 2004) that fades out towards the top owing to the progressive subsidence of Site 959 through time (Holbourn et al., 1999; Wagner

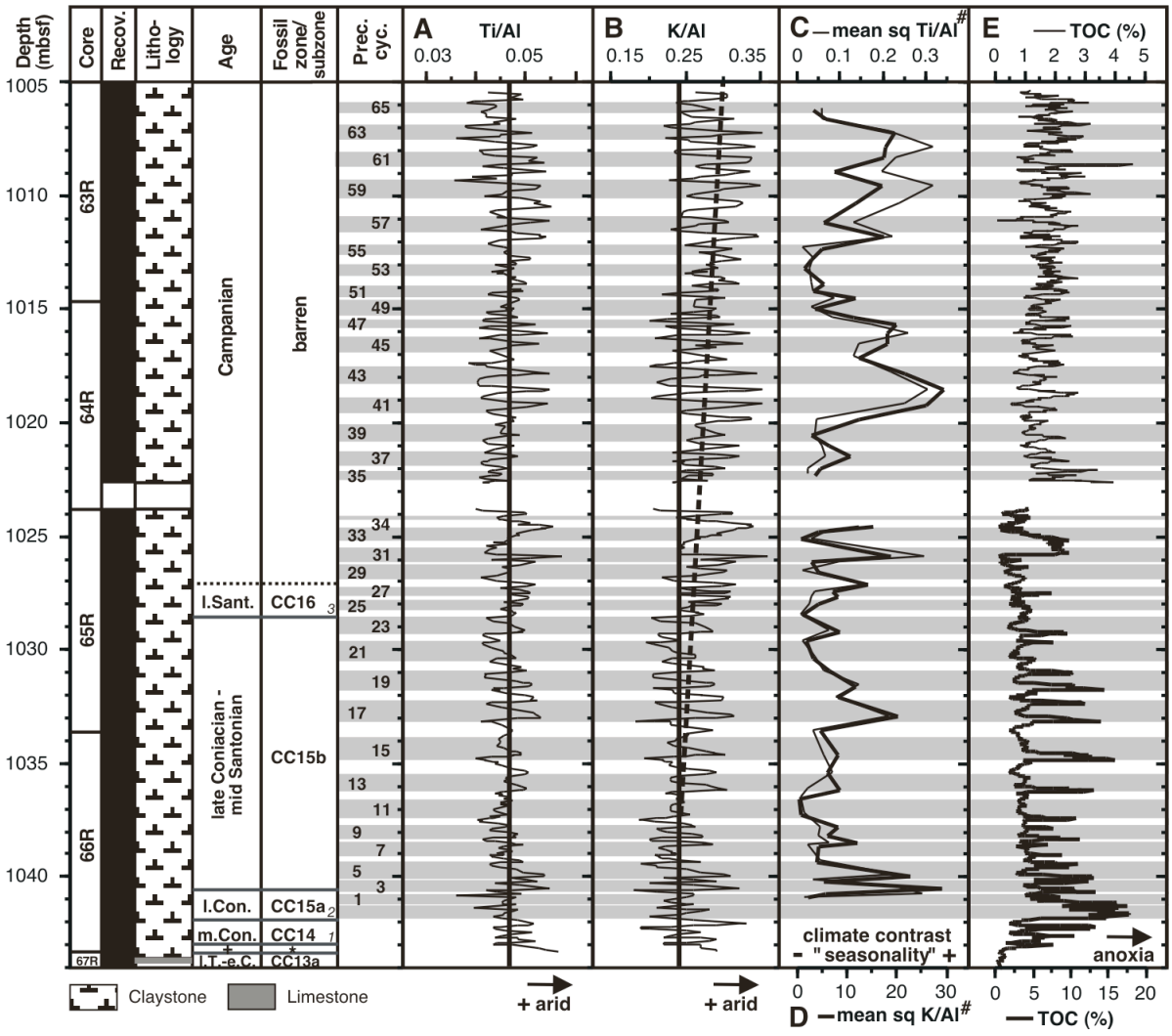

Fig. 2: Upper Cretaceous (Coniacian to Campanian) records from ODP Site 959. **(a)** Ti/Al ratio, average value indicated by solid black line. **(b)** K/Al ratio, average value for lower part of the profile indicated by solid line, mean values starting from 1034 mbsf, marked by dashed line. Both proxies (a, b) serve as a measure of fluctuations between tropical and arid climate conditions; higher values indicate greater aridity. **(c)** Mean square Ti/Al values (thin line). **(d)** Mean square K/Al values (heavy line). Both proxies (c, d) are calculated as the standard deviation from respective mean values for each precession cycle; higher values indicate greater seasonality, that is, more marked alternations between arid and humid conditions. **(e)** Total organic carbon content (TOC) in %; bottom axis refers to values below 1022.5 mbsf (heavy line); top axis refers to data above 1022.5 mbsf (thin line). Higher values (15-20%) indicate anoxia. Recov., recovery. Fossil zone/subzone and Age from Kuhnt et al. (1998) and Watkins et al. (1998); l. Sant. = late Santonian, l. Con. = late Coniacian, m. Con. = mid Coniacian, l. T. – e. C. = late Turonian to early Coniacian; + = early Coniacian; * = CC13b; absolute ages [25]; ***1*** = 87.2 Ma, ***2*** = 85.5 Ma, ***3*** = 84.8 Ma; # = value multiplied by 10^4. Precession cycles (numbered from bottom to top), below 1024 mbsf based on previous work (Hofmann et al., 2003, Wagner et al., 2004).

et al., 2002; Fig. 2e). Despite the decline in amplitudes, maxima in OC generally coincide with minima in K/Al and Ti/Al, that is, with periods of enhanced detrital input from tropical regions.

OC accumulation within individual cycles exhibits a distinct pattern (Fig. 2e) characterized by an initial sharp increase followed by a plateau and a gradual decrease. Only peak OC deposition was associated with the development of sea floor anoxia and photic zone euxinia (Wagner et al., 2004). A compilation of OC data from Late Coniacian-Mid Santonian nannofossil zone CC 15 reveals that maximum black shale sedimentation on average lasted for a quarter cycle, that is, ~5 kyr (Beckmann et al., 2005). The robustness of this pattern across the record points to an external control that caused episodic anoxic conditions in the tropical eastern Atlantic over more than one million years. A previous investigation (Hofmann et al., 2003) proposed that black shale formation was triggered by discharge of freshwater and nutrients to the semi-enclosed Deep Ivorian Basin (DIB) resulting in a circulation reversal and the development of ocean anoxia/euxinia (Hofmann et al., 2003; Wagner et al., 2004). Although less well constrained, a similar mechanism and long-term climate trend has been suggested for the conjugate South-American Maracaibo Basin during OAE 3 (Rey et al., 2004).

The implications from the records of Site 959 were validated using global climate model GENESIS v.2.0 (Thompson & Pollard, 1995). (Details of the model and experimental set-up of GENESIS v. 2.0 are available as Supplementary Information.) Five simulations with changing orbital configurations were conducted: a control run with no precession and four runs covering one precessional cycle, each shifting the closest annual approach of the Earth to the Sun (perihelion) into a different season.

Of specific relevance to the black shale mode is total freshwater discharge (TD). Previous simulations emphasized the importance of continental discharge for climate change and ocean response, for example, during the ice-free Early Eocene (Bice et al., 1997). All simulations performed in this study yielded a pronounced wet season in spring and early summer (March to June, Fig. 3) with enhanced TD accounting for 56 - 71 % of the total annual discharge (Table 1), and a dry season (July to February). Strongest seasonal contrasts occurred during orbital case A, representing the orbital configuration when spring is coincident with perihelion. Weakest contrasts are recognized for case C, suggesting most balanced conditions when perihelion coincided with autumn configuration. The two remaining orbital cases (B and D) describe “transitional” modes. During case A, total annual TD was elevated by about 43 % relative to case C. During the months of wettest conditions and largest divergence (March-June) TD was elevated by 79 % (~487 km^3/yr), but reduced by 27 % (~105 km^3/yr) during dry seasons (July-February) for case A relative to case C (Table 1).

The fluctuations in TD for orbital configurations A to D provide a robust mechanism to explain the observed pattern in ocean redox conditions and OC burial. Black shale formation apparently was restricted to case A, when maximum insolation (northern spring equinox is at perihelion) occurred during wet seasons, both fostering seasonal contrasts and massive spring TD (Fig. 3). These conditions apparently were not reached during orbital configurations B, C,

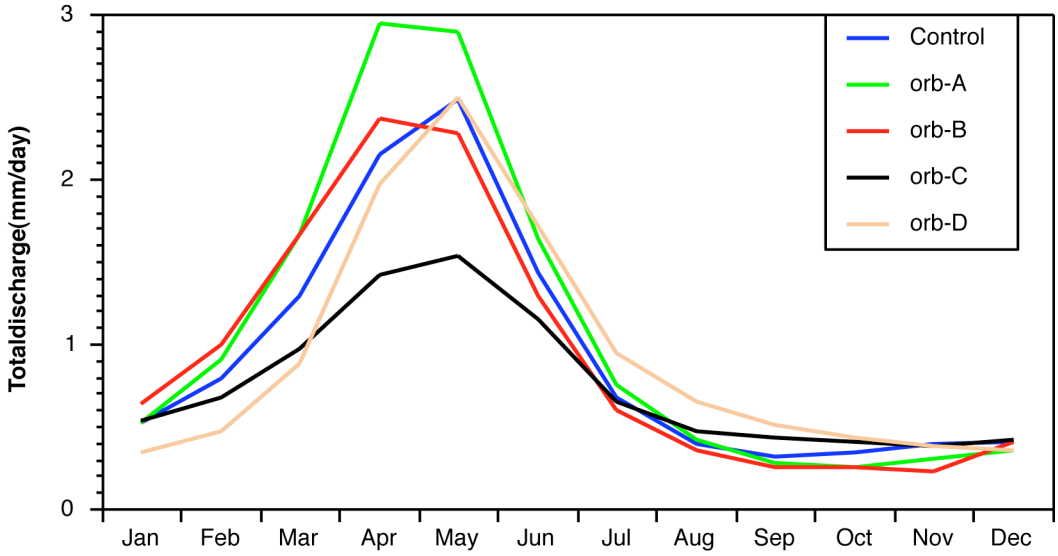

Fig. 3: Simulated total continental freshwater discharge over the course of one precession cycle (orbital cases A to D) compared to control run conditions. Total continental freshwater discharge (TD) was drastically enhanced during spring conditions (April-May), independent of orbital configuration. Highest levels of up to 3 mm/day were achieved during orbital configuration A (warm spring/cold autumn in the Northern Hemisphere), in parallel with strongest seasonal contrasts. From orbital case A to C climate contrast diminishes, resulting in more balanced cold spring/warm autumn conditions and a decrease in TD by about a factor of 2 during orbital case C. Orbital cases B and D represent transitional phases.

and D. The runoff data suggest that a threshold in excess of 125 km^3/yr was necessary to maintain a year-round or multi-year freshwater cap that triggered a reversal in ocean circulation in the DIB and a shift into a black shale mode. The estimated thickness of a freshwater cap ranges from 1.0 m during orbital case A to 0.7 m during orbital case C (Table 1), providing values comparable to the modern Black Sea (0.7 m; Vladimirov, 1999) but 2-3 times higher than for the modern Arctic Ocean (0.36 m; Alychunskaya & Ivanov, 1978). The direct linkage of African TD patterns and black shale formation in the DIB implies that fluctuations in ocean properties were short, i.e., on seasonal time-scales, but had a major effect on the Upper Cretaceous carbon cycle.

The results of this study demonstrate how sensitive and rapid tropical marine areas close to continental margins react even to relatively moderate increases in continental freshwater discharge. The freshwater threshold required to shift sheltered and semi-enclosed areas of the modern ocean into an anoxic mode are unknown, but the progressive emission of greenhouse gases to the modern atmosphere is gradually shifting Earth towards a greenhouse mode with an accelerated hydrological cycle. At present it is hardly possible to estimate where we are on that long-term climate trend, but once that threshold is passed, a substantial impact on biochemical cycling of continental margins may be expected.

Orbital case	perihelion at	Northern hemisphere	Seasonal contrasts	Total annual discharge in km^3/yr *(relative to Orb C)*	Wet season relative to annual discharge (%)	Wet season discharge in km^3/yr *(Mar-Jun)*	Dry season discharge in km^3/yr *(Jul-Feb)*	Thickness of annual freshwater lid in m
Orb A	northern spring equinox	warm spring/ cold autumn	maximum	1556 (+43%)	71	1101 (+79%)	288 (-27%)	1.00
Orb B	northern winter solstice	transitional	transitional	1365 (+25%)	67	917 (+49%)	276 (-30%)	0.88
Orb C	northern autumn equinox	cold spring/ warm autumn	minimum	1091 (0%)	56	614 (0%)	393 (0%)	0.70
Orb D	northern summer solstice	transitional	transitional	1343 (+23%)	63	851 (+39%)	407 (+4%)	0.86

Table 1 Simulated continental freshwater discharge for the investigated region. Analysed area was situated in tropical, Upper Cretaceous Africa and South-America (3,945,198.69 km^2); the resulting thickness of freshwater lid in the Equatorial Atlantic for all simulations expressed as total numbers in km^3/yr, relative proportions, and meters.

5.3 Acknowledgements

We thank the Ocean Drilling Program to provide the sample material and technical assistance. Helga Heilmann, Renate Henning, and Brit Kockisch (Bremen), Mrs Gölden, Sonja Berg, Almuth Katzemich, Stefan Reiss (Cologne), Mithun Aiyswaryan, Rüdiger Kunze (IFM-GEOMAR) and Dave Pollard (Pennsylvamia State University) are thanked for analytical assistance.

5.4 Methods

5.4.1 Original data

Site 959 was drilled during ODP Leg159 off Ivory Coast and Ghana at 3°37.656'N, 2°44.149'W in approximately 2100m water-depth. Samples were taken continuously in 1cm increments, dried at 35°C and homogenized before analysis. Determination of OC was performed after removal of inorganic carbon with 0.25N HCl on every other sample. Major element chemistry was determined by X-ray fluorescence analysis on samples with average spacing of every 8cm.

5.4.2 Cycle model

The cyclostratigraphic model for the record of Hole 959D between 1005.43 and 1046.09 mbsf is based on the analysis of geochemical cycles within the interval below 1022.5 mbsf, in particular on biozone CC15b (Hofmann et al., 2003). In this biozone, the number of cycles in the Si/Al and K/Al records were matched to precession by counting the number of cycles in a biostratigraphic well-defined time interval. The cycle pattern with respect to the Si/Al, Ti/Al, K/Al and TOC records is not restricted to biozone CC15b but clearly extends over the entire interval between 1005.43 and 1046.09 mbsf. The biostratigraphic time control above 1022.5 mbsf, however, prohibits extending the approach described for biozone CC15b. Time –frequency analysis in CC15 reveals one prominent frequency of more than 3 cycles/m at the base that shifts to about 1.3 cycles/m above1037 mbsf. The upper part of the profile 1022.69 and 1005.43 mbsf also shows one prominent frequency at about 1.8 cycles/m that progressively decreases upward to about 1.3 cycles/m. No persistent signal components are detected at shorter wavelength. The period of the dominant cycle in the time domain was estimated by analysing the data from nannofossil biozone CC15 above 1041 mbsf in a chronostratigraphic framework. Time frequency analysis for TOC and K/Al displays one prominent frequency at about 35 cycles/Myr throughout the main parts of the record. Based on the age model, this frequency corresponds to a period of about 28 kyr; this is close enough to 22 kyr to support precession as the dominant frequency. See Supplementary Information for further details.

5.4.3 Global circulation model

The general features of the GENESIS (Global Environmental Ecological Simulation of Interactive Systems) 2.0, designed for paleoclimate research, have been presented before (DeConto et al., 1999). Boundary conditions were set for Cenomanian-Turonian simulations (see Supplementary Information for specification on experimental set-up, paleogeography, astronomical forcing, and validation of GENESIS v. 2.0). Five simulations with changing orbital forcing were carried out.

5.5 Supplementary Information

The supplement provides information on the time-frequency analysis as well as specifications on experimental setup of GENESIS 2.0.

5.5.1 Time-frequency analysis

Temporal changes in amplitude of signal components were estimated using a modified harmonic-filtering algorithm (Ferraz-Mello, 1981), which fits sinusoidal waves to a time series by means of least-squares. This method can process unevenly spaced time series directly, that is, without the requirement of prior interpolation. To obtain time-dependent amplitude estimates, the input time series is analyzed within a moving window of width $T_w = w \times T_f$, where $w = 3$ is a width–factor and T_f denotes the signal periodicity of interest (e.g. 20 ky). The window is shifted consecutively by one data point along the time axis of the input time series. Each "window segment" is linearly detrended prior to tapering with a Hanning window. The resulting amplitude and phase of the best-fit sinusoid are saved *vs.* the average of the observation times within the current segment and are used to reconstruct the signal component as function of time. The result of this procedure is equivalent to band-pass filtering (Hinnov et al., 2002). The selected value of w offers a good compromise between statistical and systematic errors and results in a half-amplitude bandwidth of approximately $0.5/T_f$ cycles/My. Note that due to the finite window width, a step-like increase in signal amplitude appears $w \times T_f$ wide. Applying the above filtering algorithm over a predefined range of frequencies allows us to detect changes in signal components in time-frequency space (Schulz et al., 1999). The dependence of window width, T_w on frequency leads to a change in temporal resolution with frequency. At low (high) frequencies wide (narrow) windows result in a low (high) temporal resolution. This scale dependence of the temporal resolution is similar to that of wavelet analysis. A program for time-frequency analysis (TIMEFRQ, version 4.3) is available from www.palmod.uni-bremen.de/~mschulz. In the following we apply the algorithm to the time and to the depth domain. To avoid double meaning, we refer to the method in both cases as time-frequency analysis.

5.5.2 Time-series analysis of nannofossil zone CC15 and the upper part of the profile

To detect persistent periodicities in the geochemical records we conducted time-frequency analysis using TOC and K/Al records from ODP Site 959 using the above method. Initially, analyses were performed in the depth domain in the intervals 1022.69 – 1005.43 mbsf (CC16, Figure 4a, b) and 1041.81 – 1028.62 mbsf (CC15, Figure 4c, d). The time-frequency analysis in CC15 reveal only one prominent frequency of more than 3 cycles/m at the base that shifts to about 1.3 cycles/m above 1037 mbsf. No persistent signal components are detected at shorter wavelength. The low-frequency signal near 0.7 cyles/m recognized between ~1035 and 1036 m for TOC (Fig 4d) is an artefact, reflecting the interruption of the typical TOC cycle pattern in that interval. The upper part of profile between 1022.69 – 1005.43 mbsf (Figure 4a, b) also shows one prominent frequency at about 1.8 cycles/m that progressively decreases upward to about 1.3 cycles/m. This dominant frequency disappears

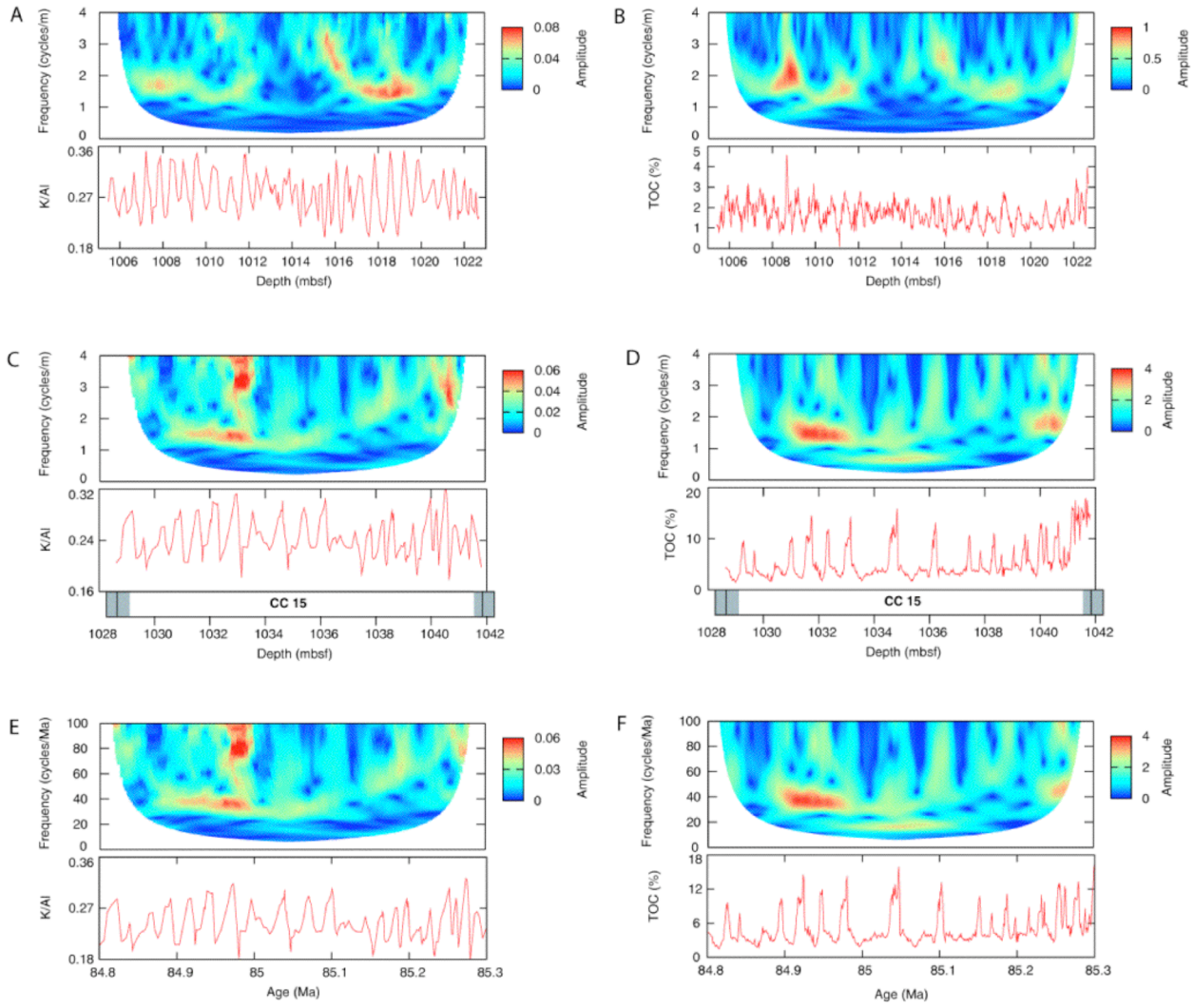

Fig. 4: Time-frequency analysis of K/Al and TOC records from ODP Site 959. Analysis were performed in the depth domain separately for the upper (A, B) and lower (C, D) parts of the record. Time-domain analysis was only carried out for the older part of the series (E, F). Bottom panel in each graph shows the record being analysed (K/Al and TOC in [wt. %]), while top panel shows signal amplitudes (in the same units as the data being analyzed) as function of depth/time and frequency. Shaded bars for the lower part of the record (C, D) indicate uncertainties in biozone-boudaries.

between 1016 and 1012 mbsf due to the strong attenuation of amplitudes in that part of the section (see records in Figs 4a, b). These results support the notion that only one dominant cycle persists throughout the record and that the frequency of this cycle varies only slightly from ~1037 mbsf upward. Minor variations in sedimentation rate across the section likely explain small modulations in the prominent m-scale frequency.

In a second step, we attempted to estimate the period of the dominant cycle in the time domain, by analyzing the data from nannofossil biozone CC15 above 1041 mbsf in a chronostratigraphic framework. This approach bears some uncertainties and limitations that have to be addressed prior to the presentation of the results from time-frequency analysis. A high-quality age model is pivotal for any precise identification of periodic signal components. This requirement poses a fundamental problem for any Cretaceous high-resolution record.

Providing such a high-quality age model for Site 959 that resolves with sufficient reliability orbital-scale variability has been shown to be critical if not impossible. This is primarily due to poor preservation of calcareous tests from foraminifera and coccoliths (Bellier, 1998; Watkins et al., 1998) but also because of deposition of the sediments during Magnetochron C34n (121-83 Ma), the "Cretaceous Quiet Zone" (Pletsch et al., 2001). Watkins et al. (1998) describe non-calcareous claystone between 1027 – 870 mbsf, excluding any biostratigraphic time control in the upper part of the study section. Below 1027 mbsf, nannofossil assemblages are sparse but fortunately sufficient to allow the assignment of nannofossil biozones CC16 to CC14 (Watkins et al., 1998).

The central part of the OAE 3 at Site 959 thus reveals two reasonably well located biostratigraphic age fixpoints, i.e. the first occurrence of *Reinhardtites anthophorus* (boundary CC14/CC15) and the first occurrence of *Lucianorhabdus cayeuxii* (boundary CC15/CC16). The uncertainty in boundary location for both fixpoints range from 56 cm at CC14/CC15 to 84 cm at CC15/CC16 (Watkins et al., 1998); the total length of CC15 in the core may thus vary between 14 m and 12.6 m, the uncertainty being equivalent to about two geochemical cycles. Both datum events also vary in absolute age depending of the chronostratigraphy applied. Gradstein et al. (1995) give ages of 85.66 and 84.9 Ma for the boundaries of CC14/CC15 and CC15/CC16, respectively. In a more recent chronostratigraphy, numerical ages of 85.5 and 84.8 Ma are given for both datum events (Shipboard Scientific Party, 2004). The total age uncertainty for CC15 is therefore about 0.1 Ma, without consideration of any error of these datums. Finally, sedimentological evidence strongly supports that sedimentation rates at Site 959 have not been constant across the study interval. Hardgrounds, reworked debris, and condensed sections indicate strongly reduced sedimentation rates below about 1040.5 mbsf (about 2.5 m/Ma; Watkins et al., 1998; Pletsch et al., 2001). In the middle and upper part of CC15 sedimentation rates increase by one order of magnitude to values of 20-40 m/Ma (Wagner et al., 2004) consistent with a palaeobathymetric position at upper continental margin at that time (Holbourn et al., 1999); linear interpolation of absolute age between the aforementioned age fixpoints of biozone CC15 must therefore result in an erroneous age model if the drastic change in sedimentation rate is not taken into account. We conclude that uncertainties in the duration of nannofossil biozone CC15, the location of boundaries of biozone CC15 at Site 959, and drastic changes in sedimentation rate in the lower part of the section at Site 959 are significantly variable; a fact that allows for a rather large inaccuracy of statistically-deduced time frequencies.

To minimize at least the uncertainty due to drastic changes in sedimentation rate for time-series analysis we omitted data below 1041.17 mbsf, i.e. the lowermost two cycles in CC15 that were before tentatively assigned to 100 ka eccentricity cycles [11]. Using the chronostratigraphy from ODP Leg 207 (Shipboard Scientific Party, 2004), we linearily interpolated ages between 1041.17 mbsf (85.3 Ma, subtracting 200 ka for the two omitted 100 ka cycles) and 1028.62 mbsf (84.8 Ma, top of CC15). The time-frequency analysis for TOC

and K/Al display one prominent frequency at about 35 cycles/Ma throughout main parts of the record (Figure 4e, f). Based on the age model, this frequency corresponds to a period of about 28 ka. Considering the potential uncertainties of the age model, this period lies in the range of orbital frequencies and close enough to 22 ka to support precession as the prominent frequency. Considering the outlined uncertainties at Site 959 we consider this conclusion as robust as possible and difficult to improve.

Time-frequency analysis does not identify other significant frequencies that persist across the record. The only hint comes from the records of mean square values of K/Al and Ti/Al that may suggest a 400 ka frequency. A 100 ka and/or 41 ka component is not identified in the time-series analysis. This result may come as a surprise given the high time-resolution and continuity of the records. One argument to explain this observation may be the location of the study area a few degrees south of the palaeo-equator. At this latitude it appears reasonable to expect a prominent precessional signal (even doubling of the precessional frequency). However, we do not have a conclusive physical explanation for the absence of the 100 ka and 41 ka signals.

The second part of the supplement provides specifications on experimental setup of GENESIS 2.0, paleogeography, astronomical forcing, and significance and effectiveness including sensitivity tests and other critical aspects to model sensitivity and validation of the simulated data.

5.5.3 Global circulation model GENESIS 2.0 and experimental setup

GENESIS v. 2.0 consists of an atmosphere general circulation model coupled to a non-dynamic 50-m slab ocean model. The atmospheric component has 18 vertical layers with a spectral resolution of T31, corresponding to a Gaussian latitude-longitude grid of 3.758° x 3.758°. Coupled to the atmospheric models are surface models having a 2° x 2° resolution: sea-ice, snow, vegetation and a six-layer model of soil. Boundary conditions set for Cenomanian-Turonian simulations are as follows: The solar constant was specified to be 98.62 % (1337.0 W/m^2) of the present value of 1365.0 W/m^2 based on estimates of solar luminosity. Heat transport in the slab ocean model was prescribed with values similar to those of today. Atmospheric CO_2 was specified as 1881.6 ppm, about five times the 2003 average value of 376.3 ppm. Recent re-evaluation of CO_2-values has shown that Upper Cretaceous values have been in the range between 1.5 and 7 times "present", with 5x being the best estimate (Royer et al., 2004). Concentrations of atmospheric CH_4 and N_2O were set at pre-industrial levels, 0.800 ppm and 0.288 ppm, respectively. A single vegetation, "Type 6" (broadleaf trees with groundcover – savannah; Dorman & Sellers, 1989) was specified and assumed to cover all land areas. The soil was specified as consisting of 51% sand, 29% silt, and 20% clay, distributed uniformly over all land areas. The model was allowed to spin up for 25 years, datasets were then compiled by averaging years 15 through 25.

5.5.3.1 Paleogeography

The paleogeographic boundary conditions (land-sea distribution) were provided by a global paleogeographic reconstruction for the early Turonian prepared for these simulations (Balukhovsky et al., 2004). This map was constructed using the techniques involved in producing the Paleozoic and Mesozoic-Cenozoic Atlases of "Lithological-Paleogeographic Maps of the World" (Ronov et al., 1989). The original data, from which the maps are constructed, taken from the literature and other sources, are originally plotted on large-scale equal area maps of each continent. The lithologic information is interpreted in the context of the paleogeographical environments and tectonic regimes which governed erosion and sediment deposition. The data are then smoothed and transferred onto a smaller scale global present day map. Elevations are originally estimated qualitatively based on the masses and grain size of the detrital sediment eroded and deposited in adjacent basins. The quantitative topographic interpretation is based on an interpretation of the denudation rate over the eroded region calculated from the volume of sediment supplied to the adjacent basins, using an estimate of the erosion-rate/elevation relationship. The map shows continents in their present-day configurations. It was digitized and the appropriate areas assigned to the continental blocks and terranes. Using a plate tectonic reconstruction program (www.odsn.de), these fragments were rotated back to their Turonian (93 Ma) position. The paleogeography, terrestrial elevations, and vegetation of this plate tectonic map were then converted to the 2° x 2° resolution of the surface model used to define paleo-shorelines and land-surface boundary conditions.

5.5.3.2 Astronomical Forcing

Five simulations with changing orbital forcing were carried out. For the control run, we assume that the Earth's orbit around the Sun was circular (eccentricity = 0) and had an obliquity of 23.5°. The remaining four simulations were computed with different positions of the earth in the precession cycle (0 = spring, 90 = winter, 180 = autumn, and 270 = summer). The so-called "climatic precession" determines which season coincides with perihelion (Earth's smallest distance to the sun). This allows analysis of the changes during one complete precessional cycle, including both of the solstice end members and the two equinoctial passages. Eccentricity for these runs was fixed at a value of 0.05. Obliquity was fixed at the present value of 23.5°. By definition the origin (0°) and end (360°) of the precession cycle are set at the northern hemisphere vernal equinox.

5.5.3.3 Model sensitivity and validation

Global paleoclimate modes such as GENESIS 2.0 are not specifically designed to simulate regional precipitation and discharge patterns, and seasonality for small geographic areas with large precision. We therefore conducted sensitivity tests and considered various other critical aspects to validate the quality of the simulated data.

The sensitivity experiments addressed surface runoff, drainage, continental discharge, and wind velocities. First we compare simulated precipitation data from GENESIS for modern NW-Africa (9-19°N / 9°W-9°E) to measured and modelled data from the literature. Modern annual precipitation for the region of 10-20°N / 10°W-10°E is measured to be 638 mm/year (Shver & Struzer, 1978). GENESIS 2.0 provides modern annual precipitation values of 642 mm/day at 2 m height above surface (D. Pollard, Pennsylvania State University, unpublished data), which are above the 95% confidence level of the predicted values provided by satellite measurements (*http://www.cpc.ncep.noaa.gov/products/african_desk/meteosat/*) testifying to the quality and significance of GENESIS 2.0-derived modelling data

Recent advances focus on the implementation of an explicit river routing scheme for the use in paleoclimate GCM (Markwick & Valdes, 2004). An explicit river routing scheme is currently developed for a future version of GENESIS but is not available yet. We want to emphasize that application of river routing scheme, although desirable, is not necessary for the central aims and interpretations of our study. This is because our conclusions base on estimates of total continental freshwater discharge that flows into the mid-Cretaceous Deep Ivorian Basin. It is not critical to specifically know where the local total continental freshwater discharge in the chosen rectangle (25-55°W, 1-17°S) emerged on the Mid-Cretaceous African coast. From previous studies (Poulsen et al., 1999; Flögel, 2002; Floegel et al., 2005) we know that we would get similar results as described in our study because precipitation and discharge patterns in GENESIS do not vary considerably over small scales.

The application of a river routing treatment would delay the seasonal peak of discharge by several weeks, at least while the fresh water is en route towards the coast. For the modern Amazon basin, for example, the delay may actually be up to several months (peak precipitation in January - peak river discharge in May; Marengo et al., 1994). Since the Mid-Cretaceous river system in low-latitude N-Africa may be assumed to be considerably shorter than the present day Amazon one, it appears reasonable to expect a delay time on the order of a few weeks. The point we want to make is that this time delay has *no impact* on the principle conclusions drawn from our modeling results. Instead, it is the amplitude of peak continental freshwater discharge for the four orbital cases that is critical for understanding Upper Cretaceous black shale formation.

We finally considered the question of alternative hypotheses/processes, such as upwelling. The geochemical records from ODP Site 959 do not support such a mechanism. Instead they show that periods of organic carbon burial follow humid time intervals with

indication for high continental discharge and not intervals with enhanced wind strength (Hofmann et al., 2003; Wagner et al., 2004; Beckmann et al., 2005). This interpretation is also supported by supplementary results from modelling (S. Flögel, IFM-GEOMAR, unpublished results). We analyzed global and regional pressure systems and wind velocities, focusing on the study area. The results from wind field patterns for all five models suggest that upwelling was not likely to have occurred in the Deep Ivory Basin. Only southerly sideshore winds blowing parallel to the coastline would be able to invoke Ekman transport of surface water away from the continent, therefore enabling upwelling. Offshore winds in addition could invoke coastal upwelling. No offshore or sideshore winds have been simulated for the coastal areas of the Deep Ivorian Basin using AGCM. Based on these independent and consistent results from geochemical data and simulations we did not put effort in running an additional ocean model.

Chapter 6. Summary, conclusions, and perspectives

Deposits from the eastern tropical Atlantic at ODP Site 959 off Ivory Coast and Ghana, provide a unique record of Coniacian to Campanian OC-rich sedimentation that covers the OAE 3. Investigations comprise detailed sedimentological, geochemical, isotopical, and biomarker analyses of a 40 m long drilled core to develop a model for black shale formation. The reconstruction of mechanisms and feedbacks of orbital forcing, land-sea interaction, and phasing of terrigenous and marine records in the tropical Atlantic Ocean during greenhouse conditions were of special interest during the study. The obtained continuous multi-disciplinary proxy records of Mid-Cretaceous African climate development were coupled with global climate modeling to understand controls of rapid change during past extreme warmth.

Fluctuations in several continental proxy records were associated with changes in the atmospheric circulation pattern, likely related to the repetitive latitudinal displacement of the paleo-ITCZ and African climate belts. Riverine nutrient supply and the periodic development of an estuarine circulation generating a freshwater cap were identified as main triggers for productivity cycles in the DIB. Long-term development of continental climate proxies indicate that transport mechanisms, which were controlling sediment delivery from different African source areas, persisted throughout the entire OAE 3; as did the pattern of phases with strong contrasts in climate modes (maximum arid and tropical conditions) and periods of reduced divergence in climate modes (moderate arid and tropical conditions). The molecular and bulk geochemical data supports a highly dynamic climate-ocean system with major impact on the structure and redox conditions of equatorial Atlantic surface waters during the peak greenhouse and enhanced OC burial over longer time periods.

The persistent and well-expressed cyclicity in various parameters with mainly precessional frequency acted as basis for a cyclostratigraphic age model that was proposed for nannofossil biozone CC15 and later continued into the lower Campanian sequences. This orbital age model allows detailed time control and ultimately determination of sedimentation and accumulation rates during an interval of sparse biostratigraphic fixpoints. It provides estimates for transitions between two sedimentological extremes (i.e., black shale deposition and formation of the background signal with low OC accumulation rates) on the order of thousand years or less, and permits the deduction of long-term trends and shorter-scale variations in the tropical ocean-atmosphere system.

Numerical simulations using the GCM GENESIS v. 2.0 support the assumption that ocean anoxia and black shale sedimentation were restricted to specific periods of maximum river discharge resulting in circulation reversal in the upper Cretaceous DIB. Simulations display a pronounced wet season (March to June) and a dry season (July to February). Black shale formation was confined to a situation when maximum insolation (i.e., northern spring

equinox at perihelion) occurred during the wet season with maximum seasonal contrasts and massive spring river discharge.

Black shale deposition in the eastern tropical Atlantic was ultimately triggered by changes in continental climate, vegetation belts and atmospheric circulation pattern with a major contribution by input of terrigenous material from continental Africa via run-off. In the future, a high-resolution study on OAE 3 samples from the conjugate South American margin at ODP Sites 1259 and 1261 at Demerara Rise will focus on the evolution of BS formation in response to forcing from the South American continent. To assess paleoclimatic conditions, several proxies for paleo-SSTs will be applied. The utilisation of the new organic geochemical SST proxy TEX_{86} (e.g., Schouten et al., 2002; 2003; 2004), which is based on the distribution of archaeal tetraether lipids, allows the assessment paleotemperatures. Additionally, the newly developed BIT proxy (e.g., Hopmans et al., 2004), based on the ratio of terrestrially derived tetraether lipids versus crenarchaeol, permits a quantification of the fluvial input of terrestrial OM. By applying these new proxies to samples from ODP Site 959 verification of data obtained from GCM is anticipated. In a further step the eastern and western equatorial Atlantic sedimentary regimes will be compared with regard to orbital forcing and its mechanisms, influence of the continents on studied sites, and the reaction of BS formation on these forcing factors.

In order to compare results from ODP Site 959 with other OAE 3 sites (apart from ODP Leg 207) with regard to onset, expansion, and termination of the event, a new or more specific definition of OAEs in general and the OAE 3 in particular is crucial. In the DIB the OAE 3 was not related to an appreciably positive $\delta^{13}C$ excursion due to elevated marine productivity and thus hampering the correlation with other OAE 3 occurrences. Furthermore, black shale formation during the OAE 3 was restricted to marginal marine settings while the deep oceans were fully oxic during that interval. It is thus questionable among researchers if the event can be called a "global" event at all. More and detailed investigations of potential upper Cretaceous sites, especially in the Pacific realm are needed to decide whether the OAE 3 was a truly global event or just represents a more regional phenomenon. Apart from that discussion on the event itself, further investigations during the climatically important interval of the upper Cretaceous are needed to obtain information on climate development during past extreme climates. A possible question deals with the importance of the Tropics in controlling global climate via ocean-atmosphere circulation during extreme warmth (e.g., Wilson et al. 2002; Norris et al., 2002) in contrast to the mid-latitudes representing the most important area in global climate development as indicated by Flögel & Wagner (in press). Only by gaining more information on former greenhouse intervals we might be able to further understand future climate evolution.

References

Alberdi-Genolet, M., Tocco, R., 1999. Trace metals and organic geochemistry of the Machiques Member (Aptian-Albian) and La Luna Formation (Cenomanian-Campanian), Venezuela: Chemical Geology, v. 160, p. 19-38.

Allen, M.R., Ingram, W.J., 2002. Constraints on future changes in climate and the hydrologic cycle: Nature, v. 419, p. 224-232.

Alychunskaya, N.M., Ivanov, V.V., 1978. Fresh-water balance of the world - Water inflow fom land. In: Korzun, V.I. (Ed.) World Water Balance and Water Resources of the Earth: Paris, UNESCO, Studies and Reports in Hydrology, v. 25, p. 568-574.

Archer, D., Ganopolski, A., 2005. A moveable trigger: Fossil fuel CO_2 and the onset of the next glaciation: Geochemistry, Geophysics, Geosystems, v. 6, no. 5, Q05003, doi:10.1029/2004GC000891.

Arthur, M.A., Dean, W.E., 1991. A holistic geochemical approach to cyclomania: examples from Cretaceous pelagic limestone sequences. In: Einsele, G., Ricken, W., Seilacher, A. (Eds.) Cycles and Events in Stratigraphy: Berlin, Springer, p. 126-166.

Arthur, M.A., Fisher, A.G., 1977. Upper Cretaceous-Paleocene magnetic stratigraphy at Gubbio, Italy I. Lithostratigraphy and sedimentology: Geological Society of America, Bulletin, v. 88, p. 367-371.

Arthur, M.A., Sageman, B.B., 1994. Marine black shales: depositional mechanisms and environments of ancient deposits: Annual Review of Earth Planetary Sciences, v. 22, p. 499-551.

Arthur, M.A., Schlanger, S.O., 1979. Cretaceous „Oceanic Anoxic Events“ as Causal Factors in Development of Reef-Reservoired Giant Oil Fields: American Association of Petroleum Ggeologists, Bulletin, v. 63, p. 870-885.

Arthur, M.A., Schlanger, S.O., Jenkyns, H.C., 1987. The Cenomanian-Turonian Oceanic Anoxic Event, II. Palaeoceanographic controls on organic-matter production and preservation. In: Brooks, J., Fleet, A.J. (Eds.) Marine Petroleum Source Rocks: Oxford, Geological Society, Special Publication, v. 26, p. 401-420.

Arthur, M.A., Dean, W.E. and Pratt, L.M., 1988. Geochemical and climatic effects of increased marine organic carbon burial at the Cenomanian/Turonian boundary: Nature, v. 335, p. 714-717.

Arthur, M.A., Jenkyns, H.C., Brumsack, H.-J., Schlanger, S.O., 1990. Stratigraphy, Geochemistry, and Paleoceanography of Organic Carbon-Rich Cretaceous Sequences. In: Ginsburg, R.N., Beaudoin, B. (Eds.) Cretaceous Resources, Events and Rhythms: Dordrecht, NATO ASI Series, Series C, v. 304, p.75-119.

Arthur, M.A., Dean, W.E., Neff, E.D., Hay, B.J., King, J., Jones, G., 1994. Varve calibration records of carbonate and organic carbon accumulation over the last 2000 years in the Black Sea: Global Biochemical Cycles, v. 8, p. 195-217.

Balukhovsky, A.N., Floegel, S., Hay, W.W., Migdisov, A., Wold, C.N., 2004. A paleogeographic map for the Lower Turonian: EarthRef Digital Archive http://earthref.org/cgi-bin/erda.cgi?n=220.

Barron, E.J., Fawcett, P.J., Peterson, W.H., Pollard, D., Thompson, S.L., 1995. A “simulation” of mid-Cretaceous climate: Paleoceanography, v. 10, p. 953-962.

Beckmann, B., Wagner, T., Hofmann, P., 2005. Linking Coniacian-Santonian (OAE3) black shale deposition to African climate variability: A reference section from the eastern tropical Atlantic at orbital time scales (ODP Site 959, of Ivory Coast and Ghana). In: Harris, N.B. (Ed.) The deposition of Organic Carbon-Rich Sediments: Models, Mechanisms, and Consequences: Washington, SEPM (Society for Sedimentary Geology), Special Publication, v. 82, p. 125-143.

Beckmann, B., Flögel, S., Hofmann, P., Schulz, M., Wagner, T., 2005. Orbital forcing of Cretaceous river discharge in tropical Africa and ocean response: Nature, in press.

Bellier, J.P., 1998. Cretaceous planktonic foraminifers, eastern Equatorial Atlantic. In: Mascle, J., Lohmann, G. P., Moullade, M. (Eds.) Proceedings of the Ocean Drilling Program, Scientific Results: College Station, v. 159, p. 335-345.

Berger, A., Loutre, M.-F., Laskar, J., 1992. Stability of astronomical frequencies over the Earth's history for paleoclimatic studies: Science, v. 255, p. 560-566.

Berner, R.A., 1992. Palaeo-CO_2 and climate: Nature, v. 358, p. 114.

Berner, R.A., 1994. GEOCARB 2: A revised model of atmospheric CO_2 over Phanerozoic time: American Journal of Science, v. 294, p. 56-91.

Berner, R.A., Raiswell, R., 1983. Burial of organic carbon and pyrite sulfur in sediments over Phanerozoic time: a new theory: Geochimica et Cosmochimica Acta, v. 47, p. 862-885.

Bice, K.L., Barron, E.J., Peterson, W.H., 1997. Continental runoff and early Cenozoic bottom-water sources: Geology 25, 951-954.

Bice, K.L., Huber, B.T., Norris, R.D., 2003. Extreme polar warmth during the Cretaceous greenhouse? The paradox of the late Turonian $\delta^{18}O$ record at DSDP Site 511: Paleoceanography, v. 18, doi: 10.1029/2002PA000848.

Bottjer, R. J., Stein, J. A., 1994. Relationship of stratigraphic traps to submarine unconformities: examples from the Tocito Sandstone, San Juan Basin, New Mexico and Colorado. In: Dolson, J.C., Hendricks, M.L., Wescott, W.A. (Eds.). Unconformity-Related Hydrocarbons in Sedimentary Sequence: Denver, Rocky Mountain Association of Geologists, p. 181-208.

Bralower, T.J., Thierstein, H.R., 1987. Organic carbon and metal accumulation rates in Holocene and mid-Cretaceous sediments: palaeoceanographic significance. In: Brooks, J., Fleet, A.J., (Eds.) Marine Petroleum Source Rocks: Oxford, Geological Society, Special Publication, v. 26, p. 345-369.

Bralower, T.J., Arthur, M.A., Leckie, R.M., Sliter, W.V., Schlanger, S.O., 1994. Timing and Paleoceanography of Oceanic Dysoxia/Anoxia in the Late Barremian to Early Aptian (Early Cretaceous): Palaios, v. 9, p. 335-369.

Brassell, S.C., Wardroper, A.M.K., Thompson, I.D., Maxwell, J.R., Eglinton, G., 1981. Specific acyclic isoprenoids as biological markers of methanogenic bacteria in marine sediments: Nature, v. 290, p. 693-696.

Breit, G. N., Wanty, R.B., 1991. Vanadium accumulation in carbonaceous rocks: A review of geochemical controlls during deposition and diagenesis: Chemical Geology, v. 91, p. 83-97.

Broecker, W.S., 1997. Thermohaline Circulation, the Achilles Heel of Our Climate System: Will Man-Made CO_2 Upset the Current Balance?: Science, v. 278, p. 1582-1588.

Brüchert, V., Jørgensen, B.B., Neumann, K., Riechmann, D., Schlösser, M., Schulz, H., 2003. Regulation of bacterial sulfate reduction and hydrogen sulfide fluxes in the central Namibian coastal upwelling zone: Geochimica et Cosmochimica Acta, v. 67, p. 4505-4518.

Brumsack, H.-J., 1986. The inorganic geochemistry of Cretaceous black shales (DSDP Leg 41) in comparison to modern upwelling sediments from the Gulf of California. In: Summerhayes, C.P., Shackleton, N.J. (Eds.) North Atlantic Palaeoceanography: London, Geological Society, Special Publications, v. 21, p. 447-462.

Brumsack, H.-J., 1988. Rezente, Corg-reiche Sedimente als Schlüssel zum Verständnis fossiler Schwarzschiefer: Habilitation Thesis, University of Göttingen, 166 p.

Brumsack, H.-J., 1991. Inorganic geochemistry of the German "Posidonia Shale": palaeoenvironmental consequences. In: Tyson, R.V., Pearson, T.H. (Eds.) Modern and Ancient Continental Shelf Anoxia: London, Geological Society, Special Publications, v. 58, p. 353-362.

Bush, A.B.G., Philander, S.G.H., 1997. The late Cretaceous: Simulation with a coupled atmosphere-ocean general circulation model: Paleoceanography, v. 12, p. 495-516.

Calvert, S.E., 1976. The mineralogy and geochemistry of nearshore sediments. In: Riley, J.P., Chester, R. (Eds.) Treatise on Chemical Oceanography: San Diego, Academic Press, v. 6, p. 187-280.

Calvert, S.E., Fontugne, M.R., 2001. On the late Peistocene-Holocene sapropel record of climatic and oceanographic variability in the eastern Mediterranean: Paleoceanography, v. 16, p. 78-94.

Calvert, S.E., Pedersen, T.F., 1993. Geochemistry of Recent oxic and anoxic marine sediments: Implications for the geological record: Marine Geology, v. 113, p. 67-88.

Clark, P.U., Pisias, N.G., Stocker, T.F. Weaver, A.J., 2002. The role of the thermohaline circulation in abrupt climate change: Nature, v. 415, p. 863-869.

Cotillon, P., Picard, A., Tribovillard, N., 2000. Compared cyclicity and diagenesis of two ancient deposits in the Caribbean domain: the Pleistocene-Holocene of Cariaco Basin (Site 1002) and the upper Cretaceous La Luna-Querecual Formation (North Venezuela). In: Leckie, R.M., Sigurdsson, H., Acton, G.D., Draper, G. (Eds.) Proceedings of the Ocean Drilling Program, Scientific Results: College Station, (Ocean Drilling Program), v. 165, p. 125-140.

Crespo de Cabrera, S., Sliter, W.V., Jarvis, I., 1999. Integrated foraminiferal biostratigraphy and chemostratigraphy of the Querecual formation (Cretaceous), eastern Venezuela: Journal of Foraminiferal Research, v. 29, p. 487-499.

Dam, G., Nøhr-Hansen, H., Christiansen, F. B., Bojesen-Koefoed, J. A., Laier, T., 1998. The oldest marine Cretaceous sediments in West Greenland (Umiivik-1 borehole) – record of the Cenomanian–Turonian Anoxic Event?: Geology of Greenland Survey, Bulletin, v. 180, p. 128-137.

Davis, C., Pratt, L., Sliter, W., Mompart, L., Murat, B., 1999. Factors influencing organic carbon and trace metal accumulation in the Upper Cretaceous La Luna Formation of the western Maracaibo Basin, Venezuela. In: Barrera, E., Johnson, C.C. (Eds.) The evolution of Cretaceous ocean/climate systems: Boulder, Geological Society of America, Special Paper, v. 332, p. 203-230.

Dean, W.E., Arthur, M.A., 1989. Iron-sulfur-carbon relationships in organic-carbon-rich sequences. I: Cretaceous Western Interior Seaway: American Journal of Science, v. 289, p. 708-743.

Dean, W.E., Arthur, M.A., 1998. Geochemical expressions of cyclicity in Cretaceous pelagic limestone sequences: Niobrara Formation, Western Interior Seaway. In: Dean, W.E., Arthur, M.A. (Eds.) Stratigraphy and Paleoenvironments of the Cretaceous Western Interior Seaway, USA: Tulsa, SEPM (Society for Sedimentary Geology), Concepts in Sedimentology and Paleontology, v. 6, p. 227-255.

Dean, W.E., Arthur, M.A., 1999. Sensitivity of the north Atlantic basin to cyclic climatic forcing during the Early Cretaceous: Journal of Foraminiferal Research, v. 29, p. 465-486.

Dean, W.E., Arthur, M.A., Stow, D.A.V., 1984. Origin and geochemistry of Cretaceous deep-sea black shales and multi-colored claystones, with emphasis on Deep Sea Drilling Project Site 530, southern Angola Basin. In: Hay, W.W., Sibuet, J.C., et al. (Eds.) Initial Reports of the Deep Sea Drilling Project, 75: Washington, Deep Sea Drilling Project, p. 819-844.

Dean, W.E., Arthur, M.A., Claypool, 1986. Depletion of ^{13}C in Cretaceous marine organic matter: Source, diagenetic, or environmental signal?: Marine Geology, v. 70, p. 119-157.

Dean, W. E., Piper, D. Z., Peterson, L. C., 1999. Molybdenum accumulation in Cariaco Basin sediment over the past 24 k.y.: A record of water-column anoxia and climate: Geology, v. 27, p. 507-510.

DeConto, R.M., Hay, W.W., Thompson, S.L., Bergengren, J., 1999. Late Cretaceous climate and vegetation interactions: Cold continental interior paradox. In: Barrera, E., Johnson, C.,

(Eds.) The evolution of Cretaceous ocean/climate systems: Geological Society of America Special Publication, v. 332, 391-406.

DeConto, R.M., Brady, E.C., Bergengren, J., Hay, W.W., 2000. Late Cretaceous climate, vegetation, and ocean interactions. In: Huber, B.T., MacLeod, K.G., Wing, S.L. (Eds.) Warm Climates in Earth History, Cambridge, Cambridge University Press, p. 275-296.

De Graciansky, P.C., Deroo, G., Herbin, J.P., Jacquin, T., Magni, F., Montadert, L., Müller, C., 1986. Ocean-wide stagnation episodes in the Late Cretaceous: Geologische Rundschau, v. 75, p.17-41.

De Romero, L.M., Truskowski, I.M., Bralower, T.J., Bergen, J.A., Odreman, O., Zachos, J.C., Galea-Alvarez, F.A., 2003. An Intergrated Calcareous Microfossil Biostratigraphic and Carbon-Isotope Stratigraphic Framework for the La Luna Formation, Western Venezuela: Palaios, v. 18, p. 349-366.

Deroo, G., Herbin, J. P., Huc, A. Y., 1984. Organic geochemistry of Cretaceous black shales from Deep Sea Drilling Project Site 530, Leg 75, Eastern South Atlantic. In: Hay, W.W., Sibuet, J.C., et al. (Eds.) Proceedings of the Deep Sea Drilling Project, Washington, Initial Reports, v. 75, p. 983-999.

Diester-Haass, L., Chamley, R.C., 1993. Palaeoceanographic and palaeoclimatic evolution in the Wedell Sea (Antarctica) during the middle Eocene-late Oligocene, from a coarse sediment fraction and clay mineral data (OCP 689): Marine Geology, v. 114, p. 233-250.

Dorman, J.L., Sellers, P.J., 1989. A global climatology of albedo, roughness, length and stomatal resistance for atmospheric general circulation models as represented by the simple biosphere model (SiB): American Meteorological Society, v. 28, p. 833-855.

Eglinton, T. I., Sinninghe Damsté, J. S., Kohnen, M. E. L., de Leeuw, J. W., 1990. Rapid estimation of the organic sulfur content of kerogens, coals and asphaltenes by pyrolysis-gas chromatography: Fuel, v. 69, p. 1394-1404.

Emeis, K.C., Morse, J.W., 1993. Zur Systematik der Kohlenstoff-Schwefel-Eisen-Verhältnisse in Auftriebssedimenten: Geologische Rundschau, v. 82, p. 604-618.

Emeis, K.-C., Sakamoto, T., Wehausen, R., Brumsack, H.J., 2000. The sapropel record of the eastern Mediterranean Sea—Results of Ocean Drilling Program Leg 160: Palaeogeography, Palaeoclimatology, Palaeoecology, v. 158, p. 371–395.

Erba, E., 1994. Nannofossils and superplumes: The early Aptian "nannoconid crisis": Paleoceanography, v. 9, p. 483-501.

Erba, E., 2004. Calcareous nannofossils and Mesozoic oceanic anoxic events: Marine Micropaleontology, v. 52, p. 85-106.

Erbacher, J., Thurow, J., 1997. Influence of oceanic anoxic events on the evolution of mid-Cretaceous radiolaria in the North Atlantic and western Tethys: Marine Micropaleontology, v. 30, p. 139-158.

Erbacher, J., Thurow, J., Littke, R., 1996. Evolution patterns of radiolaria and organic matter variations: A new approach to identify sea level changes in mid-Cretaceous pelagic environments: Geology, v. 24, p. 599-602.

Erbacher, J., Huber, B. T.; Norris, R. D., Markey, M., 2001. Increased thermohaline stratification as a possible cause for an ocean anoxic event in the Cretaceous period: Nature, v. 409, p. 325-327.

Erlich, R.N., Astorga, A., Sofer, Z., Pratt, L.M., Palmer, S.E.,1996. Palaeoceanography of organic-rich rocks of the Loma Chumico Formation of Costa Rica, Late Cretaceous, eastern Pacific: Sedimentology, v. 43, p. 691-718.

Erlich, R.N., Palmer-Koleman, S.E., Antonieta Lorente, M., 1999. Geochemical characterization of oceanographic and climatic changes recorded in upper Albian to lower Maastrichtian strata, western Venezuela: Cretaceous Research, v. 20, p. 547-581.

Espitalié, J., Laporte, J.L., Madec, J., Marquis, F., Leplat, P., Paulet, J., Boutefeau, A., 1977. Méthode rapide de characterisation des roches mers de leur potential pétrolier et de leur degré d'évolution: Révenue Institute Français du Pétrole, v. 33, p. 23-42.

Espitalié, J., Makadi, K.S., Trichet, J., 1984. Role of the mineral matrix during kerogen pyrolysis: Organic Geochemistry, v. 6, p. 365-382.

Farrington, J.W., Davis, A.C., Sulanowski, J., McCaffrey, M.A., McCarthy, M., Clifford, C.H., Dickinson, P., Volkman, J.K., 1988. Biogeochemistry of lipids in surface sediments of the Peru Upwelling Area at 15°S: Organic Geochemistry, v. 13, p. 607-617.

Fassell, M.L., Bralower, T.J., 1999. Warm, equable mid-Cretaceous: Stable isotope evidence. In: Barrera, E., Johnson, C.C. (Eds.) Evolution of the Cretaceous Ocean-Climate-System: Boulder, Geological Society of America Special Paper, v. 332, p. 121-142.

Ferraz-Mello, S., 1981. Estimation of periods from unequally spaced observations: Astronomical Journal, v. 86, p. 619-624.

Flögel, S., 2001. On the influence of precessional Milankovitch cycles on the Late Cretaceous climate system: Comparison of GCM-results, geochemical, and sedimentary proxies for the Western Interior Seaway of North America: Doctoral Thesis, University of Kiel, 231 p.

Floegel, S., Hay, W.W., DeConto, R.M., Balukhovsky, A.N., 2005. Formation of sedimentary bedding couplets in the Western Interior Seaway of North America – implications from climate system modelling: Palaeogeography, Palaeoclimatology, Palaeoecology, v. 218, 125-143.

Flögel, S., Wagner, T., 2005. Insolation-control on the Late Cretaceous hydrological cycle and tropical African climate - global climate modelling linked to marine climate records: Palaeogeography, Palaeoclimatology, Palaeoecology, in press.

Föllmi K.B., Weissert, H., Bisping, M., Funk, H., 1994. Phosphogenesis, carbon-isotope stratigraphy, and carbonate platform evolution along the lower Cretaceous northern Tethyan margin: American Association of Petroleum Geologists, Bulletin, v. 106, p. 729-746.

Frakes, L.A., Francis, J.E., Syktus, J.I., 1992. Climate modes of the Phanerozoic: the history of the Earth's climate over the past 600 Million years. Cambridge, Cambridge University Press, 274 p.

Francis, J.E., Poole, I., 2002. Cretaceous and early Tertiary climates of Antarctica: evidence from fossil wood: Palaeogeography, Palaeoclimatology, Palaeoecology, v. 182, p. 47-64.

Freeman, K.H., Wakeham, S.G., Hayes, J.M., 1994. Predictive isotopic biogeochemistry: Hydrocarbons from anoxic marine basins: Organic Geochemistry, v. 21, p. 629-644.

Galeotti, S., Bellagamba, M., Kaminski, M.A., Montanari, A., 2002. Deep-sea benthic foraminiferal recolonisation following a volcaniclastic event in the lower Campanian of the Scaglia Rossa Formation (Umbria-Marche Basin, central Italy): Marine Micropaleontology, v. 44, p. 57-76.

Gradstein, F.M., Agterberg, F.P., Ogg, J.G., Hardenbol, J., van Veen, P., Thierry, J., Huang, Z., 1995. A Triassic, Jurassic and Cretaceous time scale. In*:* Berggren, W.A., Kent, D.V., Aubra, M.P., Hardenbol, J. (Eds.) Geochronology, Time Scales and Global Stratigraphic Correlation: Washington DC, SEPM (Society for Sedimentary Geology), Special Publication, v. 54, p. 95-126.

Grice, K., Schouten, S., Nissenbaum, A., Charrach, J., Sinninghe Damsté, J.S., 1998. Isotopically heavy carbon in the C21 to C25 regular isoprenoids in halite-rich deposits from the Sdom Formation, Dead Sea Basin, Israel: Organic Geochemistry, v. 29, p. 349-359.

Gröcke, D., Hesselbo, S.P., Jenkyns, H.C., 1999. Carbon-isotope composition of Lower Cretaceous fossil wood: ocean-atmosphere chemistry and relation to sea-level change: Geology, v. 27, p. 155-158.

Haq, B.U., Hardenbol, J., Vail, P.R., 1987. Chronology of Fluctuating Sea Levels Since the Triassic: Science, v. 235, p. 1156-1167.

Hardenbol, J., Thierry, J., Farley, M.B., Jacquin, T., de Graciansky, P.-C., Vail, P.R., 1998. Mesozoic and Cenozoic sequence chronostratigraphic framework of European basins. In: de Graciansky, P.-C., Hardenbol, J., Jacquin, T., Vail, P.R. (Eds.) Mesozoic and Cenozoic sequence stratigraphy of European basins: Washington DC, SEPM (Society for Sedimentary Geology), Special Publication, v. 60, p. 3-13.

Haug, G. H., Hughen, K. A., Sigman, D. M., Peterson, L. C., Röhl, U., 2001. Southward migration of the Intertropical Convergence Zone through the Holocene: Science, v. 293, p. 1304-1307.

Hay, W.W., DeConto, R.M., Wold, C.N., 1997. Climate: Is the past the key to the future?: Geologische Rundschau, v. 86, p. 471-491.

Hay, W.W., DeConto, R.M., Wold, C.N., Wilson, K.M., Voigt, S., Schulz, M., Rossby Wold, A., Dullo, W.C., Ronov, A.B., Söding, E., 1999. An alternative global Cretaceous paleogeography. In: Barrera, E., Johnson, C.C. (Eds.) The evolution of the Cretaceous ocean-climate system: Boulder, Geological Society of America, Special Paper, v. 332, p. 1-48.

Herbert, T., Gee, J., DiDonna, S., 1999. Precessional cycles in Upper Cretaceous pelagic sediments of the South Atlantic: Long term patterns from high-frequency climate variations. In: Barrera, E., Johnson, C.C. (Eds.) The evolution of the Cretaceous ocean-climate system, Boulder, Geological Society of America Special Paper, v. 332, p. 105–120.

Hesselbo, S.P., Gröcke, D., Jenkyns, H.C., Bjerrum, C.J., Farrimond, P., Morgans Bell, H.S., Green, O., 2000. Massive dissociation of gas hydrate during a Jurassic oceanic anoxic event: Nature, v. 406, p. 392-395.

Hinnov, L.A., Schulz, M., Yiou, P., 2002. Interhemispheric space-time attributes of the Dansgaard-Oeschger oscillations between 100 and 0 ka: Quaternary Science Review, v. 21, p. 1213-1228.

Hofmann, P., Ricken, W., Schwark, L., Leythaeuser, D., 1999. Coupled oceanic effects of climatic cycles from late Albian deep-sea sections of the North Atlantic. In: Barrera, E., Johnson, C.C. (Eds.) The evolution of Cretaceous ocean/climate systems: Geological Society of America Special Publication, v. 332, p. 143-159.

Hofmann, P., Ricken, W., Schwark, L., Leythaeuser, D., 2000. Carbon-sulfur-iron relationships and $\delta^{13}C$ of organic matter for late Albian sedimentary rocks from the North Atlantic Ocean: paleoceanographic implications: Palaeogeography, Palaeoclimatology, Palaeoecology, v. 163, p. 97-113.

Hofmann, P., Ricken, W., Schwark, L., Leythaeuser, D., 2001. Geochemical signature and related climatic-oceanographic processes for early Albian black shales: Site 417D, North Atlantic Ocean: Cretaceous Research, v. 22, p. 243-257.

Hofmann, P., Wagner, T., Beckmann, B., 2003. A millennial- to centennial-scale record of African climate variability and organic carbon accumulation in the Coniacian-Santonian eastern tropical Atlantic (Ocean Drilling Program Site 959, off Ivory Coast and Ghana): Geology, v. 31, p. 135-138.

Holbourn, A.E.L., Kuhnt, W., El Albani, A., Pletsch, T., Luderer, F., Wagner, T., 1999. Upper Cretaceous palaeoenvironments and benthonic foraminiferal assemblages of potential source rocks from the western African margin, Central Atlantic. In: Cameron, N.R., Bate, R.H., Clure, V.S. (Eds.) The Oil and Gas Habitats of the South Atlantic: London, Geological Society, Special Publication, v. 153, p. 195-222.

Holtar, E., Forsberg, A.W., 2000. Postrift development of the Walvis Basin, Namibia: results from the exploration campaign in Quadrant 1911. In: Mello, M.R., Katz, J. (Eds.) Petroleum systems of South Atlantic margins: American Association of Petroleum Geologists Memoir, v. 73, p. 429-446.

Hopmans, E.C., Weijers, J.W.H., Schefuß, E., Herfort, L., Sinninghe Damsté, J.S., Schouten, S., 2004. A novel proxy for terrestrial organic matter in sediments based on branched and isoprenoid tetraether lipids: Earth and Planetary Science Letters, v. 224, p. 107-116.

Hu, X., Jansa, L., Wang, C., Sarti, M., Bak, K., Wagreich, M., Michalik, J. Soták, J., 2005. Upper Cretaceous oceanic red beds (CORBs) in the Tethys: occurrences, lithofacies, age, and environments: Cretaceous Research, v. 26, p. 3-20.

Huber, B.T., 1998. Tropical Paradise at the Cretaceous Poles?: Science Magazine, v. 282, p. 2199-2200.

Huber, B.T., Hodell, D.A., Hamilton, C.P., 1995. Mid- to Late Cretaceous climate of the southern high latitudes: Stable isotopic evidence for minimal equator-to-pole thermal gradients: Geological Society of America, Bulletin, v. 107, p. 1164-1191.

Huber, B.T., Leckie, R.M., Norris, R.D., Bralower, T.J., CoBabe, E., 1999. Foraminiferal assemblage and stable isotopic change across the Cenomanian-Turonian boundary in the subtropical North Atlantic: Journal of Foraminiferal Research, v. 29, p. 392-417.

Huber, B.T., Norris, R.D., MacLeod, K.G., 2002. Deep-sea paleotemperature record of extreme warmth during the Cretaceous: Geology, v. 30, p. 123-126.

Hutchins, D.A., Bruland, K.W., 1998. Iron-limited diatom growth and Si:N uptake ratios in a coastal upwelling regime: Nature, v. 393, p. 561-564.

Hutchins, D.A., Hare, C.E., Weaver, R.S., Zhang, Y., Firme, G.F., Di Tullio, G.R., Alm, M.B., Riseman, S.F., Maucher, J.M., Geesey, M.E., Trick, C.G., Smith, G.J., Rue, E.L., Conn, J., Bruland, K.W., 2002. Phytoplankton iron limitation in the Humboldt Current and Peru Upwelling: Limnology and Oceanography, v. 47, p. 997-1011.

Jahren, A.H., 2002. The biogeochemical consequences of the mid-Cretaceous superplume: Journal of Geodynamics, v. 34, p. 177-191.

Jenkyns, H.C., 1980 Cretaceous anoxic events: from continents to oceans: Journal of the Geological Society of London, v. 137, p. 171-188.

Jenkyns, H.C., 1999. Mesozoic anoxic events and palaeoclimate: Zentralblatt für Geologie und Paläontologie, v. 7-9, p. 943-949.

Jenkyns, H.C., 2003. Evidence for rapid climate change in the Mesozoic-Palaeogene greenhouse world: Philosophical Transactions of the Royal Society of London, A, v. 361, p. 1885-1916.

Jenkyns, H.C., Gale, A.S., Corfield, R.M., 1994. Carbon- and oxygen-isotope stratigraphy of the English Chalk and Italian Scaglia and its palaeoclimatic significance: Geological Magazine, v. 131, p. 1-34.

Jenkyns, H.C., Forster, A., Schouten, S., Sinninghe Damsté, J.S., 2004. High temperatures in the Late Cretaceous Arctic Ocean: Nature, v. 432, p. 888-892.

Jones, B., Manning, D.A.C., 1994. Comparison of geochemical indices used for the interpretation of paleoredox conditions in ancient mudstones: Chemical Geology, v. 111, p. 111-129.

Jones, E.J.W., Cande, S.C., Spathopoulos, F., 1995. Evolution of a major oceanographic pathway: The Equatorial Atlantic. In: Scrutton, R.A., Stoker, M.S., Shimmield, G.B., Tudhope, A.W. (Eds.) The Tectonics, Sedimentation and Paleoceanography of the North Atlantic Region: London, Geological Society of London, Special Publication, v. 90, p. 199-213.

Katz, B.J., Dawson, W.C., Liro, L.M., Robison, V.D., Stonebraker, J.D., 2000. Petroleum systems of the Ogooué Delta, offshore Gabon. In: Mello, M.R., Katz, B.J. (Eds.) Petroleum Systems of South Atlantic margins: Tulsa, American Association of Petroleum Geologists, Memoir, v. 73, p. 247-256.

Kohnen, M.E.L., Sinninghe Damsté, J.S., Kock-van Dalen, A.C., ten Haven, H.L., Rullkötter, J., de Leeuw, J.W., 1990. Origin and diagenetic transformation of C25 and C30 highly branched isoprenoid sulfur compounds: further evidence for the formation of organically

bound sulfur during early diagenesis: Geochimica et Cosmochimica Acta, v. 54, p. 3053-3063.

Kolonic, S., Wagner, T., Forster, A., Sinnighe Damsté, J.S., Walsworth-Bell, B., Erba, E., Turgeon, S., Brumsack, H.-J., Chellai, E.H., Tsikos, H., Kuhnt, W., Kuypers, M.M.M., 2005. Black shale deposition on the northwest African Shelf during the Cenomanian/Turonian oceanic anoxic event: Climate coupling and global organic carbon burial: Paleoceanography, v. 20, doi:10.1029/2003PA000950.

Koopmans, M.P., van Kaam-Peters, H.M.E., Kenig, F., Schouten, S., Hartgers, A.W., de Leeuw, W.J., Damsté Sinninghe J.S., 1996. Diagenetic and catagenetic products of isorenieratane: Molecular indicators for photic zone anoxia: Geochimica et Cosmochimica Acta, v. 60, p. 4467-4496.

Koopmans, M.P., Schaeffer-Reiss, C., de Leeuw, J.W., Lewan, M.D., Maxwell, J.R., Schaeffer, P., Sinninghe Damsté, J.S., 1997. Sulfur and oxygen sequestration of n-C37 and n-C38 unsaturated ketones in an immature kerogen and the release of their carbon sceletons during early stages of thermal maturation: Geochimica et Cosmochimica Acta, v. 61, p. 2397-2408.

Köster, J., Rospondek, M., Schouten, S., Kotarba, M., Zubrzycki, A. Sinninghe Damsté, J.S., 1998. Biomarker geochemistry of a foreland basin: the Oligocene Menilite Formation in the Flysch Carpathians of Southeast Poland: Organic Geochemistry, v. 29, p. 649-669.

Kuhnt, W., 1992. An early Campanian paleoceanographic event in the North Atlantic and Western Tethys? Fourth International Conference on Paleoceanography, ICP IV: Kiel, Geomar Report, v. 15, p. 171.

Kuhnt, W., Kaminski, M.A. Moullade, M., 1989. Late Cretaceous deep-water agglutinated foraminiferal assemblages from the North Atlantic and its marginal seas: Geologische Rundschau, v. 78, p. 1121-1140.

Kuhnt, W., Nederbragt, A., Leine, L., 1997. Cyclicity of Cenomanian-Turonian organic-carbon-rich sediments in the Tarfaya Atlantic Coastal Basin (Morocco): Cretaceous Research, v. 18, p. 587-601.

Kuhnt, W., Moullade, M., Kaminski, M.A., 1998. Upper Cretaceous, K/T boundary, and Paleocene agglutinated foraminifers from Hole 959D (Côte d'Ivoire-Ghana Transform Margin). In: Mascle, J., Lohmann, G.P., Moullade, M. (Eds.) Proceedings of the Ocean Drilling Program: College Station, Scientific Results, v. 159, p. 389-411.

Kuhnt, W., El Chellai, H, Holbourn, A.E.L., Luderer, F., Thurow, J., Wagner, T., El Albani, A., Beckmann, B., Herbin, J.-P., Kawamura, H., Kolonic, S., Nederbragt, A., Street, C., Ravilious, K., 2001. Morocco basin's sedimentary record may provide correlations for Cretaceous paleoceanographic events worldwide: EOS Transactions, v. 82, no. 33, p. 361-364.

Kuypers, M.M.M., Pancost, R.D., Sinninghe Damsté, J.S., 1999. A large and abrupt fall in atmospheric CO_2 concentration during Cretaceous times: Nature, v. 399, p. 342-345.

Kuypers, M.M.M., Pancost, R.D., Nijenhuis, I.A., Sinninghe Damsté, J.S., 2002. Enhanced productivity led to increased organic carbon burial in the euxinic North Atlantic basin during the Late Cenomanian oceanic anoxic event: Paleoceanography, v. 17-4, p. 3-1 – 3-13.

Kuypers, M.M.M., Lourens, L.J., Rijstra, I.C., Pancost, R.D., Nijenhuis, I.A., Sinninghe Damsté, J.S., 2004. Orbital forcing of organic carbon burial in the proto-North Atlantic during oceanic anoxic event 2: Earth and Planetary Science Letters, v. 228, p. 465-482.

Larsen, J.W., Parikh, H., Michels, R., 2002. Changes in the cross-link density of Paris Basin Toarcian kerogen during maturation: Organic Geochemistry, v. 33, p. 1143-1152.

Larson, R.L., 1991a. Latest pulse of Earth: evidence for a Mid-Cretaceous superplume: Geology, v. 19, p. 547-550.

Larson, R.L., 1991b. Geological consequences of superplumes: Geology, v. 19, p. 963-966.

Larson, R.L., Erba, E., 1999. Onset of the mid-Cretaceous greenhouse in the Barremian-Aptian: Igneous events and the biological, sedimentary, and geochemical responses: Paleoceanography, v. 14, p. 663-678.

Leckie, R.M., Bralower, T.J., Cashman, R., 2002. Oceanic anoxic events and plankton evolution: Biotic response to tectonic forcing during the mid-Cretaceous: Paleoceanography, v. 17, no. 3, p. 13-1-13-29.

Leine, L., 1986. Geology of the Tarfaya oil shale deposit, Morocco: Geologie en Mijnbouw, v. 65, p. 57-74.

Leith, T.L., Weiss, H.M., Mørk, A., Arhus, N., Elvebakk, G., Embry, A.F., Brooks, P.W., Stewart, K.R., Pchelina, T.M., Bro, E.G., Verba, M.L., Danyushevskaya, A., Borisov, A.V., 1993. Mesozoic hydrocarbon source-rocks of the Arctic region. In: Vorren, T.O., Bergsager, E., Dahl-Stamnes, O.A., Holter, E., Johansen, B., Lie, E., Lund, T.B. (Eds.) Arctic Geology and Petroleum Potential: Amsterdam, Elsevier, NPF Special Publication, v. 2, p. 1-25.

Leventhal, J.S., 1983. An interpretation of carbon and sulfur relationships in Black Sea sediments as indicators of environments of deposition: Geochimica et Cosmochimica Acta, v. 47, p. 133-137.

Lewan, M.D., Maynard, J.B., 1982. Factors controlling enrichment of V and nickel in the bitumen of organic sedimentary rocks: Geochimica et Cosmochimica Acta, v. 46, p. 2547-2260.

Ly, A., Kuhnt, W., 1994. Late Cretaceous benthic foraminiferal assemblages of the Casamance shelf (Senegal, NW Africa). Indication of a Late Cretaceous oxygen minimum zone: Revue de Micropaleontologie, v. 37, p. 49-74.

Madigan, T.M., Martinko, M.J., Parker, J., 2000. Biology of Microorganisms, Old Tappan, Brock Prentice Hall International, 991 p.

Macsotay, O., Erlich, R.N., Peraza, T., 2003. Sedimentary Structures of the La Luna, Navay and Querecual Formations, Upper Cretaceous of Venezuela: Palaios, v. 18, p. 334-348.

Maley, J., 1996. The African rain-forest - Main characteristics of change in vegetation and climate from the Upper Cretaceous to the Quaternary: Proceedings of the Royal Society of Edinburgh, v. 104B, p. 31-73.

Manabe, S., Stouffer, R.J., 1993. Century-scale effects of increased atmospheric CO_2 on the ocean-atmosphere system: Nature, v. 364, p. 215-218.

Marengo, J.A., Miller, J.R., Russell, G.L., Rosenzweig, C.E., Abramopoulos, F., 1994. Calculations of river-runoff in the GISS GCM: Impact of a new land-surface parameterization and runoff routing model on the hydrology of the Amazon River: Climate Dynamics, v. 10, p. 349-361.

Markwick, P.J., 1998. Fossil crocodilians as indicators of Late Cretaceous and Cenozoic climates: implications for using palaeontological data in reconstructing palaeoclimate: Palaeogeography, Palaeoclimatology, Palaeoecology, v. 137, p. 205-271.

Markwick, P.J., Valdes, P.J., 2004. Palaeo-digital elevation models for use as boundary conditions in coupled ocean–atmosphere GCM experiments: a Maastrichtian (late Cretaceous) example: Palaeogeography, Palaeoclimatology, Palaeoecology, v. 213, p. 37-63.

Martinez-Ruiz, F., Kastner, M., Paytan, A., Ortega-Huertas, M., Bernasconi, S.M., 2000. Geochemical evidence for enhanced productivity during S1 sapropel deposition in the eastern Mediterranean: Paleoceanography, v. 15, p. 200-209.

Mascle, J., Lohmann, G.P., Clift, P.D., 1996. Proceedings of the Ocean Drilling Program, Initial Reports, 159: College Station, (Ocean Drilling Program), 616 p.

McCaffrey, M.A., Farrington, J.W., Repeta, D.J., 1990. The organic geochemistry of Peru margin surface sediments: 1. A comparison of the C_{37} alkenone and historical El Niño records: Geochimica et Cosmochimica Acta, v. 54, p. 1671-1682.

Mello, M.R., Telnaes, N., Maxwell, J.R., 1995. The hydrocarbon source potential in the Brazilian Marginal basins: a geochemical and paleoenvironmental assessment. In: Huc, A.Y. (Ed.) Paleogeography, Paleoclimate, and Source Rocks: Tulsa, American Association of Petroleum Geologists, Studies in Geology, p. 233-272.

Menegatti, A.P., Weissert, H., Brown, R.S., Tyson, R.V., Farrimond, P., Strasser, A., Caron, M., 1998. High-resolution $\delta^{13}C$ stratigraphy through the early Aptian „Livello Selli" of the Alpine Tethys: Paleoceanography, v. 13, p. 530-545.

Menzel, D., Hopmans, E.C., van Bergen, P.F., de Leeuw, J.W., Sinninghe Damsté, J.S., 2002. Development of photic zone euxinia in the eastern Mediterranean Basin during deposition of Pliocene sapropels: Marine Geology, v. 189, p. 215-226.

Meyers, S.R., Sageman, B.B., Hinnov, L.A.,2001. Integrated quantitative stratigraphy of the Cenomanian-Turonian Bridge Creek Limestone Member using evolutive harmonic analysis and stratigraphic modeling: Journal of Sedimentary Research, v. 71, p. 628-644.

Mongenot, T., Tribovillard, N.-P., Desprairies, A., Lallier-Vergès, E., Laggoun-Defarge, F., 1996. Trace elements as palaeoenvironmental markers in strongly mature hydrocarbon source rocks: the Cretaceous La Luna Formation of Venezuela: Sedimentary Geology, v. 103, p. 23-37.

Morse, J.W., Emeis, K.C., 1992. Carbon/sulphur/iron relationships in upwelling sediments. In: Summerhayes, C.P., Prell, W.L., Emeis, K.C. (Eds.) Upwelling Systems: Evolution Since the Early Miocene: London, Geological Society, Special Publications, v. 64, p. 247-255.

Müller, P.J., Suess, E., 1979. Productivity, sedimentation rate, and sedimentary organic matter in the oceans – I. Organic carbon preservation: Deep-Sea Research, v. 26A, p. 1347-1362.

Naqvi, S.W.A., Jayakumar, D.A., Narvekar, P.V., Naik, H., Sarma, V.V.S.S., D'Souza, W.D., Joseph, S., George, M.D., 2001. Increased marine production of N_2O due to intensifying anoxia on the Indian continental shelf: Nature, v. 408, p. 346-349.

Nguyen Tu, T.T., Bocherens, H., Mariotti, A., Baudin, F., Pons, D., Broutin, J., Derenne, S., Largeau, C., 1999. Ecological distribution of Cenomanian terrestrial plants based on $^{13}C/^{12}C$ ratios: Palaeogeography, Palaeoclimatology, Palaeoecology, v. 145, p. 79-93.

Nijenhuis, I.A., Bosch, H.-J., Sinninghe Damsté, J.S., Brumsack, H.-J., De Lange, G.J., 1999. Organic matter and trace element rich sapropels and black shales: a geochemical comparison: Earth and Planetary Science Letters, v. 169, p. 277-290.

Nijenhuis, I.A., Becker, J., De Lange, G.J., 2001. Geochemistry of coeval marine sediments in Mediterranean ODP cores and a land section: implications for sapropel formation models: Palaeogeography, Palaeoclimatology, Palaeoecology, v. 165, p. 97-112.

Norris, R.D., Wilson, P.A., 1998. Low-latitude sea-surface temperatures for the mid-Cretaceous and the evolution of planktic foraminifera: Geology, v. 26, p. 823-826.

Norris, R.D., Bice, K.L., Magno, E.A., Wilson, P.A., 2002. Jiggling the tropical thermostat during the Cretaceous hot house: Geology, v. 30, p. 299-302.

Oboh-Ikuenobe, F.E., Yepes, O. Gregg, J.M., 1998. Palynostratigraphy, palynofacies, and thermal maturation of Cretaceous-Paleocene sediments from the Cote d'Ivoire-Ghana Transform Margin. In: Mascle, J. Lohmann, G.P., Moullard, M. (Eds.) Proceedings of the Ocean Drilling Program: College Station, Scientific Results, v. 159, p. 277-318.

Oglesby, R.J. Park, J., 1992. Cyclic sedimentation, climate and orbital insolation changes in the Cretaceous: Encyclopedia of Earth System Science, v. 2, p. 13-27.

Otto-Bliesner, B.L., Brady, E.C., Shields, C., 2002. Late Cretaceous ocean: Coupled simulations with the National Center for Atmospheric Research Climate System Model: Journal of Geophysical Research, v. 107, no. D2, p. ACL 11-1 – 11-14.

Park, J., Oglesby, R.J., 1991. Milankovitch rhythms in the Cretaceous: A GCM modeling study: Palaeogeography, Palaeoclimatology, Palaeoecology, v. 90, p. 329-355.

Parrish, J.T., 1995. Paleogeography of Corg-rich rocks and the preservation versus production

controversy. In: Huc, A.Y. (Ed.) Paleogeography, Paleoclimate, and Source Rocks: Tulsa, American Association of Petroleum Geologists, Studies in Geology, v. 40, p. 1-20.

Passier, H.F., Bosch, H.J., Nijenhuis, I.A., Lourens, L.L., Böttcher, M.E., Leenders, A., Sinninghe Damsté, J.S., De Lange, G.J., De Leeuw, J.W., 1999. Sulphidic Mediterranean surface waters during Pliocene sapropel formation: Nature, v. 397, p. 146-149.

Pearson, P.N., Ditchfield, P.W., Singano, J., Hartcourt-Brown, K.G., Nicholas, C.J., Olsson, R.K., Shackleton, N.J., Hall, M.A., 2001. Warm tropical sea surface temperatures in the Late Cretaceous and Eocene epochs: Nature, v. 413, p. 481-487.

Perez-Infante, J., Farrimond, P., Furrer, M., 1996. Global and local controls influencing the deposition of the La Luna Formation (Cenomanian-Campanian), western Venezuela: Chemical Geology, v. 130, p. 271-288.

Peterson, C.C., Haug, G.H., Hughen, K.A. Röhl, U., 2000. Rapid changes in the hydrological cycle of the tropical Atlantic during the last glacial: Science, v. 290, p. 1947-1951.

Philander, S.G., Fedorov, A.V., 2003. Role of tropics in changing the response to Milankovich forcing some three milion years ago: Paleoceanography, v. 18, doi:10.1029/2002PA000837.

Pickett, E.A., Allerton, S., 1998. Structural observations from the Côte d'Ivoire-Ghana Transform Margin. In: Mascle, J., Lohmann, G. P. Moullade, M. (Eds.) Proceedings of the Ocean Drilling Program, Scientific Results, 159: College Station, TX (Ocean Drilling Program), p. 3-11.

Pierrehumbert, R.T., 2002. The hydrologic cycle in deep-time climate problems: Nature, v. 419, p. 191-198.

Pletsch, T., Erbacher, J., Holbourn, A.E.L., Kuhnt, W., Moullade, M., Oboh-Okuenobe, F.E., Söding, E., Wagner, T., 2001. Cretaceous separation of Africa and South America: the view from the West African margin (ODP Leg 159): Journal of South American Earth Sciences, v. 14, p. 147-174.

Poulsen, C.J., Barron, E.J., Johnson, C.C., Fawcett, P., 1999. Links between climatic factors and regional oceanic circulation in the mid-Cretaceous. In: Barrera, E., Johnson, C.C. (Eds.) The evolution of Cretaceous ocean/climate systems: Geological Society of America, Special Paper, v. 332, p. 73-89.

Poulsen, C.J., Barron, E.J., Arthur, M.A., Peterson, W.H., 2001. Response of the mid-Cretaceous global oceanic circulation to tectonic and CO_2 forcings: Paleoceanography, v. 16, p. 576-592.

Poulsen, C.J., Gendaszek, A.S., Jacob, R.L., 2003. Did the rifting of the Atlantic Ocean cause the Cretaceous thermal maximum?: Geology, v. 31, p. 115-118.

Prahl, F.G., Dymond, J., Sparrow, M.A., 2000. Annual biomarker record for export production in the central Arabian Sea: Deep-Sea Research II, v. 47, p. 1581-1604.

Premoli Silva, I., Sliter, W.V., 1999. Cretaceous paleoceanography: evidence from planktonic foraminiferal evolution. In: Barrera, E., Johnson, C. (Eds.) The evolution of Cretaceous ocean/climate systems: Boulder, Geological Society of America, Special Paper, v. 332, p. 301-328.

Rahmstorf, S., 2002. Ocean circulation and climate during the past 120,000 years: Nature, v. 419, p. 207-214.

Raiswell, R., Berner, R.A., 1985. Pyrite formation in euxinic and semi-euxinic sediment: American Journal of Science, v. 285, p. 710-724.

Rangel, A., Parra, P., Nino, C., 2000. The La Luna formation: chemostratigraphy and organic facies in the Middle Magdalena Basin: Organic Geochemistry, v. 31, p. 1267-1284.

Rey, O., Simo, J.A., Lorente, M.A., 2004. A record of long- and short-term environmental and climatic change during OAE3: La Luna Formation, Late Cretaceous (Santonian-early Campanian), Venezuela: Sedimentary Geology, v. 170, p. 85-105.

Robison, C.R., Smith, M.A. Royle, R.A., 1999. Organic facies in Cretaceous and Jurassic

hydrocarbon source rocks, Southern Indus basin, Pakistan: Coal Geology, v. 39, p. 205-225.

Ronov, A.B., Khain, V., Balukhovsky, A., 1989. Atlas of Lithological-Paleogeographical Maps of the World, Mesozoic and Cenozoic of Continents and Oceans Barsukov, V., Laviorov, N. Eds.): Leningrad, Academy of Sciences,79 p.

Rowland, S.J. Robson, J.N., 1990. The widespread occurrence of highly branched acyclic C_{20}, C_{25} and C_{30} hydrocarbons, Recent Sediments and Biota - A review: Marine Environmental Research, v. 30, p. 191-216.

Royer, D.L., Berner, R.A., Montanez, I.P., Tabor, N.J., Beerling, D.J., 2004. CO_2 as a primary driver of Phanerozoic climate: Geological Society of America Today, v. 14, no. 3, p. 4-10.

Rusk, D.C., 2001. Libya: Petroleum potential of the underexplored basin centers-a twenty-first century challenge. In: Downey, M.W., Threet, J.C., Morgan, W.A. (Eds.) Petroleum Provinces of the twenty-first Century, Tulsa, American Association of Petroleum Geologists, Memoir, v. 74, p. 429-452.

Sageman, B., Rich, J., Arthur, M.A., Dean, W.E., Savrda, C.E., Bralower, T.J., 1998. Multiple Milankovitch cycles in the Bridge Creek Limestone (Cenomanian-Turonian), Western Interior Basin. In: Dean, W.E., Arthur, M.A. (Eds.) Stratigraphy and Paleoenvironments of the Cretaceous Western Interior Seaway, USA: Tulsa, SEPM (Society for Sedimentary Geology), Concepts in Sedimentology and Paleontology, v. 6, p. 153-171.

Schlanger, S.O., Jenkyns, H.C., 1976. Cretaceous oceanic anoxic events: causes and consequences: Geologie en Mijnbouw, v. 55, p. 179-184.

Schmittner, A., Appenzeller, C., Stocker, T.F., 2000. Enhanced Atlantic freshwater export during El Niño: Geophysical Research Letters, v. 27, p. 1163-1166.

Schoellkopf, N.B., Patterson, B.A., 2000. Petroleum systems of offshore Cabinda, Angola. In: Mello, M.R., Katz, J. (Eds.) Petroleum systems of South Atlantic margins: Tulsa, American Association of Petroleum Geologists, Memoir, v. 73, p. 361-376.

Schouten, S., Hoefs, M.J.L., Sinninghe Damsté, J.S., 2000. A molecular and stable carbon isotopic study of lipids in late Quaternary sediments from the Arabian Sea: Organic Geochemistry, v. 31, p. 509-521.

Schouten, S., Hopmans, E.C., Schefuß, E., Sinninghe Damsté, J.S., 2002. Distributional variations in marine crenarchaeotal membrane lipids: a new tool for reconstructing ancient sea water temperatures?: Earth and Planetary Science Letters, v. 204, p. 265-274.

Schouten, S., Hopmans, E.C., Forster, A., van Breugel, Y., Kuypers, M.M.M., Sinninghe Damsté, J.S., 2003. Extremely high sea-surface temperatures at low latitude during the middle Cretaceous as revealed by archael membrane lipids: Geology, v. 31, p. 1069-1072.

Schouten, S., Hopmans, E.C., Sinninghe Damsté, J.S., 2004. The effect of maturity and depositional redox conditions on archaeal tetraether lipid palaeothermometry: Organic Geochemistry, v. 35, p. 567-571.

Schröder-Adams, C.J., Cumbaa, S.L., Bloch, J., Leckie, D.A., Craig, J., Seif El-Dein, S.A., Simons, D.-J., Kenig, F., 2001. Late Cretaceous (Cenomanian to Campanian) paleoenvironmental history of the Eastern Canadian margin of the Western Interior Seaway: bonebeds and anoxic event: Palaeogeography, Palaeoclimatology, Palaeoecology, v. 170, p. 261-289.

Schulz, M., Berger, W.H., Sarnthein, M., Grootes, P.M., 1999. Amplitude variations of 1470-year climate oscillations during the last 100,000 years linked to fluctuations of continental ice mass. Geophysical Research Letters, v. 26, p. 3385-3388.

Scotese, C.R., 1997. Paleogeographic atlas, PALEOMAP progress report 90-0497: Arlington, Texas, University of Texas, Department of Geology, 37 p.

Shipboard Scientific Party, 2004. Explanatory notes. In: Erbacher, J., Mosher, D.C., Malone, M.J., et al. (Eds.) Proceedings of the Ocean Drilling Program, College Station, Initial Reports, v. 207, p. 1-94 [CD-ROM].

Sinninghe Damsté, J.S., de Leeuw, J.W., 1990. Analysis, structure and geochemical significance of organically-bound sulphur in the geosphere: State of the art and future research: Organic Geochemistry, v. 16, p. 1077-1101.

Sinninghe Damsté, J.S., Köster, J., 1998. A euxinic southern North Atlantic Ocean during the Cenomanian/Turonian oceanic anoxic event: Earth and Planetary Science Letters, v. 158, p. 165-173.

Sinninghe Damsté, J.S., van Koert, E.R., Kock-van Dalen, A.C., de Leeuw, J.W., Schenk, P.A., 1989. Characterization of highly branched isoprenoid thiophenes occurring in sediments and immature crude oils: Organic Geochemistry, v. 14, p. 555-567.

Sinninghe Damsté, J.S., Eglinton, T.I., Rijpstra, W.I.C., de Leeuw, J.W., 1990. Characterization of organically bound sulfur in high-molecular-weight, sedimentary organic matter using flash pyrolysis and Raney Ni desulfurization. In: Orr, W.L., White, C.M. (Eds.) Geochemistry of sulfur in fossil fuels: Washington DC, American Chemical Society, Symposium Series, v. 429, p. 486-528.

Sinninghe Damsté, J.S., Wakeham, S.G., Kohnen, E.L., Hayes, J.M., de Leeuw, J.W., 1993. A 6,000-year sedimentary molecular record of chemocline excursions in the Black Sea: Nature, v. 362, p. 827-829.

Sinninghe Damsté, J.S., Rijpstra, W.I.C., Schouten, S., Peletier, H., van der Maarel, M.J.E.C., Gieskes, W.W.C., 1999. A C25 branches isoprenoid alkene and C25 and C27 n-polyenes in the marine diatom *Rhizosolenia setigera*: Organic Geochemistry, v. 30, p. 95-100.

Sinninghe Damsté, J.S., Schouten, S., van Duin, A.C.T., 2001. Isorenieratane derivates in sediments: possible controls on their distribution: Geochimica et Cosmochimica Acta, v. 65, p. 1557-1571.

Sinninghe Damsté, J.S., Kuypers, M.M.M., Schouten, S., Schulte, S., Rullkötter, J., 2003. The lycopane/C31 n-alkane ratio as a proxy to assess palaeooxicity during sediment deposition: Earth Planetary Science Letters, v. 209, p. 215-226.

Shver, T.A., Struzer, L.R., 1978. Water balance and water resources of continents - Africa. In: Korzun, V.I., Sokolov, A.A., Budyko, M.I., Voskresensky, K.P., Kalinin, G.P., Konoplyantsev, A.A., Korotkevich, E.S., Kuzin, P.S., Lvovich, M.I. (Eds.) World water balance and water resources of the Earth: Studies and reports in hydrology, v. 25, p. 256-265.

Sloan, L.C., Huber, M., 2001. Eocene Oceanic Responses to Orbital Forcing on Precessional Time Scales: Paleoceanography, v. 16, p. 101-111.

Stach, E. Mackowsky, M.T., Teichmüller, M., Taylor, G.H., Chandra, D., Teichmüller, R., 1982. Stachs' Textbook of Coal Petrology: Berlin, Gebrüder Bornträger, 535 p.

Stein, R., Rullkötter, J., Welte, D.H., 1989. Changes in paleoenvironments in the Atlantic Ocean during Cretaceous times: results from black shales studies: Geologische Rundschau, v. 78, p. 883-901.

Stocker, T.F., Schmittner, A., 1997. Influence of CO_2 emission rates on the stability of the thermohaline circulation: Nature, v. 388, p. 862-865.

Tarduno, J. Brinkman, D.B., Renne, P.R., Cottrell, R.D., Scher, H., Castillo, P., 1998. Evidence for Extreme Climatic Warmth from Late Cretaceous Arctic Vertebrates: Science, v. 282, p. 2241-2244.

Thiede, J., van Andel, T.H., 1977. The deposition of anaerobic sediments in the Late Mesozoic Atlantic Ocean: Earth and Planetary Science Letters, v. 33, p. 301-309.

Thompson, S.L., Pollard, D. 1995. A global climate model (GENESIS) with a land-surface-transfer scheme (LSX). Part 1: Present-day climate: Journal of Climate, v. 8, p. 732-761.

Thurow, J., Brumsack, H.-J., Rullkötter, J., Littke, R., Meyers, P., 1992. The Cenomanian/Turonian Boundary Event in the Indian Ocean - a key to understand the global picture. In: Duncan, R.A. (Ed.) Synthesis of Results from Scientific Drilling in the Indian Ocean: Washington DC, American Geophysical Union, Geophysical Monograph

Series, v. 70, p. 253-273.
Timmermann, A., Oberhuber, J., Bacher, A., Esch, M., Latif, M., Roeckner, E., 1999. Increased El Niño frequency in a climate model forced by future greenhouse warming: Nature, v. 398, p. 694-697.
Tissot, B.P., Welte, D.H., 1984. Petroleum Formation and Occurrence: Berlin, Springer-Verlag, 699 p.
Tyson, R.V., 1995. Sedimentary organic matter: organic facies and palynofacies: London, Chapman and Hall, 615 p.
Valdes, P.,2000. Warm climate forcing mechanisms. In: Huber, B.T., MacLeod, K.G., Wing, S.L. (Eds.) Warm Climates in Earth History: Cambridge, Cambridge University Press, p. 3-20.
Van Andel, T.H., Heath, G.R., Moore, T.C., 1975. Cenozoic history and paleoceanography of the central equatorial Pacific Ocean: Geological Society of America Memoirs, v. 143, 134 p.
Van Andel, T.H., Thiede, J., Sclater, J.G., Hay, W.W., 1977. Depositional history of the South Atlantic Ocean during the last 125 million years: Journal of Geology, v. 85, p. 651-698.
Van Buchem, F.S.P., de Boer, P.L., McCave, I.N., Herbin, J.-P., 1995. The organic carbon distribution in Mesozoic marine sediments and the influence of orbital climatic cycles (England and the western North Atlantic). In: Huc, A.Y. (Ed.) Paleogeography, Paleoclimate, and Source Rocks: Tulsa, American Association of Petroleum Geologists, Studies in Geology, v. 40, p. 303-336.
Van der Weijden, C.H., Reichart, G.J., Visser, H.J., 1999. Enhanced preservation of organic matter in sediments deposited within the oxygen minimum zone in the northeastern Arabian Sea: Deep Sea Research I, v. 46, p. 807-830.
van Gemereden, H., Mass, J., 1995. Ecology of phototrophic sulfur bacteria. In: Blankenship, R.E., (Ed.) Anoxygenic Photosynthetic Bacteria: Dodrecht, Kluwer Academic Publication, p. 49-85.
Vergara, L. S., 1997. Cretaceous Black Shales in the Upper Magdalena Valley, Colombia. New Organic Geochemical Results (Part II): Journal of South American Earth Sciences, v. 10, p. 133-145.
Vine, J.D., Tourtelot, E.B., 1970. Geochemistry of black shale deposits – a summary report: Economic Geology, v. 65, p. 253-272.
Vladimirov, V. L., 1999. http://www.grid.unep.ch/bsein/index.html.
Volkman, J.K., Barrett, S.M., Dunstan, G.A., 1994. C_{25} and C_{30} highly branched isoprenoids alkenes in laboratory cultures of two marine diatoms: Organic Geochemistry, v. 21, p. 407-413.
Wagner, T., 2002. Late Cretaceous to early Quaternary organic sedimentation in the eastern Equatorial Atlantic: Palaeogeography, Palaeoclimatology, Palaeoecology, v. 179, p. 113-147.
Wagner, T., Pletsch, T., 1999. Tectono-sedimentary controls on Cretaceous black shale deposition along the opening Equatorial Atlanttic Gateway (ODP Leg 159). In: Cameron, N.R., Bate, R.H., Clure, V.S. (Eds.) The Oil and Gas Habitats of the South Atlantic: London, Geological Society, Special Publication, v. 153, p. 241-265.
Wagner, T., Sinninghe Damsté, J.S., Hofmann, P., Beckmann, B., 2004. Euxinia and primary production in Late Cretaceous eastern equatorial Atlantic surface waters fostered orbitally driven formation of marine black shales: Paleoceanography, v. 19, doi:10.1029/2003PA000898.
Wakeham, S.G., Peterson, M.L., Hedges, J.I., Lee, C., 2002. Lipid biomarker fluxes in the Arabian Sea, with a comparison to the equatorial Pacific Ocean: Deep Sea Research Part II, v. 49, p. 2265-2301.

Wang, C., Hu, X., Sarti, M., Scott, R.W., Li, X., 2005. Upper Cretaceous oceanic red beds in southern Tibet: a major change from anoxic to oxic, deep-sea environments: Cretaceous Research, v. 26, p. 21-32.

Watkins, D.K., Shafik, S. and Shin, I.C., 1998. Calcareous nannofossils from the Cretaceous of the Deep Ivorian Basin. In: Mascle, J., Lohmann, G. P., Moullade, M. (Eds.) Proceedings of the Ocean Drilling Program: College Station, Scientific Results, v. 159, p. 319-333.

Wedepohl, K.H., 1971. Environmental influences on the chemical composition of shales and clays. In: Ahrens, L.H., Runcorn, S.K., Urey, H.C. (Eds.) Physics and Chemistry of the Earth, v. 8: Oxford, Pergamon, p. 305-333.

Wehausen, R., Brumsack, H.-J., 1999. Cyclic variations in the chemical composition of eastern Mediterranean Pliocene sediments: a key for understanding sapropel formation: Marine Geology, v. 153, p. 161-176.

Whelan, J.K., Thompson-Rizer, C.L., 1993. Chemical methods for assessing kerogen and protokerogen types and maturity. In: Enger, M.H., Macko, S.A. (Eds.) Organic Geochemistry, New York, Plenum Press, p. 289-353.

Wilson, P.A., Norris R.D., 2001. Warm tropical ocean surface and global anoxia during the mid-Cretaceous period: Nature, v. 412, p. 425-429.

Wilson, P.A., Norris, R.D., Cooper, M.J., 2002. Testing the mid-Cretaceous greenhouse hypothesis using "glassy" foraminiferal calcite from the core of the Turonian tropics on Demerara Rise: Geology, v. 30, p. 607-610.

Yarincik, K.M., Murray, R.W., Peterson, L.C., 2000. Climatically sensitive eolian and hemipelagic deposition in the Cariaco Basin, Venezuela, over the past 578,000 years: Results from Al/Ti and K/Al: Paleoceanography, v. 15, p. 210-228.

Zabel, M., Schneider, R.R., Wagner, T., Adegbie, A.T., de Vries, U., Kolonic, S., 2001. Late Quaternary Climate Changes in Central Africa as Inferred from Terrigenous Input to the Niger Fan. Quaternary Research, v. 56, p. 207-217.

Zapata, E., Padron, V., Madrid, I., Kertznus, V., Truskowski, I., Lorente, M.A., 2003. Biostratigraphic, Sedimentologic, and Chemostratigraphic Study of the La Luna Formation (Late Turonian-Campanian) in the San Miguel and Las Hernández Sections, Western Venezuela: Palaios, v. 18, p. 367-377.

Acknowledgements

My first thanks go to Prof. Dr. Thomas Wagner for his idea that this "dirt" bears loads of interesting secrets and giving me the opportunity to work in such a great project. Leading me through all the ups and downs of finishing this PhD study was certainly a challenge… I thank Prof. Dr. Kai-Uwe Hinrichs for his review of my thesis – this has been a very long December!

I am grateful for the close collaboration with Dr. Peter Hofmann from the University of Cologne, who always added a second viewpoint to critical questions, not to mention analytical data and moral support. Thanks to Isabel Stüsser for making several weeks of intense work during a vacation, ääääähhh work stay on Texel in the very final weeks of this thesis a highlight of the past months.

Dr. Hermann Wehner and Georg Scheeder of the BGR in Hannover are thanked for the possibility of using their analytical equipment for Rock Eval pyrolysis. Stable isotope and biomarker analyses were made possible by the help of Dr. Stefan Schouten and Dr. Jaap S. Sinninghe Damsté of the NIOZ, Holland.

This work would have been impossible without the support of my colleagues in Bremen: Andrea, Babette, Bastian, Bec, Brit, Gustl, Hanni, Helga, Helge, Henning, Ingo, Jens, Kalle, Käthe, Katrin, Meral, Mia, Micha, Ralph, Renate, Roberto, Stephan, Susanne, Till, and Prof. Dr. Rüdiger Henrich. Special thanks are reserved for Christine and reGina who helped me, among other things, to improve this thesis, for Jörg who solved severe technical problems, and for Sadat who luckily found us in the middle of nowhere.

Ein besonderer Dank gilt meiner Familie, speziell meinen Eltern, für die großen und kleinen Hilfestellungen in all den Jahren bis zur Fertigstellung dieser Arbeit. Sie haben immer gewußt, daß aus dem Kind nochmal was wird… Ja, es gibt ein Leben außerhalb der Geologie!

My husband Olaf was the biggest, most steady help during these past years working on the thesis. He patiently endured my long nights at the office, chaotic schedules, endless discussions about Cretaceous black shales and lab work in general without being a geologist, panic-attacks related to any possible deadline, conferences, dirty dishes, and non-ironed shirts without any complaints. I still don't want a dog… Our daughter Finja might be too young to be thanked, but I am still grateful for her being such a quiet girl during the last few months of 2004, as well as being such a happy, easy, and smiling person ever since.